Numerical analysis of adhesively bonded joints

Milohanić, Darian

UNIVERSITY OF ZAGREB
FACULTY OF MECHANICAL ENGINEERING AND NAVAL ARCHITECTURE

MASTER THESIS

Darian Milohanić

Zagreb, 2023.

UNIVERSITY OF ZAGREB
FACULTY OF MECHANICAL ENGINEERING AND NAVAL ARCHITECTURE

MASTER THESIS

Mentor:

Dr. sc. Lana Virag, mag. ing.

Student:

Darian Milohanić

Zagreb, 2023.

Izjavljujem da sam ovaj rad izradio samostalno koristeći znanja stečena tijekom studija i navedenu literaturu.

Posebna zahvala ide mojoj obitelji na podršci, razumijevanju i pomoći tokom čitavog perioda studiranja, posebice za vrijeme boravka i pisanja ovog rada u Švedskoj. Zahvaljujem se docentici dr.sc. Lani Virag na mentorstvu i pruženoj pomoći oko izrade ovog rada. Zahvaljujem se i mojim mentorima iz kompanije AFRY, Robinu Kristianssonu i Mikaelu Hannebergu, na velikoj pomoći, kvalitetnim raspravama i ugodnoj radnoj atmosferi.

Darian Milohanić

SVEUČILIŠTE U ZAGREBU
FAKULTET STROJARSTVA I BRODOGRADNJE
Središnje povjerenstvo za završne i diplomske ispite
Povjerenstvo za diplomske ispite studija strojarstva za smjerove:
Procesno-energetski, konstrukcijski, inženjersko modeliranje i računalne simulacije i brodostrojarski

Sveučilište u Zagrebu Fakultet strojarstva i brodogradnje	
Datum	Prilog
Klasa: **602 - 04 / 23 - 6 / 1**	
Ur.broj: **15 - 23 -**	

DIPLOMSKI ZADATAK

Student: **Darian Milohanić** JMBAG: 0035216946

Naslov rada na hrvatskom jeziku: **Numeričko modeliranje lijepljenih spojeva**

Naslov rada na engleskom jeziku: **Numerical analysis of adhesively bonded joints**

Opis zadatka:

The usage of structural adhesives in the automotive industry has in recent years surged, however the knowledge and the experience of the structural adhesive modelling and its failure predictions using the finite element field is still limited.

Thus, the objective of the thesis is to investigate and develop a methodology to analyse and evaluate adhesive structural performance for strength and durability. In this thesis, it is necessary to do the following:

1. Perform literature review to find current industrial practice and existing methods for predicting failures of adhesively bonded joint.
2. Based on the literature overview, choose the most appropriate numerical methods, and understand the element definitions and differences of the chosen methods.
3. Using data from the datasheet of an adhesive of interest, perform numerical analyses of standard experiments that are used to obtain stiffness and stress distribution within the test samples. Compare results obtained by different methods chosen in the previous step.
4. Perform sensitivity analysis on different model parameters (such as connection types or failure criteria).

All analyses must be done numerically using the finite element method. It is necessary to indicate the literature used and any help received in the thesis.

Zadatak zadan:	Datum predaje rada:	Predviđeni datumi obrane:
4. svibnja 2023.	6. srpnja 2023.	17. – 21. srpnja 2023.
Zadatak zadao:		Predsjednik Povjerenstva:
Doc.dr.sc. Lana Virag		Prof. dr. sc. Tanja Jurčević Lulić

CONTENTS

LIST OF FIGURES

LIST OF TABLES

LIST OF NOTATIONS

Symbol	Unit	Description
B	mm	Bondline width
D	Nm^2	Adherend bending stiffness
d	mm	Length of inner elastic zone
d_I	mm	Displacement in mode I
d_{II}	mm	Displacement in mode II
d_{III}	mm	Displacement in mode III
dc	m	Critical opening displacement
d_{eff}	mm	Combined relative displacement
dm	m	Maximal opening displacement
E	MPa	Young´s modulus
E_P	MPa	Adherend modulus
e_I	-	Maximum strain values in mode I
e_{II}	-	Maximum strain values in mode II
e_{III}	-	Maximum strain values in mode III
G	J/m^2	Energy per area that can be absorbed by cohesive elements
G_A	N/mm^2	Adhesive shear modulus
K	N/mm^2	
k_I	N/mm^2	Elasticity stiffness in mode I
k_{II}	N/mm^2	Elasticity stiffness in mode II
k_{III}	N/mm^2	Elasticity stiffness in mode III
k	-	Bending moment factor
L_O	mm	Bondline length
L_T	mm	Length between grips
M	Nm	Bending moment
P	N	Load
$\bar{P}$	N/m	Load per unit width
P_m	N	Maximum load
s_I	MPa	Maximum stress in mode I
s_{II}	MPa	Maximum stress in mode II
s_{III}	MPa	Maximum stress in mode III

T	MPa	Traction
t_0	mm	Adhesive thickness in a numerical model
t_P	mm	Substrate thickness
t_A	mm	Adhesive thickness
U	J	Strain energy density
V	N	Transverse force
$W1$	mm	Separation evaluated from the damage initiation to failure
B	-	Mixing coefficient
γ_e	-	Adhesive elastic shear strain
γ_P	-	Adhesive plastic shear strain
ε_I	-	Strain in mode I
ε_{II}	-	Strain in mode II
ε_{III}	-	Strain in mode III
ν	-	Poisson´s ratio
σ_I	MPa	Stress in mode I
σ_{II}	MPa	Stress in mode II
σ_{III}	MPa	Stress in mode III
$\sigma_{C,C}$	MPa	Combined stress in continuum model
$\sigma_{C,CZM}$	MPa	Combined stress in CZM
σ_{vm}	MPa	von Mises stress
σ_x	MPa	Stress in *x* direction
σ_y	MPa	Stress in *y* direction
σ_z	MPa	Stress in *z* direction
τ	MPa	Shear stress
τ_f	MPa	Shear failure strength for global yielding criterion
τ_{max}	MPa	Maximum shear stress
τ_P	MPa	Plastic adhesive shear stress
τ_{xy}	MPa	Shear stress in *xy* plane
τ_{zx}	MPa	Shear stress in *zx* plane
τ_{zy}	MPa	Shear stress in *zy* plane
Ω	-	Domain of the integral
$\boldsymbol{a}$	-	Nodal variables
$\boldsymbol{B}$	-	Gradient of the shape function matrix
$\boldsymbol{D}$	N/mm^2	Elasticity matrix
$\boldsymbol{f}$	N	Force vector
$\boldsymbol{K}$	N/mm^2	Global stiffness matrix
$\boldsymbol{k}$	N/mm^2	Element´s stiffness matrix
$\boldsymbol{N}$	-	Shape function matrix
$\boldsymbol{u}$	mm	Nodal displacement vector
$\boldsymbol{\varepsilon}$	-	Strain matrix
$\boldsymbol{\sigma}$	MPa	Stress matrix

SAŽETAK

Upotreba lijepljenih spojeva u automobilskoj industriji se sve više povećava. U isto vrijeme znanje i iskustvo o numeričkom modeliranju i analizi lijepljenih spojeva je ograničeno. Iz tog razloga, cilj ovog rada je pronaći način analiziranja lijepljenih spojeva koji će u sklopu simulacije cijelog vozila biti jednostavni, a pouzdano točni. Unutar ovog rada je u sklopu pregleda literature dan je opis problematike lijepljenih spojeva sa najvažnijim terminima. Temeljem pregleda literature su odabrane dvije metode analiziranja lijepljenih spojeva za detaljnu razradu i usporedbu rezultata – model temeljen na mehanici kontinuuma i model kohezivne zone (eng. *cohesive zone model*). Za oba modela su njihove formulacije detaljno opisane. Nadalje, na primjeru jednostruko preklopnog spoja odrađena je usporedba odabranih metoda u smislu krutosti numeričkih modela i dobivenih raspodjela naprezanja. Numerički dobiveni rezultati su također uspoređeni s eksperimentalnim podacima iz literature, kako bi se odredila njihova točnost. Na kraju je izvršena analiza senzitivnosti variranjem sljedećih parametara: veličina konačnih elemenata, debljina supstrata, debljina ljepila i dužina lijepljenog spoja.

Ključne riječi:

lijepljeni spoj, numerička analiza, kohezivni elementi, metoda kohezivne zone, metoda temeljena na mehanici kontinuuma

SUMMARY

The usage of structural adhesives has increasingly been used in the automotive industry. At the same time the knowledge and the experience about structural adhesive modelling and failure predictions in the field of numerical analysis is limited. In order to reduce these shortcomings, this thesis aims to find a solution to model adhesive behaviour in a full vehicle simulation. Thus, in this thesis, first of all, a literature review was performed. Based on this review, a description of adhesives and most relevant terms is presented. Two modelling methods – continuum mechanics and cohesive zone model – have been chosen for a further analysis and comparison. Detailed description of their formulation is presented. Next, a stiffness comparison of the models was performed on a single lap joint, after which a stress distribution of the models is analysed and compared. Also, numerical results are compared to test data extracted from literature to verify their accuracy. Lastly, sensitivity study was performed by varying following parameters: element size, adherend thickness, bondline thickness and bondline length.

Key words:
Structural adhesive, single lap joint, numerical analysis, cohesive elements

1. INTRODUCTION

1.1. Background

Adhesives have originally been used in automotive industry mainly for non-structural applications, such as sealing and damping [1]. However, the application of structural adhesives has gradually increased in the automotive industry. Unfortunately, the knowledge and the experience about the structural adhesive modelling and failure prediction in the finite element (FE) field remained limited. Hence this is an interesting topic to be explored.

1.2. Objective

The purpose of the thesis is to take initial steps towards increased understanding of modelling and more reliable simulation of adhesives. That can be performed by investigating and developing a methodology to analyse and evaluate adhesive structural performance for strength and stiffness. The investigation focused on pure metal-to-metal structures and implementations using the finite element method (FEM).

1.3. Method

Literature review was performed to find current trends in adhesive modelling in industrial practice, as well as existing methods for predicting failures of bonded joints using structural adhesives. In this thesis, a micro approach was first used to analyse chosen modelling methods. Lastly, it was determined whether a certain method is applicable for the macro approach.

1.4. Scope and limitations

This study is focusing on analysis of adhesive behaviour prior to damage initiation. Mechanics that occur after the damage initiation are not of primary concern in the thesis.

2. THEORY

In this section some basic information about adhesives are presented. That includes commonly used joint types and corresponding stress states. Furthermore, an overview of adhesive failure modes is presented. Lastly, standardized tests are described as well as some of the analytical methods developed for analysing standardized joints.

In an adhesively bonded joint at least two parts, called adherends or substrates, are connected by an adhesive. One of the main advantages of this method is the capability of joining dissimilar materials. It was shown that larger bondline area affects load distribution causing a more uniform stress distribution which results in generally stiffer structures [1]. Furthermore, when compared with traditional joining techniques, adhesively bonded joints exhibit higher resistance to cyclic loading and show improved resistance to corrosion [2].

On the other hand, there are some limitations when designing an adhesively bonded joint. Elevated temperatures and high humidity have a negative impact on adhesive strength; the decrease in strength is even more pronounced when the adhesive is submitted to a continuous load. Also, if the adhesive is submitted to a continuous load over a long period of time, creep must be considered. To achieve good cohesion, adhesively boded joints require careful surface preparation [3]. Furthermore, it is recommended to minimize peel and cleavage stresses because they cause stress concentrations, resulting in poor joint strength. Moreover, when dealing with non-permanent joint, such as fasteners or bolts, it is relatively easy to disassemble the joint and perform inspection of the parts. On the other hand, dismantling an adhesively bonded joint leads to destruction of the joint. Also, long bondlines of adhesively bonded joints usually result in a more complex design. Lastly, compared to bolts, rivets and such, adhesives exhibit complex behaviour resulting in distrust in numerically obtained results [4].

2.1. Joint types

There are many different joint types that are suitable for various load conditions. Many joint configurations can be found in specialized literature, e.g. [5]. Here, some of most common joint types are presented in Figure 1.

For the purposes of this thesis focus was put on the single lap joint (SLJ), shown first in Figure 1. This type of joint is loaded by tensile forces that are acting at the edge of the adherends. Because the forces are not in line, in addition to tension a secondary bending moment is induced causing shear and peel stresses to occur within the adhesive.

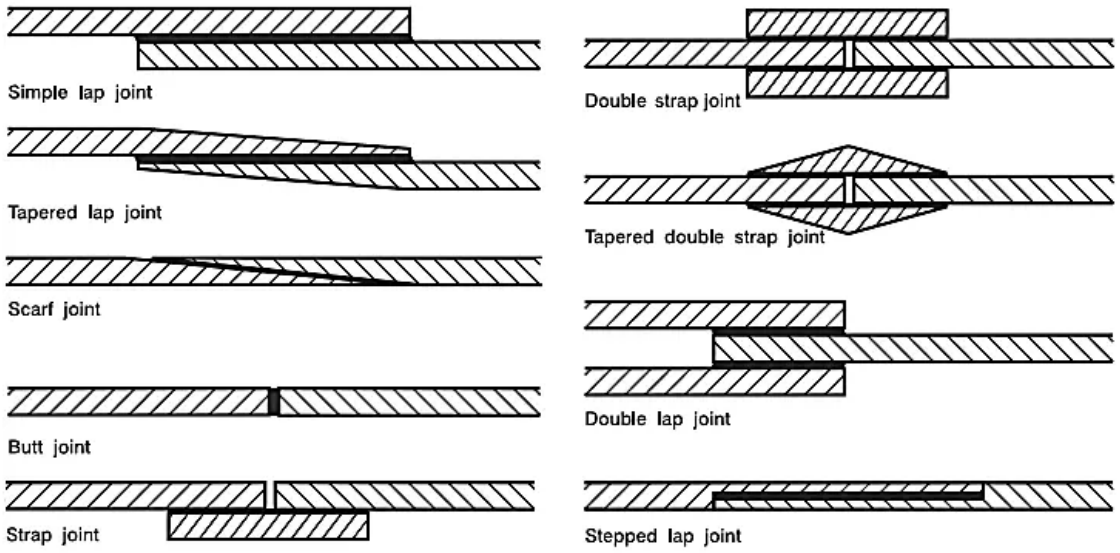

Figure 1. Joint types [5]

2.2. Joint stresses

To achieve best performance a joint should be designed in a way that result in an in-plane stress state. That way the load is distributed through the entire bondline. On the other hand, designing a joint where stress is normal to the adhesive gives poor results. Normal stress is often concentrated at the edge of the bondline creating a point at which crack initiates [6].

Types of joint stress that occur within adhesives are presented in Figure 2. Tensile, shear and compression stresses are widely known since they appear in the most common engineering problems. Peel and cleavage stresses are specific to adhesives and are characterized by a tensile force acting at one edge of the joint, resulting in a stress concentration at that edge. When it comes to the adhesive joint, one side experiences concentrated stress, while the other side theoretically undergoes compression or zero stress, depending on factors such as the thickness and material of the substrate. The difference between cleavage and peel is that cleavage occurs with two relatively rigid substrates while peel occurs when one of the substrates is flexible, resulting in even higher stress concentration compared to a cleavage joint [6].

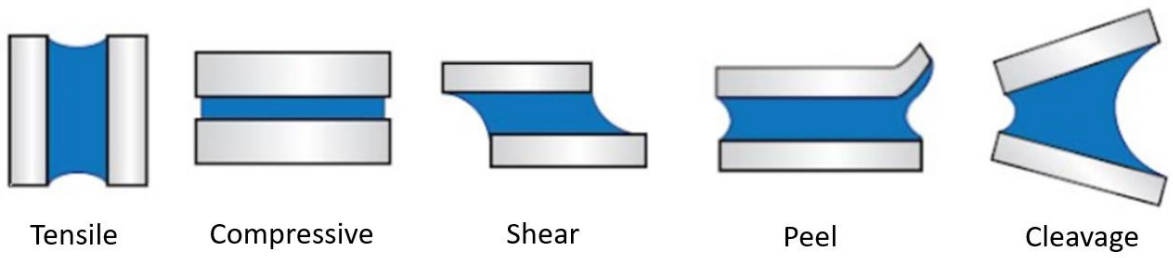

Figure 2. Types of joint stress [7]

2.3. Failure modes

Failure modes of adhesively bonded joints are presented in Figure 3. The failure mode is determined by the quality of the bond at each interface, joint geometry and loading condition [8]. Failure modes are classified, according to [9], in the following groups:

- **Adhesive failure** – "separation at the adhesive-adherend interface", see Figure 3a)
- **Cohesive failure** – "separation is within the adhesive", see Figure 3b)
- **Thin-layer cohesive failure** – "failure similar to cohesive failure, except that the failure is relatively close to the adhesive-adherend interface, characterized by a light dusting of adhesive on one adherend surface and a thick layer of adhesive left of the other", see Figure 3c)
- **Fibre-tear failure** – "failure occurring exclusively within the fibre-reinforced plastic (FRP) matrix, characterized by the appearance of reinforcing fibres on both ruptured surfaces", see Figure 3d)
- **Light-tear failure** – "failure occurring within the FRP adherend, near the surface, characterized by a thin layer of the FRP resin matrix visible on the adhesive, with few or no glass fibres transferred from the adherend to the adhesive", see Figure 3e)
- **Stock-break failure** – "this occurs when the separation is within the adherend but outside the bonded region", see Figure 4f)
- **Mixed failure** – "a mixture of different classes".

It should be noted that the mentioned failure modes characterize adhesively bonded FRP joints (ASTM D5573-99). Even so, some of the mentioned failure modes are applicable for adhesively bonded metal adherends as well.

Within this thesis, the adhesive-adherent bond is assumed to be ideal, meaning that adhesive failure will not occur. The focus of the thesis is put on analysing cohesive failure but stock-break failure is also considered.

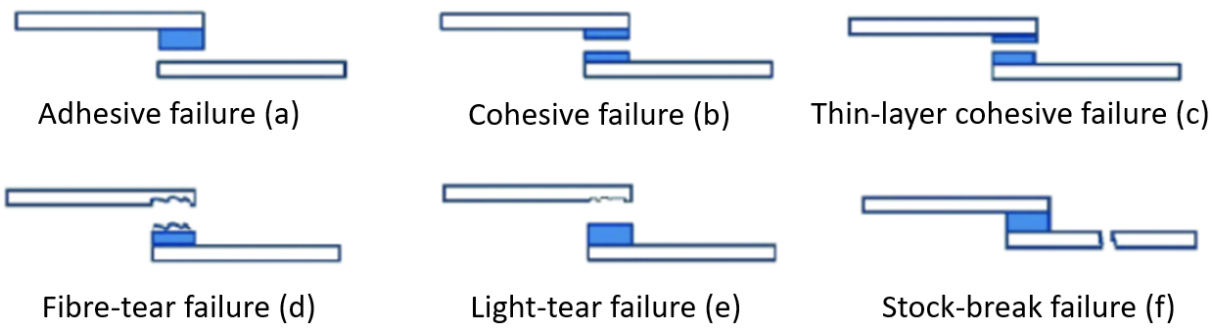

Figure 3. Failure modes [10]

2.4. Standard tests

There are various standard tests defined for adhesives by standards organizations. The tests that are of most interest for this thesis are ASTM [11] and ISO [12] norms:

- **ASTM D1002** – "standard method of test for strength properties of adhesives in shear by tension loadings (metal-to-metal)"
- **ASTM D5656** – "thick-adherend metal lap-shear joints for determination of stress-strain behaviour of adhesives in shear by tension loading"
- **ISO 527** – "test for determination of tensile properties of plastics".

Single lap joint (SLJ) is one of the standardized tests. Because SLJ with thick adherends exhibits nearly pure shear stress state due to thick substrates, it is appropriate for obtaining shear properties of the tested adhesive. Standardized dimensions of testing specimen for this experiment are shown in Figure 5. Note that while SLJ with thin adherends is also a standard test, a mixed mode (shear and tensile) stress state occurs during its exploitation. Testing specimen for this experiment can be seen in Figure 4. However, in order to obtain tensile properties, a tensile test on specimen, similar to one for testing metals, shown in Figure 6, is needed.

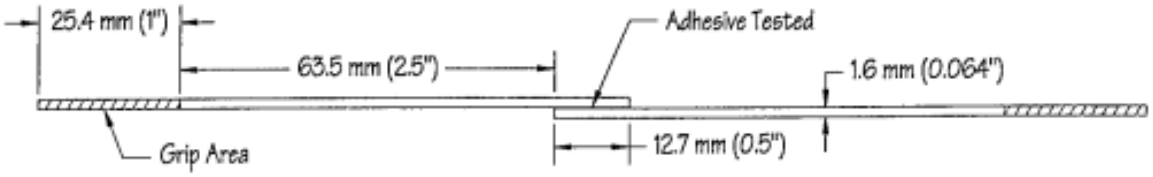

Figure 4. ASTM D1002 specimen [13]

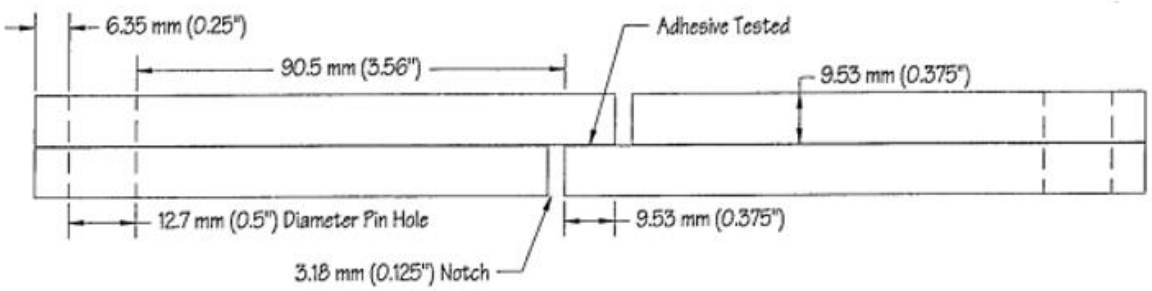

Figure 5. ASTM D5656 specimen [13]

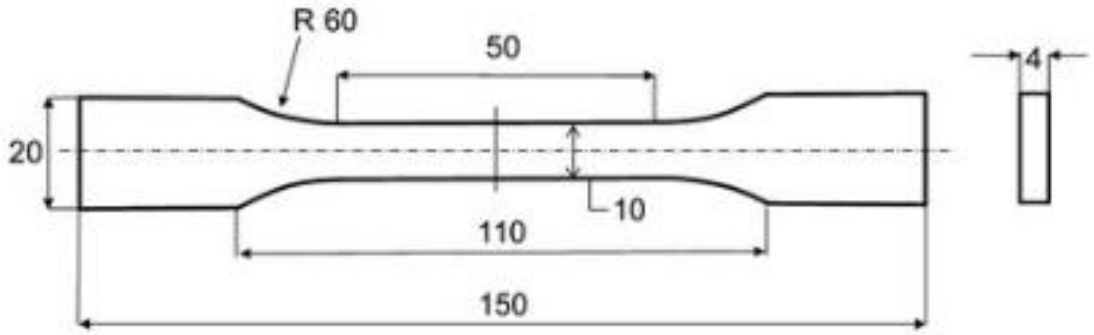

Figure 6. ISO 527 specimen [14]

2.5. Analytical methods

Through the years, a number of analytical methods have been developed that aim to analyse relatively simple problems such as the single lap joint. Some of the most known ones are presented in this chapter.

The first one to give an analytical method for the SLJ was Volkersen [15]. Volkersen's model considered the concept where adherends are under differential shear, see Figure 7. In this model, the adhesive exhibits purely shear deformation, while the adherends exhibit longitudinal deformation [15]. In the Figure 7, l is an initial bondline length and P is tensile force.

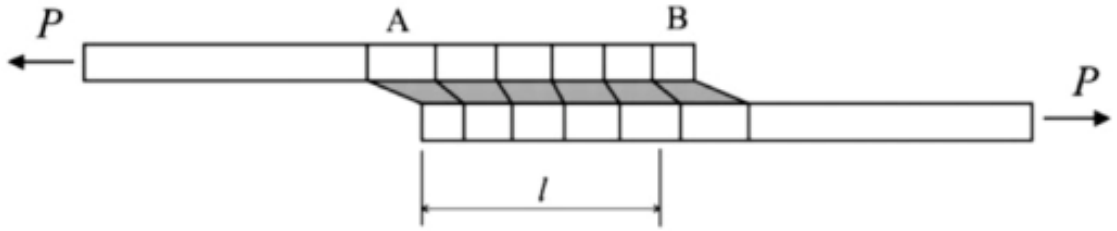

Figure 7. Deformations in a SLJ with elastic adherends [15]

The Goland and Reissner model considers that applied load $\overline{P}$ causes a bending moment M and a transverse force V due to the load eccentricity, as shown in Figure 8. As the joint is deforming under these loads, the bending moment decreases, resulting in a non-linear problem [15].

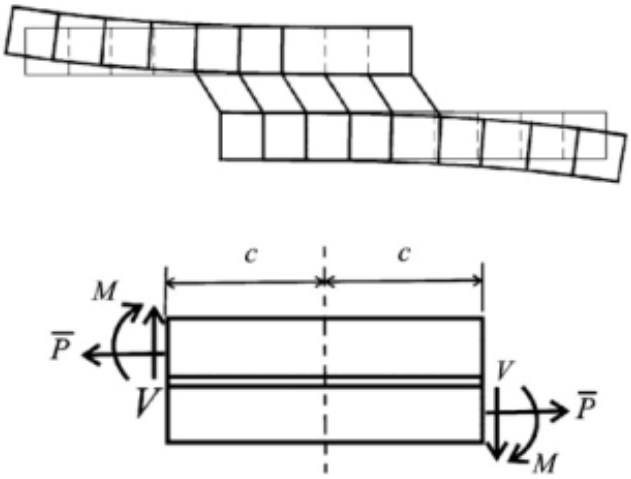

Figure 8. Goland and Reissner´s model [15]

A model by Hart-Smith was suggested that plasticization must be taken into consideration. In the model adhesive deformation under shear stress is described with an elastic-perfectly plastic model, as shown in Figure 9. The bond length was divided into three distinct zones: a central elastic zone with a length of *d*, and two outer regions exhibiting plastic behaviour [15].

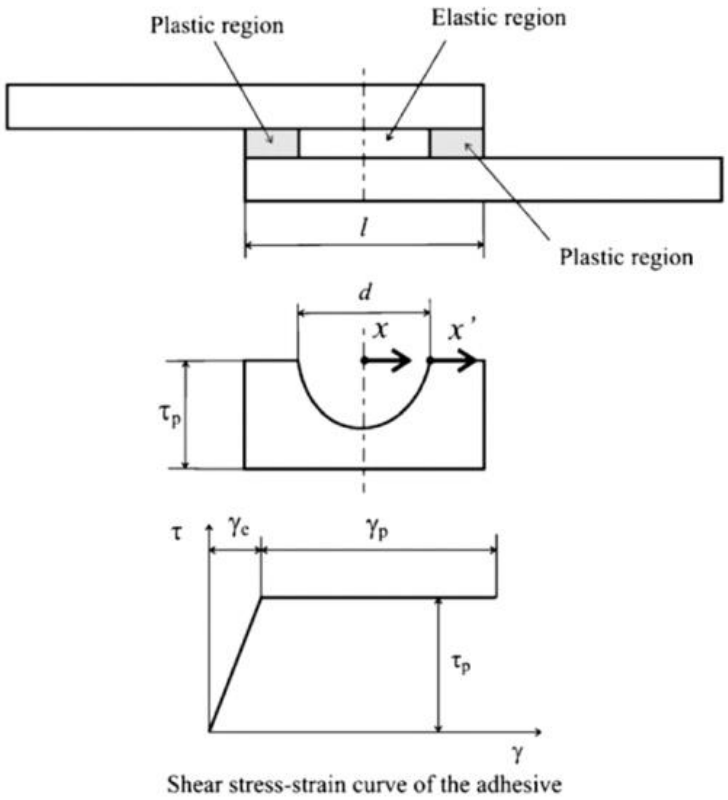

Figure 9. Schematic explanation of shear plastic deformation of the adhesive according to Hart-Smith [15]

When using elastic adherends with ductile adhesive, the strength of the joint is generally linear with the change of the bondline length. As the load increases ductile adhesives exhibit plastic deformation causing the load to be redistributed resulting in a better use of the bondline length. In this case, when the entire adhesive layer is under the adhesive shear strength, $\tau_{f,}$ it is suitable to use the global yield criterion (GY) for acquiring the maximum load, P_m [15].

2.6. Numerical methods

There are two modelling approaches depending on the degrees of freedom (DOF) of the model that is simulated. First, there is the macro approach, and it is used in models with large amount of DOF (large-scale). The second one is the micro approach, and it is used in models with small amount of DOF. With the macro approach the aim is to simulate models with large number of parts and connections. Those simulations are computationally demanding. Hence the aim is to have as simplified model as possible but still with a sufficient accuracy. An example of such model can be a full vehicle simulation. With the micro approach there are less components, and the model is usually more detailed and more accurate. An example of such model can be a simulation of a single structural part. In practice, a simpler large-scale simulation is performed to identify critical joints. The joints are then extracted and simulated in a more detailed sub-model.

2.6.1. Methods for the macro approach

Some of the most known methods for the macro approach used in the automotive industry for structural modelling of adhesive joints are, according to [16]:

- super-elements
- spring elements
- joint- line elements
- undercut element method.

Super-elements can be used to improve accuracy of macro models. Figure 10 shows a SLJ with super-elements. The super-element, labelled with number 2, that can contain good approximation of the joint behaviour is connected to other super-elements creating a simplified representation of the joint. Introducing super-elements in large-scale models offers the possibility to incorporate all geometric details. This advantage ultimately leads to reduced

processing time for addressing large problems. However, they are also restricted to linear elastic analyses [16].

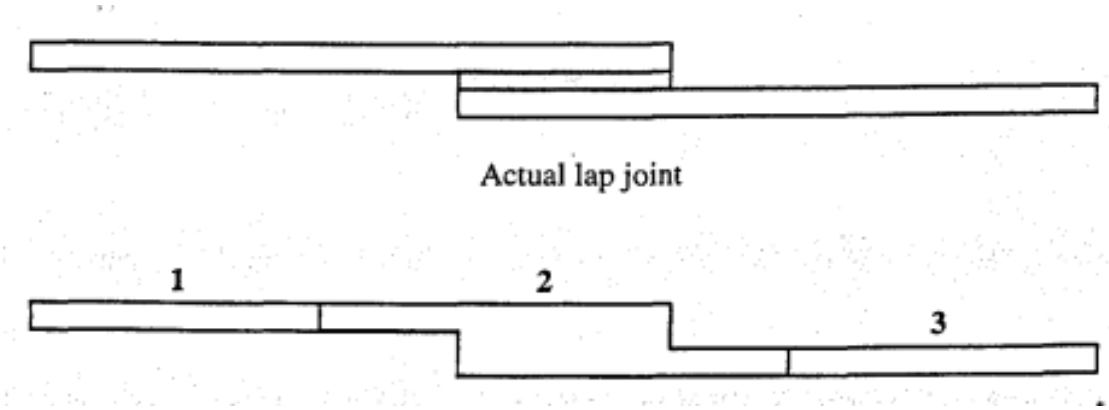

Figure 10. Super-element representation in lap joint [16]

In the next method, spring elements with six degrees of freedom are used to represent the adhesive as shown in Figure 11. Spring elements contain three DOF in translation and three in rotation. The advantage of using spring elements is a simple representation of the adhesive. On the other hand, no stress results are available and defining local co-ordinates can cause difficulties in implementation [16].

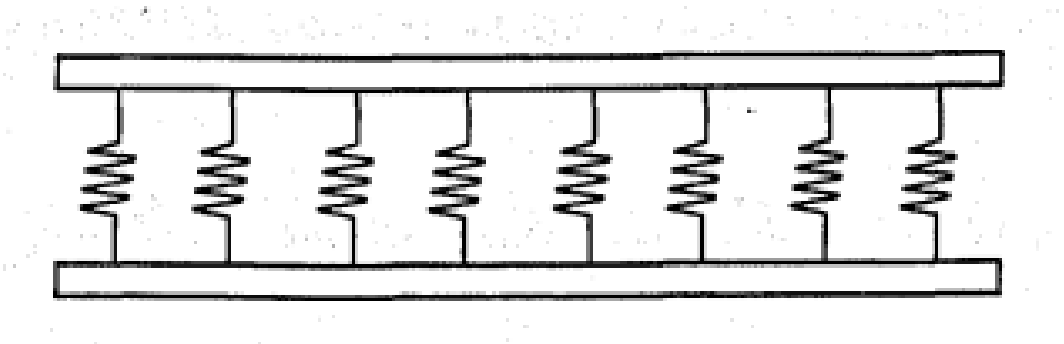

Figure 11. Spring-line element representation [16]

Joint-line elements are comprised of the complete set of geometric and material characteristics found in a real joint, including properties such as tensile and bending stiffness. Through micro models, which include geometrical details, joint properties can be obtained. In this method simplification of the real joint is achieved using joint-line elements as shown in Figure 12. The use of joint-line elements offers the ability to attain stress outputs and a straightforward modelling of the geometry. On the other hand, notable drawbacks are that representation of the geometry, and the loading effects is not accurate, as well as the necessity of using a specialized pre-processing package [16].

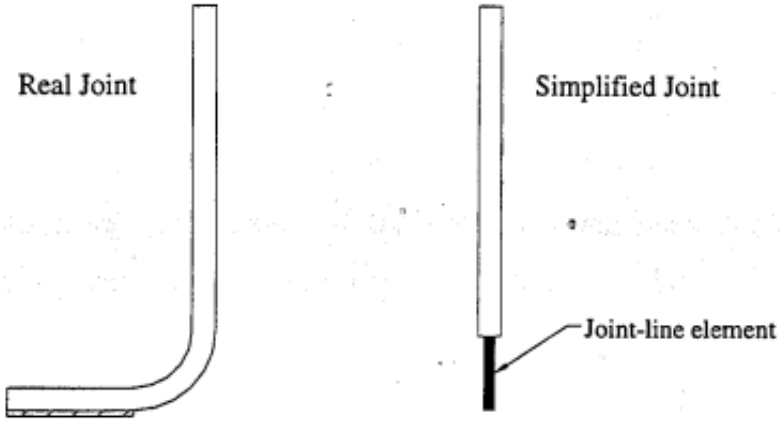

Figure 12. Inclusion of a joint-line element in a coach joint [16]

The undercut element method is a method for including joint details in large-scale models to provide more accurate and representative predictions of stiffness. Since shell to solid models with simplified geometry (i.e., with no fillets) result in overestimating stresses, and thus the joint stiffness, an intervention is required. Characteristic correction curve is used to determine the undercut distance based on the fillet ratio and bend radius. By including the undercut, excess elements are deleted resulting in lowering the joint stiffness. Results showed that this method was able to accurately predict stiffness behaviour. On the other hand, this method was developed primarily in the context of vehicle bodies constructed from steel sheets and using different materials can cause additional complications. Furthermore, although this method can be used for stress analyses, it would be necessary to use non-linear material properties [16].

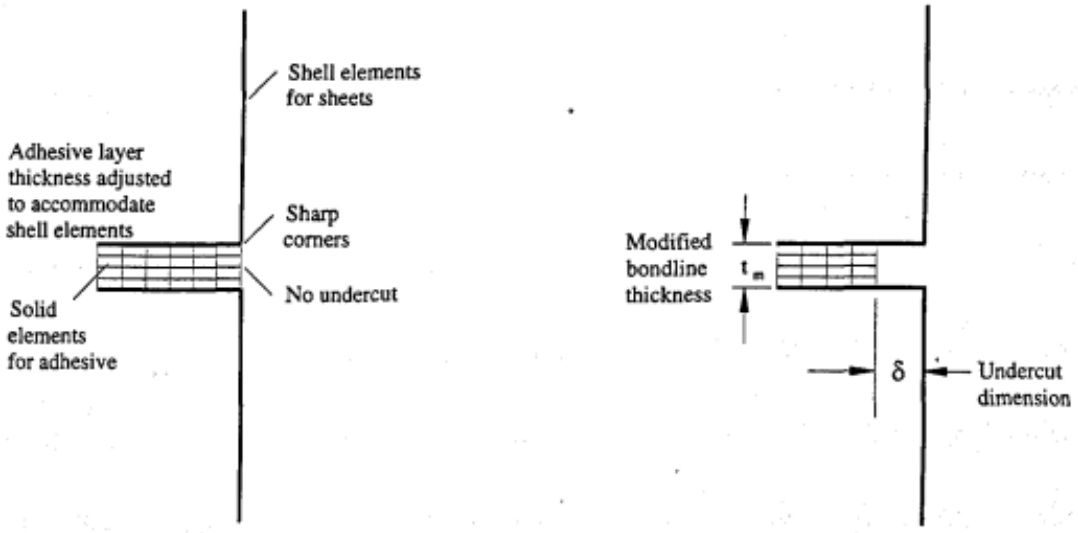

Figure 13. Application of the undercut element method in shell-solid models [16]

2.6.2. Methods for the micro approach

Some of the methods for the micro approach used for structural modelling of adhesive joints are:

- tie-break method
- continuum mechanics
- fracture mechanics
- damage mechanics.

Tie-break or contact-based method is a simple method to represent an adhesive layer. This method does not require the setup of mesh nor the use of elements to represent an adhesive [17]. The contact is typically described using two parameters – the adhesive tensile strength and shear strength. Although this method provides simple and quick implementation, representation of the adhesive behaviour can result in insufficient accuracy with large errors [18].

Continuum mechanics with linear behaviour are commonly used in general engineering and present the most straightforward method for modelling structural adhesives. This method is computationally efficient, provides simple implementation and is often used for initial evaluation. On the other hand, there are some problems involved in using this method. Typically, by comparing the stress and strain distributions attained from the finite element model to a maximum allowable value considered as the failure criterion can result in overengineering the adhesive joint [18]. Furthermore, at the interface corners where stress singularities are found, increasing mesh refinement results in increased stress levels [19].

Unlike continuum mechanics, fracture mechanics can evaluate singularities induced by material discontinuities. One major advantage of fracture mechanics is the use of energy parameters as a failure criterion making it accurate for modelling different types of materials, ranging from brittle to ductile. On the other hand, this method is reliable only for modelling problems with initial cracks. Analysing structures without initial cracks proves to be difficult since determination of a crack initiation point is not easy [19].

Damage mechanics can simulate progressive material degradation in the adhesive. This means that the adhesive stiffness is progressively reduced until reaching a failure point, where all the stiffness is gone. As a part of damage mechanics cohesive zone model (CZM) is frequently used for modelling adhesive behaviour. It can simulate adhesive behaviour from small elastic deformations to complete failure. The reason for that is the use of a mixed

formulation which includes continuum mechanics principles for damage initiation and fracture mechanics parameters for crack propagation. Cohesive elements behave according to an established cohesive law, i.e., traction-separation law. One major advantage of CZM is that strength prediction is mesh independent. This is possible since, instead of extracting values from a single point, averaging an energy criterion over an area is used for defining the damage growth [19]. Furthermore, this averaging means that overestimation of stress concentrations due to singularities found at sharp corners and defects is eliminated [18]. It is shown that CZM can provide accurate strength predictions for a wide range of joints [19]. However, there are several drawbacks with this method. Predicting stress and strain distributions in the direction perpendicular to the adhesive thickness is not possible [18]. Also, this approach typically requires the measurement of adhesive properties that are dependent on the joint geometry, e.g., adhesive shear strength being dependant on the mechanical stiffness of adherends [19].

Among the mentioned methods, continuum mechanics and cohesive zone model are chosen for further investigation. Continuum method is chosen due to its simplicity and computational efficiency. CZM is chosen due to its ability to eliminate singularities and mesh dependencies. A more detailed description of the chosen methods is presented in the following chapters.

2.6.2.1. Continuum method

In the continuum model different types of continuum elements can be used and some of them are shown in Figure 14. The FE equation for linear static system is defined as [20]:

$$\mathbf{Ku} = \mathbf{f}, \tag{1}$$

where **f** is a force vector, **K** is a stiffness matrix, and **u** is a nodal displacement vector. The nodal displacement vector is approximated by a shape function **N** and nodal variables **a**, as [20]:

$$\mathbf{u} \approx \mathbf{Na}. \tag{2}$$

Strain, **ε**, is then calculated as [20]:

$$\boldsymbol{\varepsilon} = \nabla\mathbf{u} \approx \nabla\mathbf{Na} = \mathbf{Ba}, \tag{3}$$

where **B** is a gradient of the shape function. Stress **σ**, is then calculated as [19]:

$$\boldsymbol{\sigma} = \mathbf{D}\boldsymbol{\varepsilon} \approx \mathbf{DBa}, \tag{4}$$

where **D** is an elasticity matrix.

Stiffness matrix of elements used in FEM is calculated as [20]:

$$\mathbf{k} = \int_{\Omega} \mathbf{B^T D B} \mathrm{d}\Omega., \tag{5}$$

where Ω is the domain of the integral.

Max shear stress, $\tau_{\max}$, and von Mises stress, σ_{vm}, used for analysing stress are calculated as [23]:

$$\tau_{\max} = \frac{1}{3}\left[(\sigma_x - \sigma_y)^2 + (\sigma_y - \sigma_z)^2 + (\sigma_z - \sigma_x)^2 + 6\tau_{yz}^2 + 6\tau_{zx}^2 + 6\tau_{xy}^2\right]^{\frac{1}{2}} \tag{6}$$

$$\sigma_{\mathrm{vm}} = \frac{1}{\sqrt{2}}\left[(\sigma_x - \sigma_y)^2 + (\sigma_y - \sigma_z)^2 + (\sigma_z - \sigma_x)^2 + 6\tau_{yz}^2 + 6\tau_{zx}^2 + 6\tau_{xy}^2\right]^{\frac{1}{2}}. \tag{7}$$

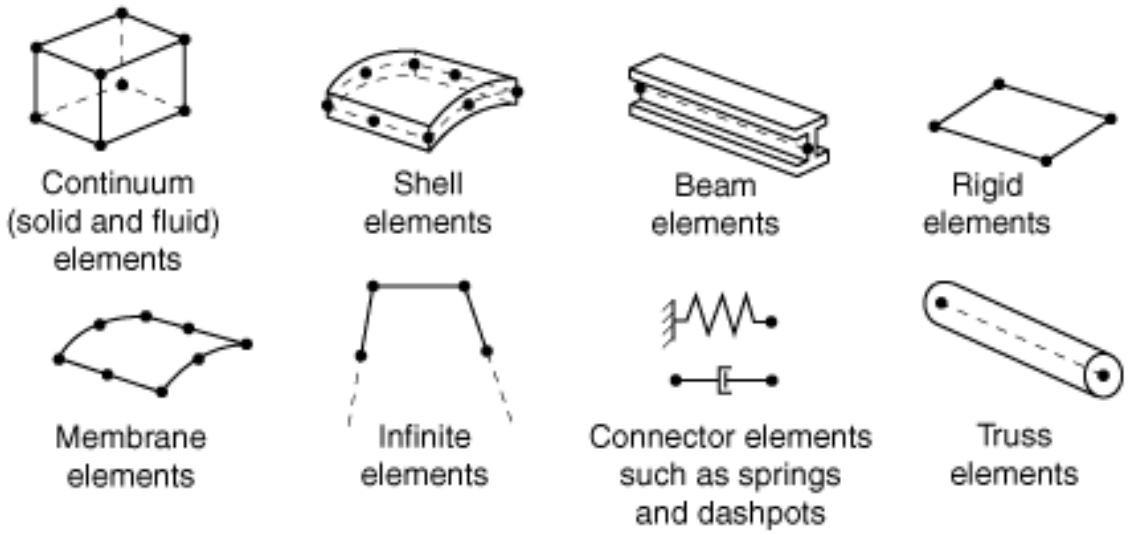

Figure 14. Commonly used continuum elements [22]

One of the most challenging parts of modelling structural adhesives is defining the material constitutive model. Constitutive models range from simple linear elastic models to advanced models that are able to predict complex adhesive behaviour [18]. Several material models are presented including linear elastic, hyperelastic, and linear elastic-plastic model.

A linear elastic model, see Figure 15, is valid for predicting behaviour at small strains and elastic, reversible deformation. In the linear elastic region, the adhesive behaviour is described by Hook´s law meaning that the stress is proportional to the strain [18]. Parameters needed to define the linear elastic model are Young's modulus and Poisson's ratio.

For some flexible structural adhesives, such as polyurethanes, hyperelastic models are appropriate for predicting large nonlinear elastic strains as can be seen in Figure 15. The stress-

strain relationship of hyperelastic materials is characterized by the strain energy density function $U(\mathbf{E})$ [18].

Material models with plasticity can predict material behaviour after reaching the yield point. The first region is linear elastic with elastic deformation but after reaching the yield point, a non-reversible deformation occurs, i.e., plasticity. Plasticity can be modelled with different hardening rules. The hardening rule defines stress – strain relationship for plastic deformations. Perfectly plastic materials exhibit constant value of yield stress with increasing plastic strain. However, real structural adhesives exhibit hardening after reaching yielding point, which can be approximated with bilinear or multilinear curves, see Figure 16. The definition of each linear segment is based on its corresponding tangent modulus. To define a general hardening curve, stress as a function of plastic strain is required [18].

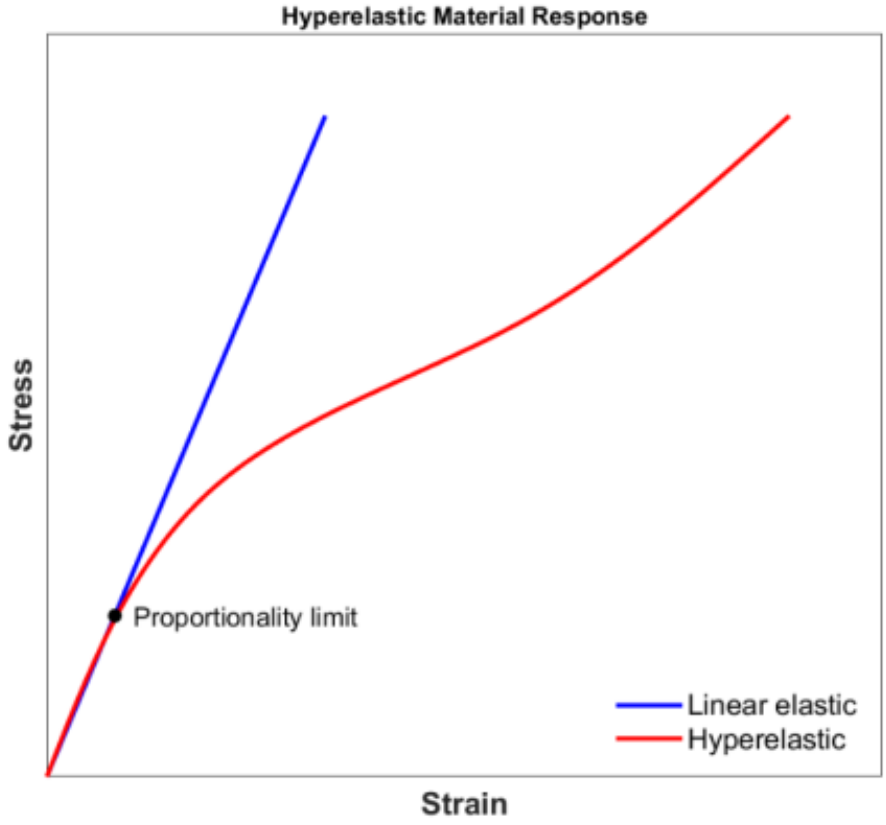

Figure 15. Material response for linear elastic and hyperelastic material models [18]

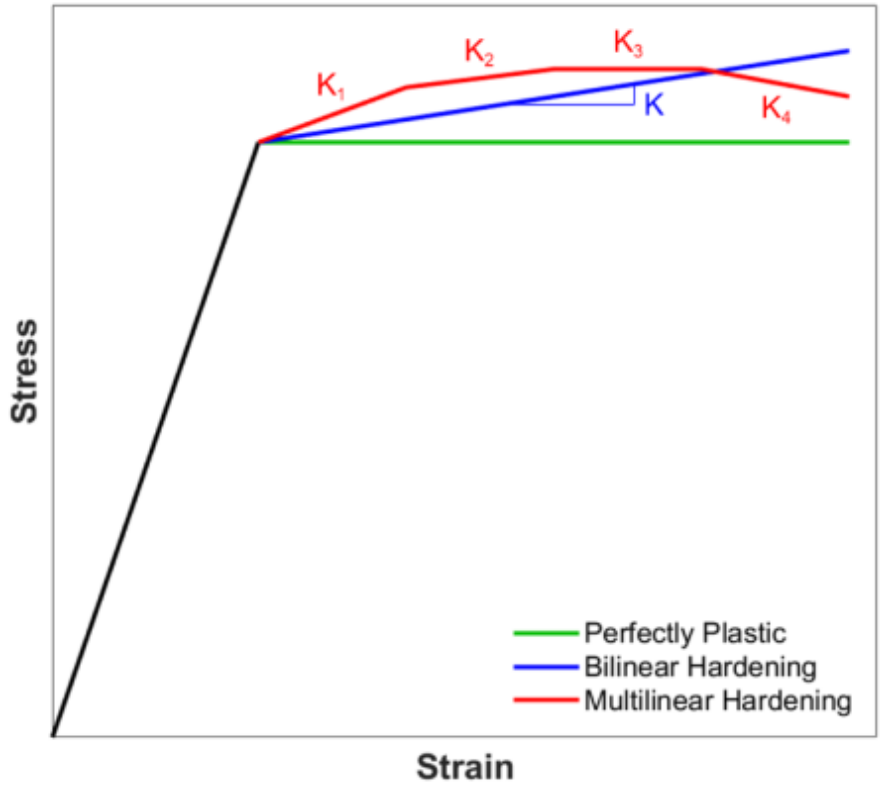

Figure 16. Material response for material models with plasticity [18]

2.6.2.2. Cohesive zone model (CZM)

In this thesis *OptiStruct v2022* is used as a solver. Therefore, CZM is described with respect to *OptiStruct* manual. When talking about cohesive elements, see Figure 17., used in CZM, there are three deformation modes as shown in Figure 18 – tensile (mode I) and two shear (modes II and III).

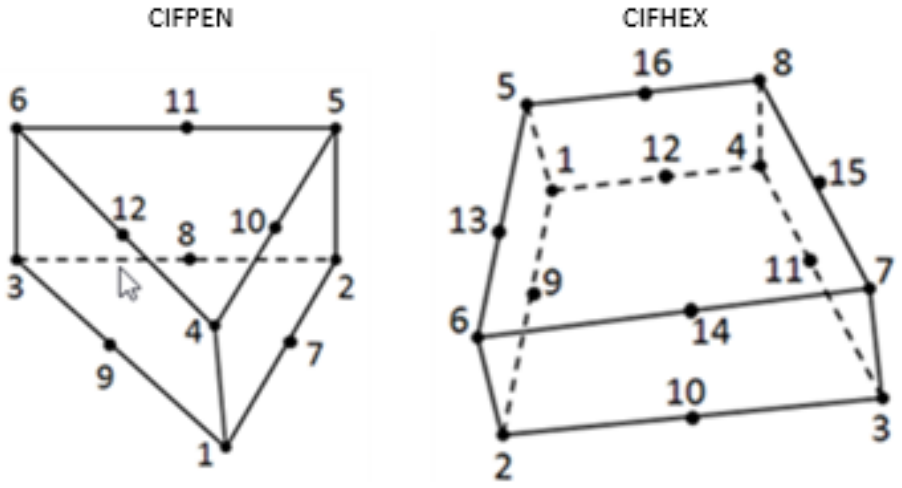

Figure 17. Cohesive elements in *OptiStruct* [17]

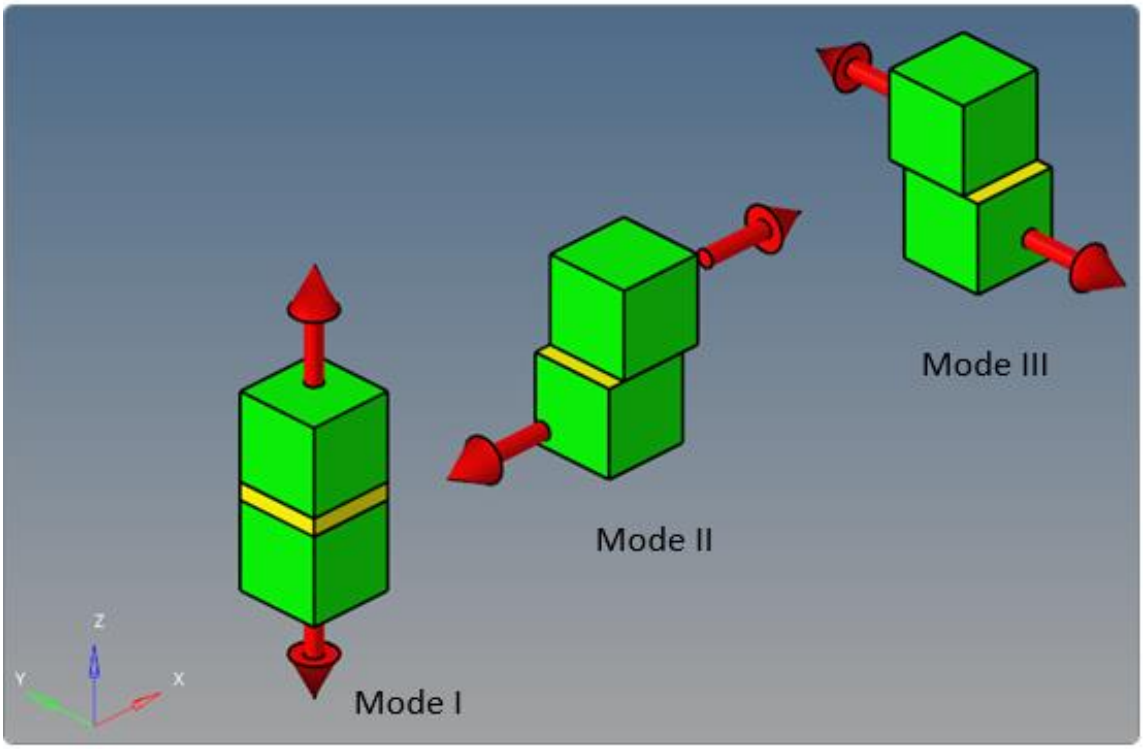

Figure 18. Deformation modes of cohesive elements [17]

In *OptiStruct* there are two approaches when using cohesive zone modelling [17]:

- potential-based
- damage-based.

In the potential-based method there are three types of traction-separation curves available, shown in Figure 19. *CRTOD* represents critical opening displacement while *MAXOD* represents maximal opening displacement and lastly *COHE* represents the energy per area that can be absorbed by the cohesive element. The calculation involves determining the relative displacement between the nodes located on the top and bottom faces. The three displacements (d_{I}, d_{II}, d_{III}) are used to derive the combined relative displacement with the mixing formulation [17]:

$$d_{eff} = \sqrt{\left(\beta d_{II}\right)^2 + \left(\beta d_{III}\right)^2 + \left(\max\left\{0.0, d_I\right\}\right)^2}, \qquad \textbf{(8)}$$

where d_{I}, d_{II} and d_{III} are openings in mode I, II and III, and β is the mixing coefficient. Based on the chosen traction-separation curve the combined traction is calculated by using the combined relative displacement d_{eff}. The equations for calculating traction T using the bilinear traction-separation curve are expressed as in [17]:

$$T = \begin{cases} \dfrac{2G}{d_m}\dfrac{d}{d_c} & 0 \le d \le d_c \\ \dfrac{2G}{d_m}\left(\dfrac{d_m - d}{d_m - d_c}\right) & d_c \le d \le d_m \\ 0 & d > d_m \end{cases}, \qquad \textbf{(9)}$$

Where d_c is the *CRTOD*, d_m is the *MAXOD*, G is the *COHE*, and d is the combined relative displacement (d_{eff}).

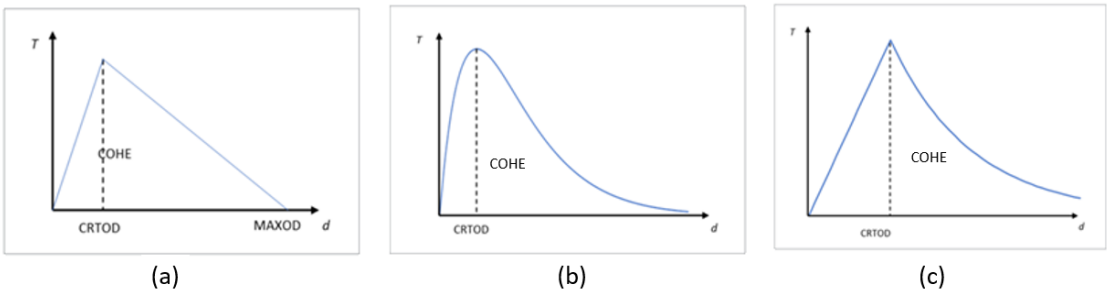

Figure 19. Traction-separation curves in *OptiStruct*, (a) bilinear, (b) exponential, (c) linear-exponential [16]

In the damage-based method, crack growth is controlled by evolution of damage in each element. The damage of an element is controlled by two indices, namely, damage initiation index and damage evolution index. Initially, both indices are zero in each element. Once damage initiation index reaches 1.0, damage appears. Next, the damage initiation index remains at 1.0 while the damage evolution index starts to increase. Upon reaching a value of 1.0, the damage is considered fully developed, resulting in the loss of cohesion, and the crack advances [17].

In the damage-based method the elastic behaviour can be written as [22]:

$$\boldsymbol{\sigma} = \begin{Bmatrix} \sigma_n \\ \sigma_s \\ \sigma_t \end{Bmatrix} = \begin{bmatrix} k_{nn} & k_{ns} & k_{nt} \\ k_{ns} & k_{ss} & k_{st} \\ k_{nt} & k_{st} & k_{tt} \end{bmatrix} \begin{Bmatrix} \varepsilon_n \\ \varepsilon_s \\ \varepsilon_t \end{Bmatrix} = \mathbf{K}\boldsymbol{\varepsilon}, \qquad \textbf{(10)}$$

where $\boldsymbol{\sigma}$ is a stress vector with components in *n*, *s* and *t* direction corresponding to mode I, II and III, respectively, i.e., $\sigma_{I,}$ $\sigma_{II,}$ σ_{III}. $\boldsymbol{\varepsilon}$ is a strain vector with components in *n*, *s* and *t* direction corresponding to mode I, II and III respectively. **K** is a fully coupled elasticity matrix, but usually an uncoupled stiffness matrix is used which is a diagonal matrix composed of only k_{nn}, k_{ss} and k_{tt} corresponding to k_I, k_{II} and k_{III} respectively.

In *OptiStruct* k_I, k_{II} and k_{III} represent elasticity moduli/penalty stiffnesses in the three directions, where k_I is for the normal direction, k_{II} and k_{III} are for the two tangential directions as depicted

in Figure 18. Like in the potential-based method the calculation involves determining the relative displacement between the nodes located on the top and bottom faces. First, by multiplying the penalty stiffness (which corresponds to elasticity modulus divided by thickness in quantity) and the opening in the three modes the calculation of the trial stress values is performed. Next, the identification of damage initiation is performed by applying predefined criteria based on strain or stress. Within strain-based damage initiation criteria there are two criteria – MAXE, see eq. (9), and QUADE, see eq. (10), based on the following formulation [17]:

$$\max\left\{\frac{\varepsilon_I}{\max(e_I)}, \frac{\varepsilon_{II}}{\max(e_{II})}, \frac{\varepsilon_{III}}{\max(e_{III})}\right\} = 1 \quad \textbf{(11)}$$

$$\left(\frac{\varepsilon_I}{\max(e_I)}\right)^2 + \left(\frac{\varepsilon_{II}}{\max(e_{II})}\right)^2 + \left(\frac{\varepsilon_{III}}{\max(e_{III})}\right)^2 = 1 \quad \textbf{(12)}$$

where e_{I}, e_{II} and e_{III} are the maximum strain values in the three directions. The actual strain is calculated as [17]:

$$\varepsilon_i = \frac{d_i}{t_0},\ i = \mathrm{I, II, III.} \quad \textbf{(13)}$$

Within stress-based damage initiation criteria there are two criteria – MAXS, see eq. (12), and QUADS, see eq. (13), based on the following formulation [17]:

$$\max\left\{\frac{\sigma_I}{\max(s_I)}, \frac{\sigma_{II}}{\max(s_{II})}, \frac{\sigma_{III}}{\max(s_{III})}\right\} = 1 \quad \textbf{(14)}$$

$$\left(\frac{\sigma_I}{\max(s_I)}\right)^2 + \left(\frac{\sigma_{II}}{\max(s_{II})}\right)^2 + \left(\frac{\sigma_{III}}{\max(s_{III})}\right)^2 = 1 \quad \textbf{(15)}$$

where s_{I}, s_{II} and s_{III} are the yield stress values in the three directions. The actual stress is calculated as [17]:

$$\sigma_i = k_i \frac{d_i}{t_0},\ i = I, II, III. \quad \textbf{(16)}$$

Combined stress is calculated as combination of stresses in each mode as [17]:

$$\sigma_{\mathrm{C,CZM}} = \sqrt{(\sigma_I)^2 + (\sigma_{II})^2 + (\sigma_{III})^2}. \quad \textbf{(17)}$$

No damage occurs unless the damage initiation criterion is satisfied. In that case the trial stress is equal to actual traction meaning that neither the initiation nor the propagation of cracks takes place. When the damage initiation criterion is met, it indicates the initiation of damage, and subsequently, the calculation of the damage evolution index is performed. There are two methods for the damage evolution index calculation based on energy dissipation and

displacement [17]. Since damage evolution is not the focus of this thesis, detailed explanation is not provided.

There are two techniques for simulating the cohesive behaviour at the corresponding interfaces [17]:

- element-based technique
- contact-based technique.

The element-based technique uses cohesive elements whose definition can be used for the potential-based and damage-based method. On the other hand, contact-based technique does not require the use of cohesive elements because the adhesive is modelled as a contact. For the contact-based technique only the damage-based method is available [17].

When the cohesive elements and their neighbouring parts have matching mesh, it is straightforward way of connecting cohesive elements with other components is simply by sharing nodes, i.e., with a node-to-node (N2N) connection. In cases where the mesh of two adjacent parts does not match, such as when the discretization level in the cohesive layer differs (usually finer) from that in the surrounding structures, a tie constraint can be used to connect the top and/or bottom surfaces of the cohesive layer with the surrounding structures [22].

In some cases, it may be difficult to obtain convergence with cohesive elements. To help achieve convergence damping stabilization can be defined in the cohesive elements [17].

2.6.2.3. Comparing stresses

To adequately compare CZM and continuum method, the same stress components should be considered. CZM calculates stress in three directions – $\sigma_{\mathrm{I}}, \sigma_{\mathrm{II}}, \sigma_{\mathrm{III}}$ (corresponding to the three modes) and a combined stress, $\sigma_{C,CZM}$, of all the modes. Therefore, two shear stress components τ_{zx} and τ_{zy}, and peel stress σ_z are considered in the continuum model. Combined stress, $\sigma_{\mathrm{C,C}}$, in continuum model, which corresponds to the combined stress in CZM, is calculated as:

$$\sigma_{\mathrm{C,C}} = \sqrt{(\sigma_{\mathrm{z}})^2 + (\tau_{\mathrm{zx}})^2 + (\tau_{\mathrm{zy}})^2}. \quad \textbf{(18)}$$

3. MODELLING AND ANALYSIS

For purposes of this thesis adhesive BETAMATE 4600F, manufactured by DuPont, is studied. The data used for modelling the adhesive was extracted from its datasheet [21]. The limitation of the datasheet is that it provides stress value for a SLJ with thin adherends meaning that mixed mode stress state occurred. This reduces the accuracy of input parameters since they should ideally consider pure stress state. Furthermore, the datasheet does not provide a force – displacement curve. This means that the behaviour of the adhesive is not completely known, hence it is not possible to compare the methods to the test results. Because of that another adhesive with similar properties was chosen from the literature that provides the needed test data. The chosen adhesive is Araldite 2015 from [15] which is characterized as a moderately ductile epoxy adhesive. Both adhesives have similar strain at break, but the tensile modulus is lower for A2015 adhesive, see Table 1. The relative difference was assumed to be sufficiently low, hence the adhesives was considered as similar. Relevant test data from [15] is shown in Figure 20 where P is force and δ is displacement.

Table 1. BETAMATE 4600F and Araldite 2015 properties [15, 21]

	BM 4600F	A2015
Tensile modulus [MPa]	2500	1850
Strain at break [%]	5	4,77

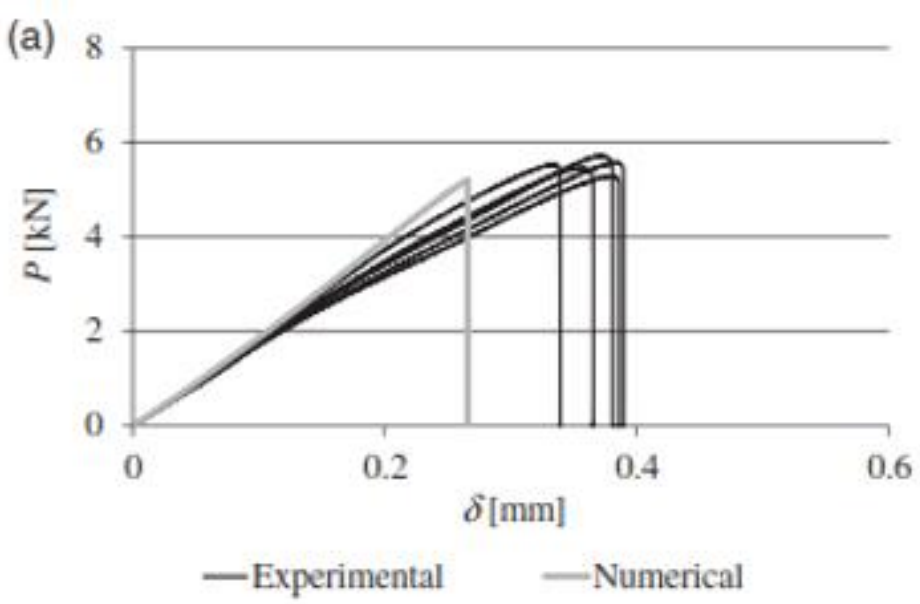

Figure 20. Experimental and CZM *P-δ* curves for the L_0 = 12,5 mm Araldite 2015 [15]

The aim was to first obtain the joint stiffness of both methods and compare it to the test data. Next, the strength of the joint can be compared. Additionally, the stress distribution within the adhesive was compared for both methods. Lastly, a sensitivity study was performed to study the effect of varying parameters on the joint stiffness and strength.

3.1. Model definition

Simulations were carried out on a single lap joint. A schematic view of the geometry and characteristic dimensions needed for modelling of the joint are shown in Figure 21. The values employed in the tests conducted in references [15] and [21] are presented in Table 2.

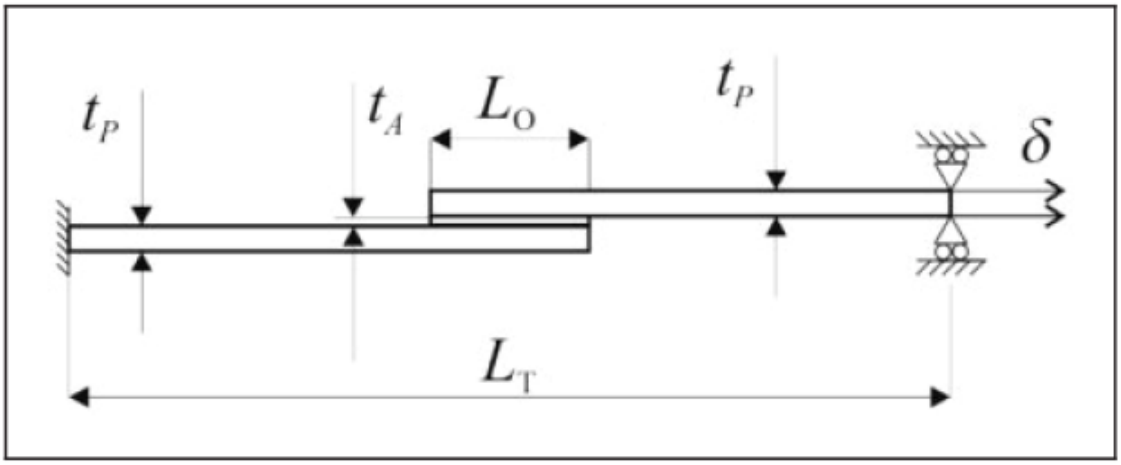

Figure 21. Schematic view of geometry and characteristic dimensions of SLJ [15]

Table 2. BM 4600F and A2015 SLJ dimensions [15, 21]

		BM 4600F	A2015
Substrate thickness [mm]	t_P	1,2	3
Adhesive thickness [mm]	t_A	0,2	0,2
Bondline length [mm]	L_0	10	12,5
Bondline width [mm]	B	25	25
Length between grips [mm]	L_T	150	180

3.1.1. Continuum model

Pre-processing was done in *ANSA* software package. In the continuum model *MAT1* material card, which defines the material properties of a linear, temperature-independent, and isotropic material, is used to define material properties of substrates and adhesive. To define the material model, Young´s modulus and Poisson´s ratio are needed, and the values used are shown in Table 3.

Boundary conditions are shown in Figure 22. Nodes at the end of the substrates were connected to a master node via RBE2 elements representing a clamped condition. The master node at Point A was constrained in all degree of freedom while Point B had constrained displacement and rotations around *y* and *z* direction, and an enforced displacement of 1 mm in *x* direction.

Two linear model configurations were used – continuum model with solid elements and continuum model with shell elements. The continuum shell model was made as computationally more efficient model compared to the solid model and is therefore more suitable for large-scale simulations. In the continuum solid model both adhesive and substrates were modelled with the first order hexahedron elements CHEXA (see Figure 17), with eight nodes and twenty-four degrees of freedom. In Figure 23 the mesh of the joint is shown. Finer mesh is used in the bond area, as shown in Figure 24, while coarser mesh is used further away from the bond area. Three layers of elements are used to model the substrates to be able to sufficiently capture the bending. Because of the thin adhesive bond, the adhesive was modelled with one layer of elements and is connected to the substrates by a node-to-node connection. In the continuum shell model, the adhesive is modelled with the first order hexahedron elements while substrates are modelled with shell elements as shown in Figure 25. The adhesive is connected to the substrates with RBE3 elements, see Figure 26.

Table 3. BM 4600F and A2015 material parameters used for continuum model

		BM 4600F	A2015	Aluminium substrate
Young´s modulus [MPa]	*E*	2500	1850	70000
Poisson´s ratio	*v*	0,4	0,33	0,33

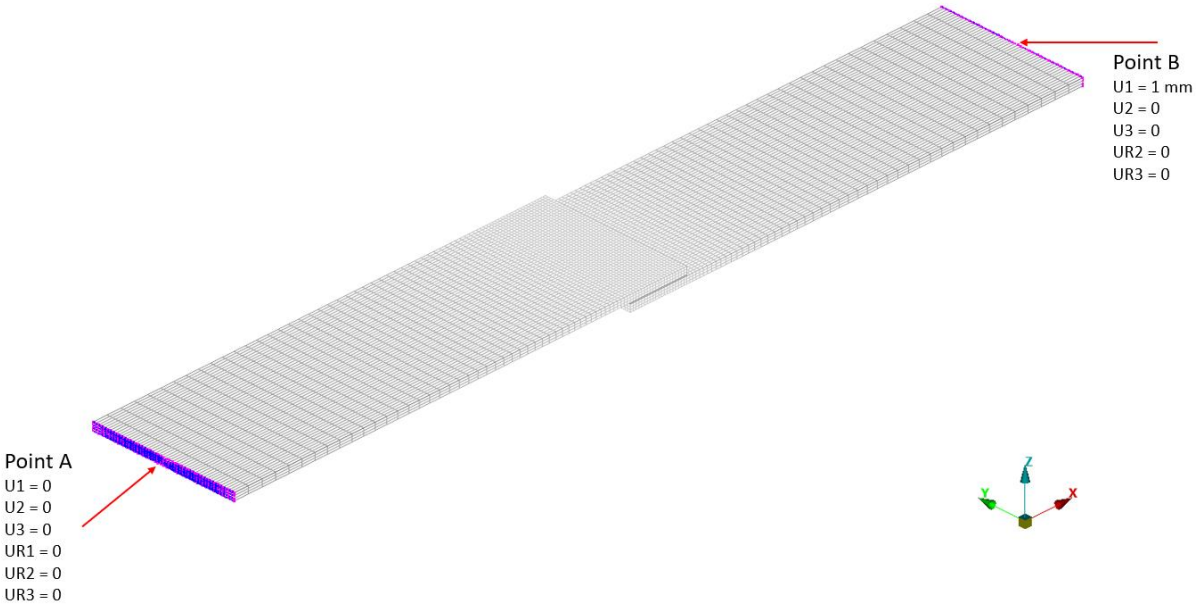

Figure 22. Boundary conditions

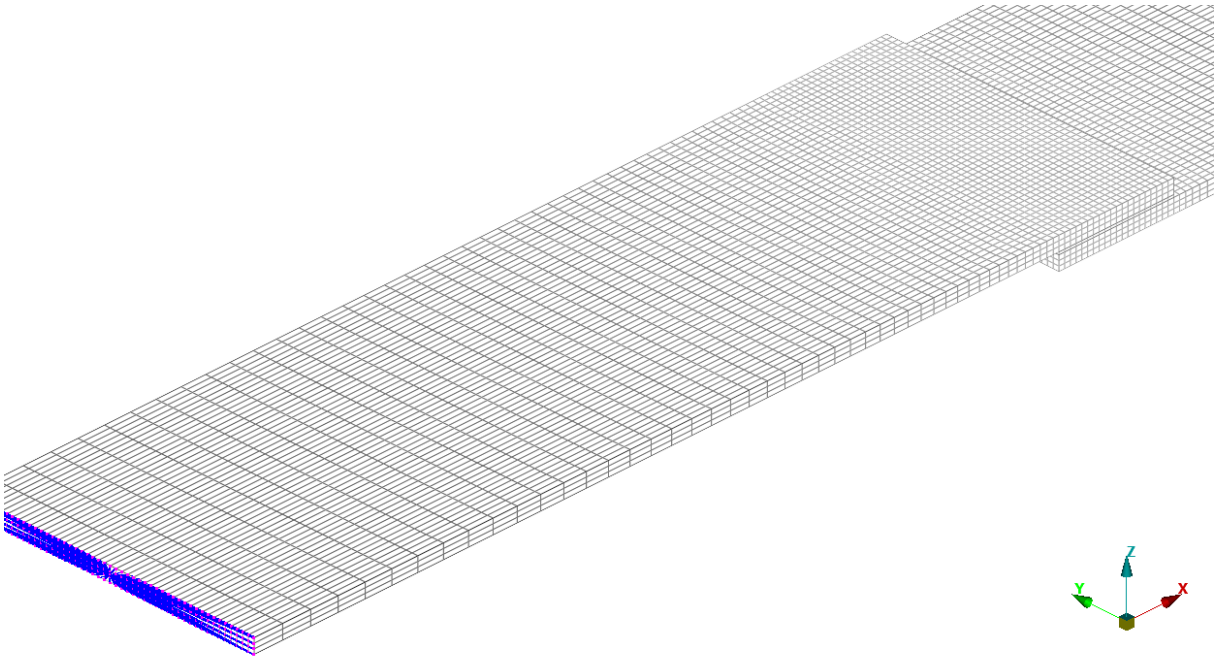

Figure 23. Mesh of continuum solid model

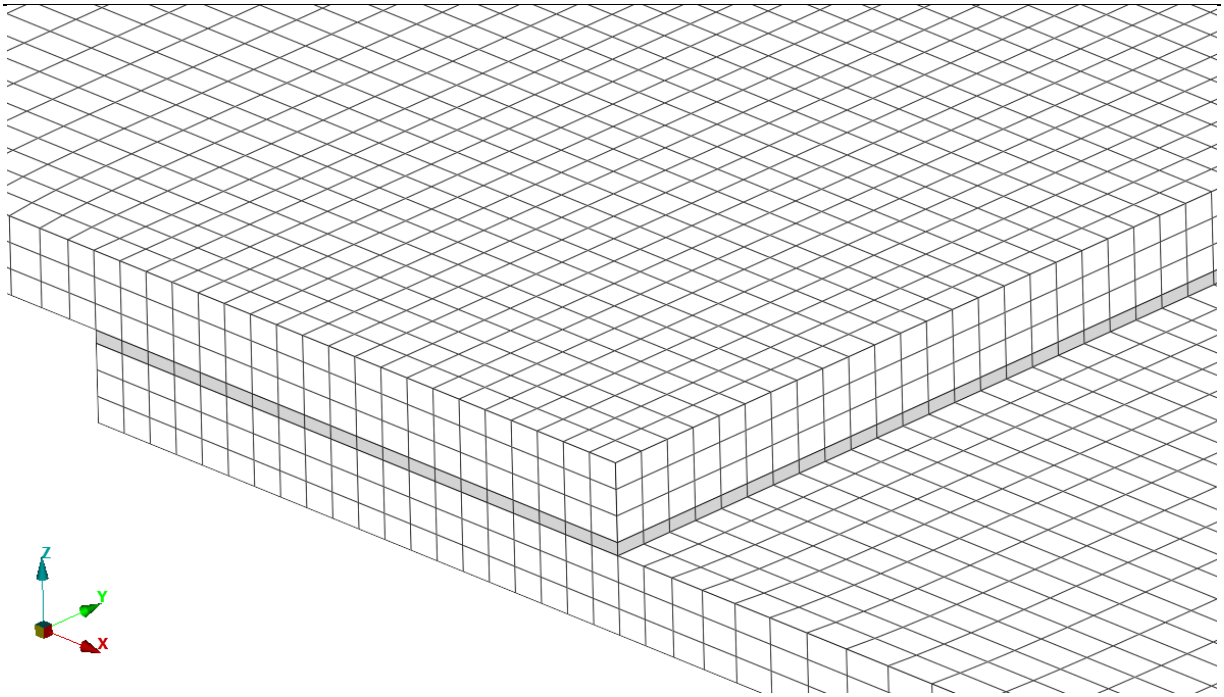

Figure 24. Mesh of the bond area in continuum solid model (substrates are white and adhesive is grey)

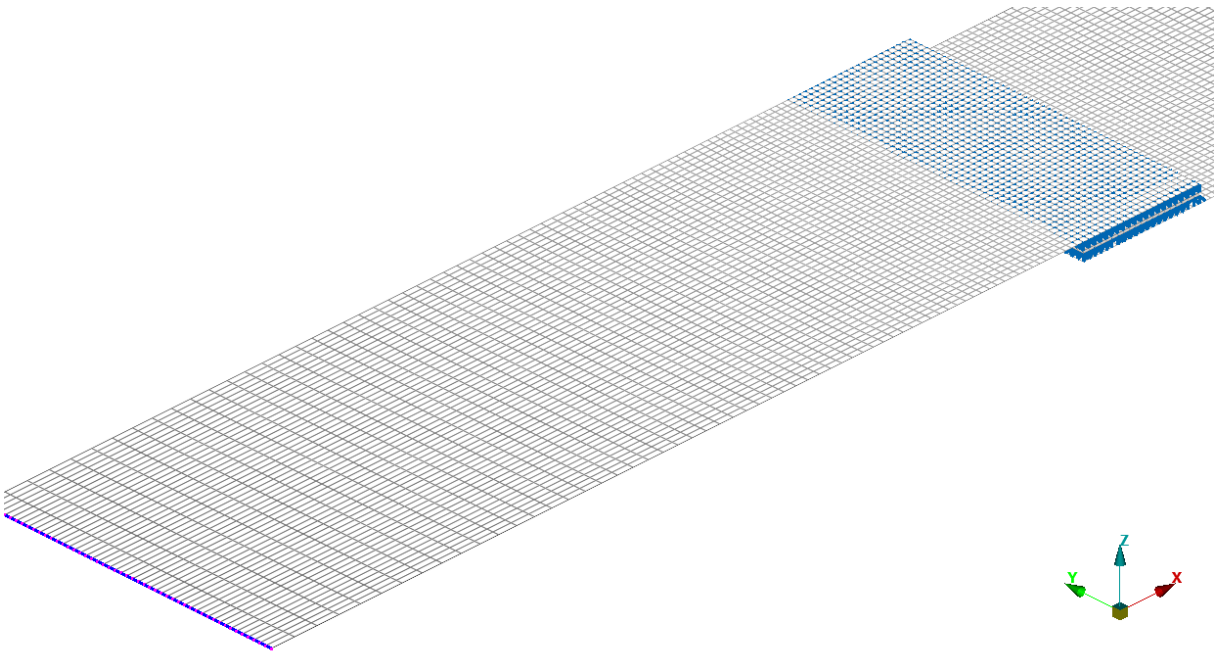

Figure 25. Mesh of continuum shell model

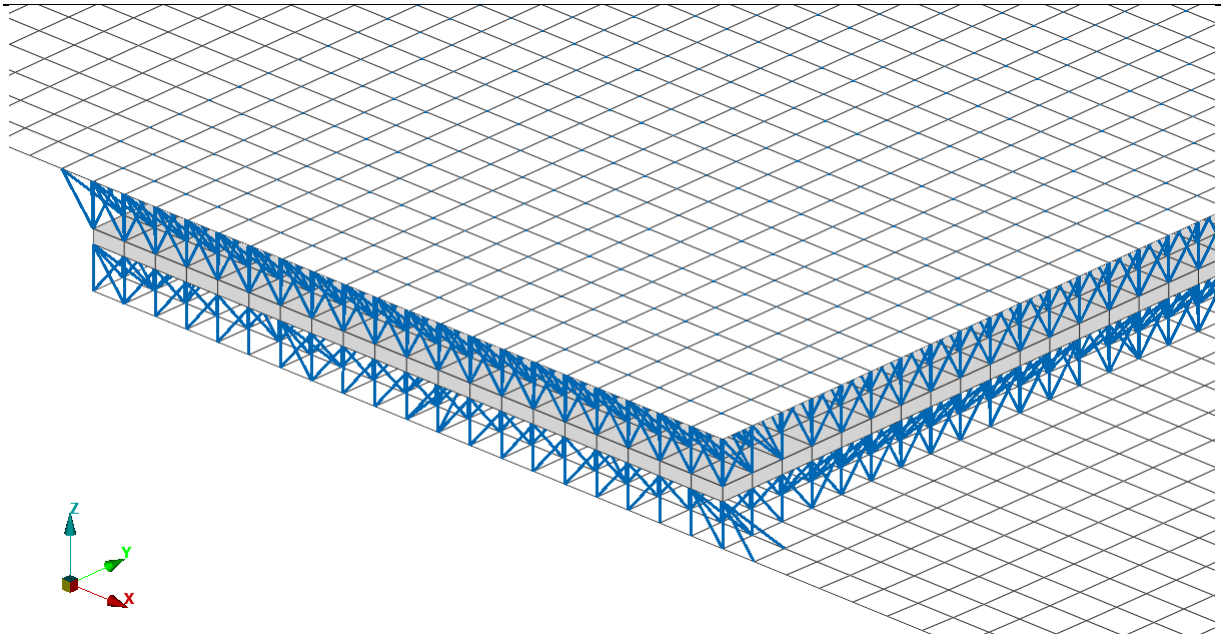

Figure 26. Mesh in the bond area of continuum solid model (substrates are white, adhesive is grey and RBE3 elements are blue lines)

3.1.2. Cohesive zone model

Modelling of the cohesive zone model was done in *ANSA* software package. Boundary conditions, material model and elements used for the substrates are the same as in the continuum model, described in the chapter 3.1.1.

The adhesive is modelled with first order cohesive elements CIFHEX, with four nodes and twelve degrees of freedom (see Figure 17). Parameters needed to define the CZM model are shown in Table 4. The mesh is the same as the one described in the previous chapter. Like in the continuum model, the adhesive elements are connected to the substrates with a node-to-node connection.

For damage evolution type *COHDISP*, where the damage is defined by the displacement, is chosen. It requires one parameter – *W1* – which represents the separation evaluated from the damage initiation to failure.

Table 4. BM 4600F and A2015 parameters used for CZM modelling

	BM 4600F	A2015
Tensile modulus [MPa]	2500	1850
Shear modulus [MPa]	893	560
Tensile strength [MPa]	51	21,63

Shear strength [MPa]	26	17,9
Damage initiation criterion	QUADS	QUADS
Damage evolution type	COHDISP	COHDISP
Damage evolution curve type	linear	linear
W1 [mm]	0,6	0,37

3.2. Analysis

Using the models described in the previous chapter simulations are done for a SLJ. Firstly, simulations are done using the CZM and continuum solid model to have as similar models as possible. The only difference between those two models is the element type used for the adhesive. Furthermore, a simulation is done using the continuum shell model.

3.2.1. Connection type

Different connection types between adhesive and substrates were used and analysed including RBE3-HEXA-RBE3, node-to-node and tie connections. As explained in chapter 2.6.2.2., N2N and tie connections are recommended to use with CZM depending on the discretization of the parts. The discretization of the parts in the CZM model is the same therefore N2N connection was used. In the continuum solid model N2N and RBE3-HEXA-RBE3 connections were used while in the continuum shell model RBE3 and tie connection were used since N2N connection is not possible to realize due to the gap between the substrates and adhesive.

3.2.2. Sensitivity study

The goal of a sensitivity study is to determine how certain parameters affect the results and then compare the results for the CZM and continuum models. Parameters chosen for the sensitivity study are:

- element size
- adherend thickness
- bondline thickness
- bondline length.

3.2.2.1. Element size

When analysing large-scale models, it is not desirable to use overly fine mesh because that generates many elements and results in long computational time and costs. Yet, using coarser mesh usually results in lowering the accuracy of the results. Therefore, a compromise between mesh refinement and computational time is needed. Five different mesh refinements of the adhesive were made. In following chapters values of 0,5, 2,5 and 5 mm were used to display the behaviour. Results with all values of element size are available in Appendix B.

Table 5. Values of element sizes used in sensitivity study

Element size [mm]
0,2
0,5
1
2,5
5

3.2.2.2. Adherend thickness

Seven different adherend thicknesses were used, see Table 6. In following chapters values of 1,2, 3 and 6 mm were used to display the behaviour. Results with all values of adherend thicknesses are available in Appendix C.

Table 6. Values of adherend thicknesses used in sensitivity study

Adherend thickness [mm]
1,2
1,5
2
3
5
6
8

3.2.2.3. Bondline thickness

Five different bondline thicknesses were used, see Table 7. In following chapters values of 0,2, 0,5 and 1,5 mm are used to display the behaviour. Results with all values of bondline thicknesses are available in Appendix D.

Table 7. Values of bondline thicknesses used in sensitivity study

Bondline thickness [mm]
0,2
0,5
1
1,5
5

3.2.2.4. Bondline length

Four different bondline lengths were used, see Table 8. In following chapters all values were used to display the behaviour.

Table 8. Values of bondline lengths used in sensitivity study

Bondline length [mm]
10
15
25
50

4. RESULTS

Results of analyses described in the previous chapter are presented and discussed in this chapter. Firstly, results of the standardized test with A2015 and BM 4600F adhesives are presented. Next, results of different connection types are presented, followed by chapters presenting the results of the sensitivity study for BM 4600F adhesive.

4.1. Standardized test

4.1.1. Stiffness analysis

Results of the simulations in terms of force vs. displacement are shown in Figure 27. Both the force and displacement are measured at the load application point B.

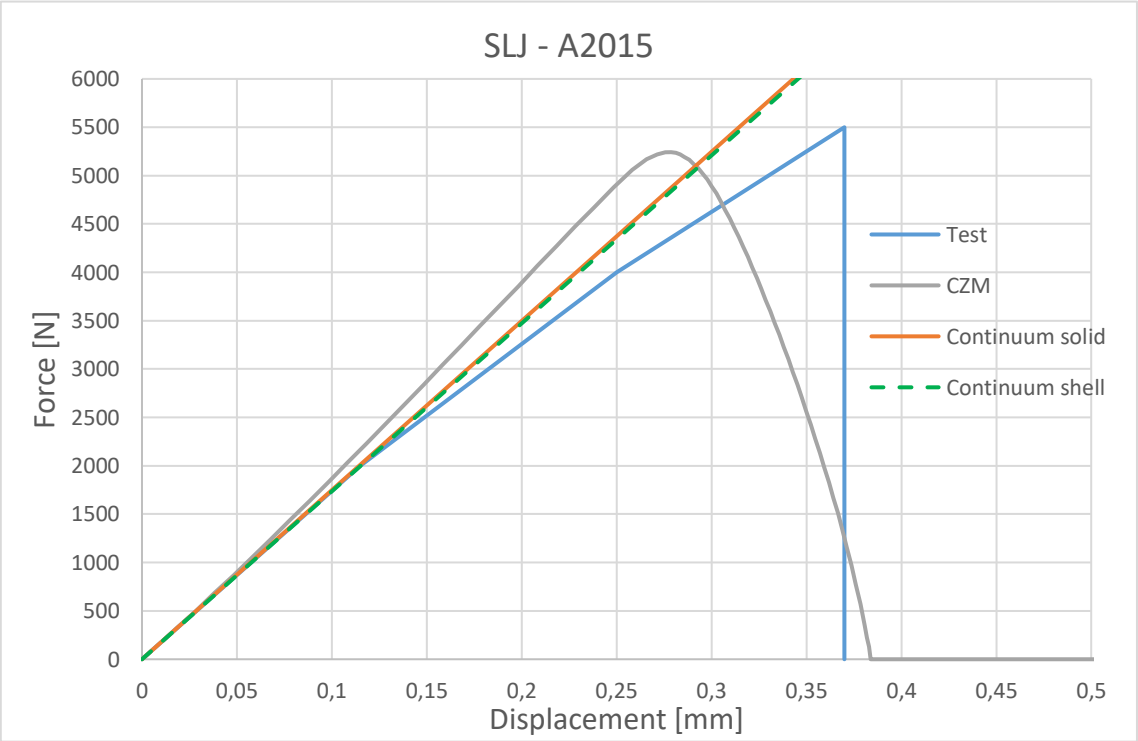

Figure 27. Force-displacement curves for A2015 adhesive

The curve from the test initially exhibits a linear behaviour but then it drops in stiffness at 0,14 mm. Due to slip of the test specimen at the clamp area the stiffness is reduced [15]. The continuum solid and shell models both exhibit the same behaviour and consequently the same stiffness. They approximate the test data sufficiently. The CZM has acceptable approximation of the test data in the beginning but then slope of the curve starts to deviate at 0,05 mm due to bending effects which are captured due to non-linearity. All models approximate the test data

with acceptable accuracy and the continuum models approximate the joint stiffness better compared to the CZM model, see Figure 27.

Next, the process was repeated for the BM 4600F adhesive. Figure 28 shows simulation results for the BM 4600F adhesive in terms of force – displacement curve.

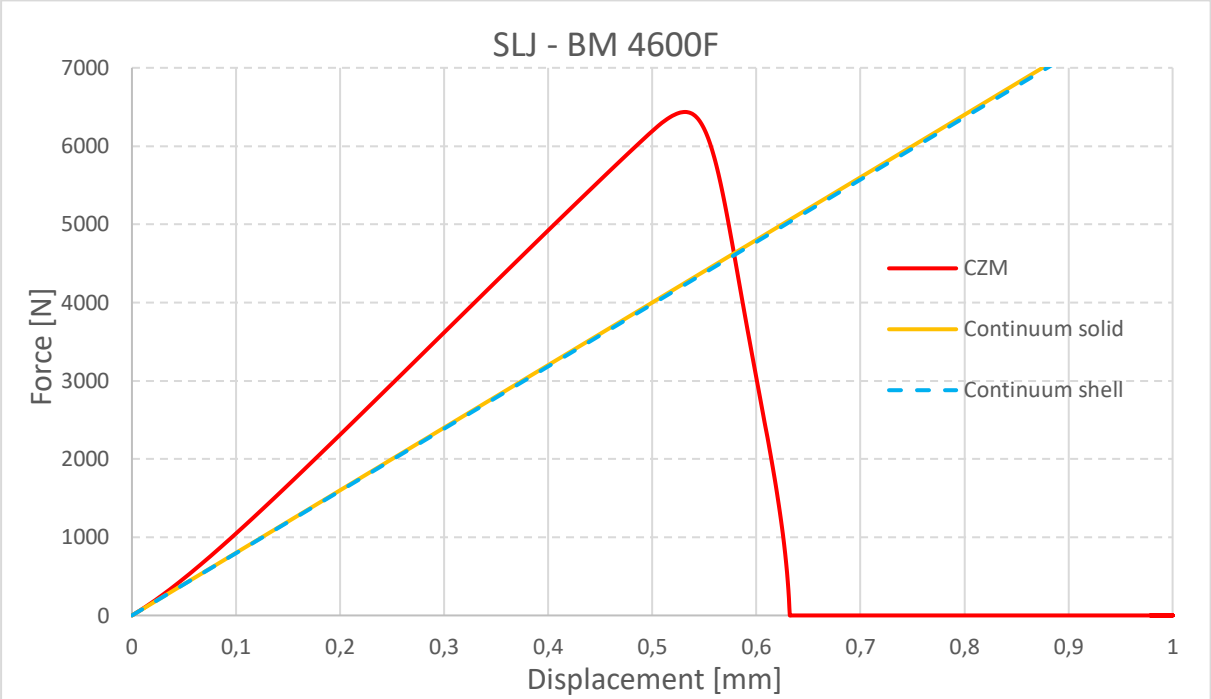

Figure 28. Force-displacement curves with continuum linear model for BM 4600F adhesive

The CZM model was anticipated to be stiffer compared to the continuum models, like shown for the A2015 adhesive in Figure 27. However, the difference in calculated stiffness for BM 4600F was approximately 50%, as seen in Figure 28. To investigate the difference in stiffness the continuum model was simulated with geometrical non-linear effects. By including non-linear geometry, large deformations are accounted for by iterative recalculation of the stiffness matrix. Continuum models with non-linear geometry match the CZM model, see Figure 29. With A2015 adhesive, continuum models were run linearly therefore the output curve is linear. However, if run with non-linear geometry, it is assumed to exhibit the same behaviour as the CZM model. Also, the reason why the BM 4600F adhesive exhibited an increased deviation in stiffness between the CZM and continuum models was because of the reduced inertia of the joint. The A2015 adhesive uses nearly three times thicker substrates making them stiffer compared to the substrates used with the BM 4600F adhesive. Since substrates have increased stiffness, they deform less, and using linear model that assumes small deformations resulted in sufficient approximation of the joint behaviour. When running a

simulation with reduced substrate thickness, by including non-linear geometry, due to large deformation, bending effect is decreased making the joint stiffer.

Effects of the non-linear geometry can be seen by comparing Figures 30 and 31. The deformation of the continuum linear model can be seen in Figure 30 while the deformation of the continuum non-linear model can be seen in Figure 31. The substrates in the linear model exhibit a bending pattern where the maximum displacement occurred near the centre of the substrates. On the other hand, with the non-linear model, the substrates exhibit significant deformation close to the bondline while the rest of the substrates remained virtually straight. Furthermore, when bending occurred in close proximity to the bondline, it resulted in a localized increase in stiffness, comparable to the behaviour observed in sheet metals.

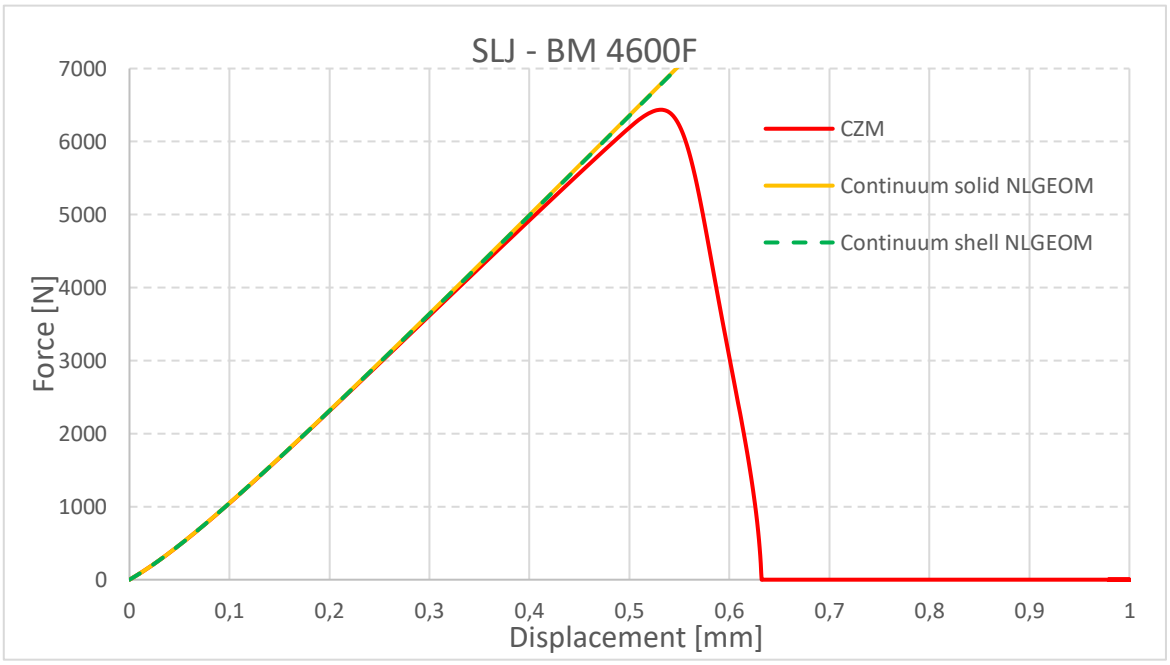

Figure 29. Force-displacement curve with continuum non-linear models for BM 4600F adhesive

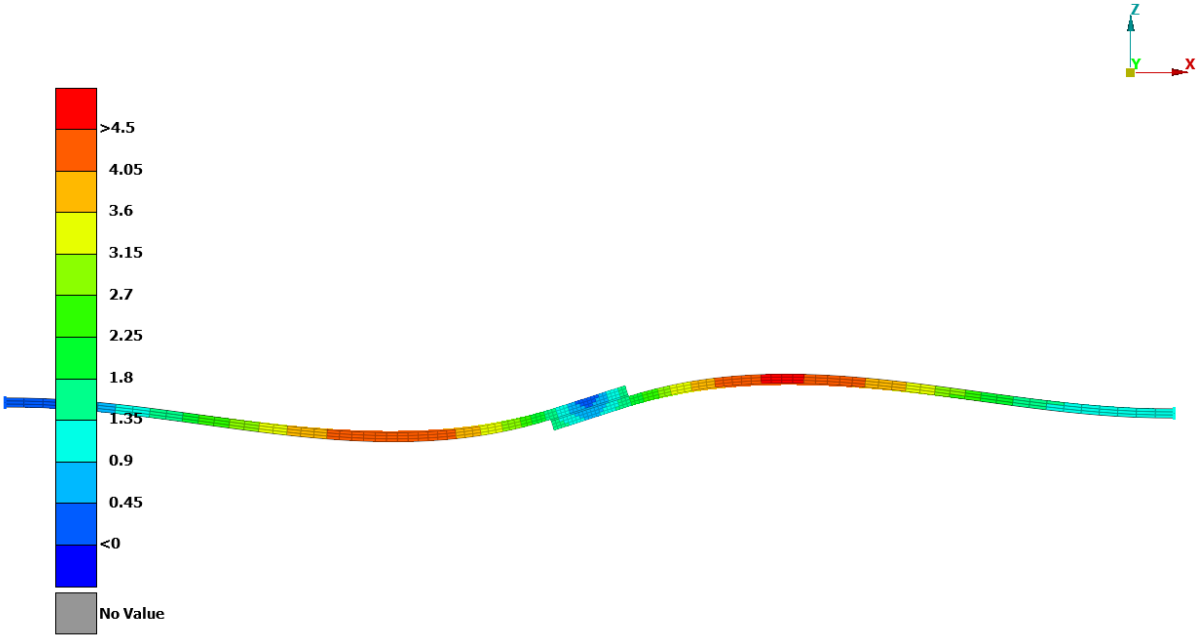

Figure 30. Displacement distribution in mm for continuum linear model for BM 4600F adhesive

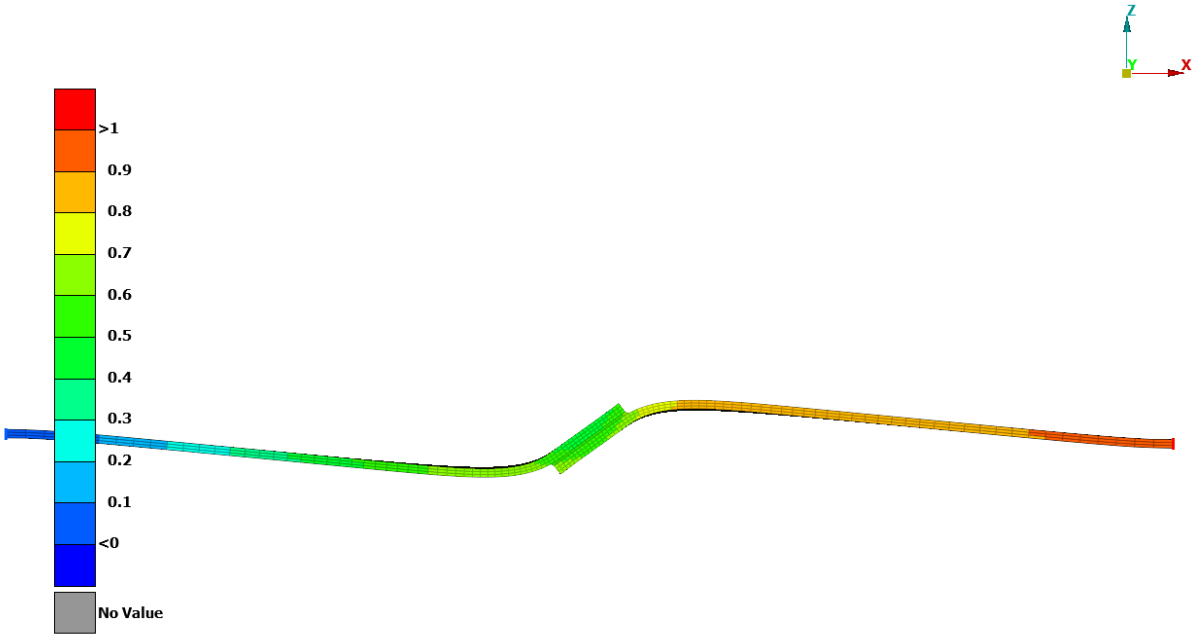

Figure 31. Displacement distribution in mm for continuum non-linear model for BM 4600F adhesive

To achieve the most objective comparison, it is preferable to have models that are as similar as possible. Therefore, in further analyses only the non-linear continuum solid model was compared to the CZM model.

4.1.2. Strength analysis

Before comparing the CZM and continuum method, the CZM behaviour is explained using Figure 32 and 33. In Figure 32, a traction vs. displacement of boundary condition, i.e., point B, is displayed for an edge and middle element of the adhesive. The element on the edge of adhesive displays linear behaviour below the yield stress, i.e., until it reached damage initiation point defined by QUADS criterion - (13). The middle element displays a non-linear behaviour. After reaching the damage initiation point the edge elements cannot take more load and the load is being redistributed. When the middle elements have reached the maximal value of stress, i.e., stress at which damage initiates, there is no more elements that can bear more load, hence a rapid degradation occurred followed by a sharp decrease in stress until complete failure.

The edge element exhibits an increase in value of stress after reaching the damage initiation point. Since maximal shear strength is reached, the element´s shear stiffness starts to slowly degrade until a certain point, resulting in decreased shear stress, as can be seen in Figure 35. On the other hand, maximal tensile strength is still not reached and peel stress continues to rise resulting in increase of combined stress.

The reason behind lower maximal combined stress values of the middle element compared the edge element can be seen in Figure 33. Unlike the adhesive edge where peel and shear stresses are high, the middle of the adhesive has low peel stress and high shear stress, leading to a lower combined stress.

In Figure 33 combined stress is displayed along the adhesive at the damage initiation point and at the moment when maximal force of the joint is reached. At the max force point the middle elements reached fully loaded state, i.e., max value of stress, due to predominant presence of shear stress, see Figure 35.

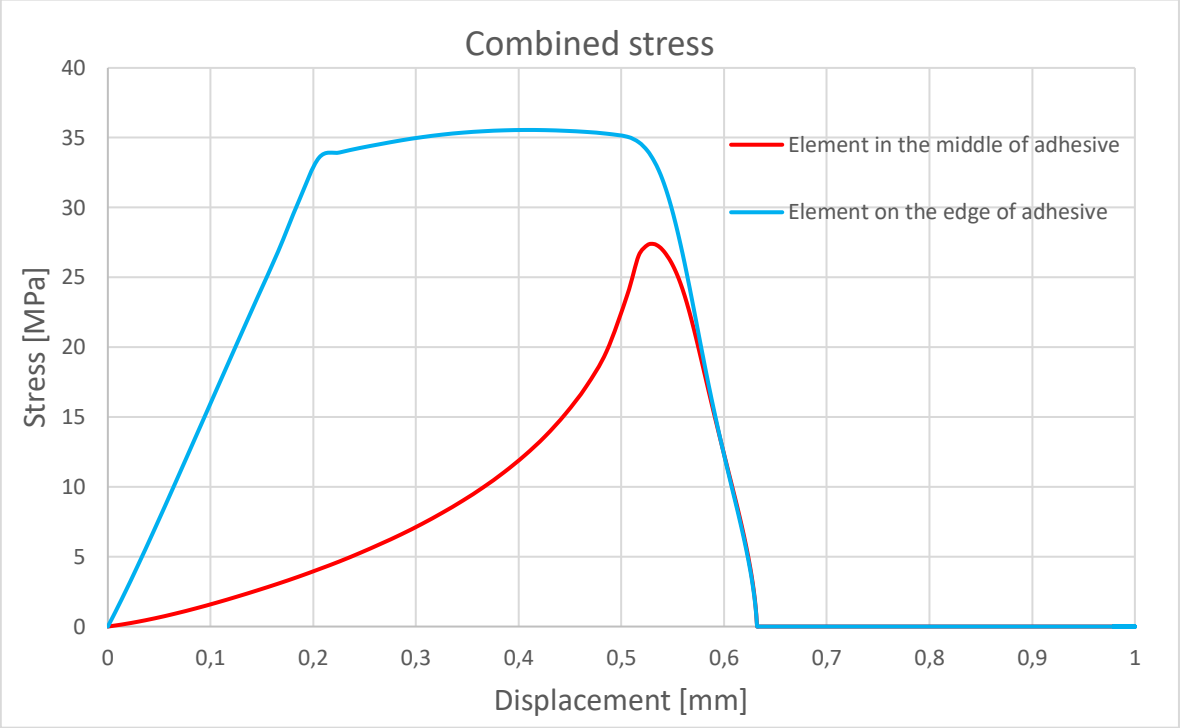

Figure 32. Stress-displacement curves for elements for BM 4600F adhesive

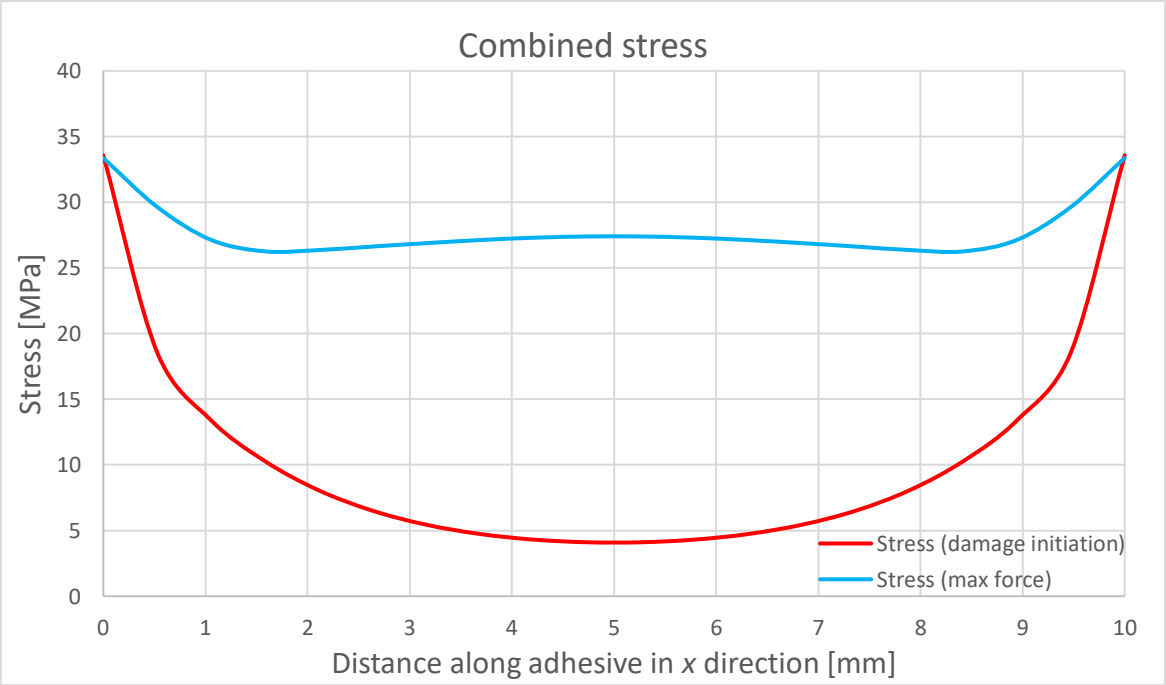

Figure 33. Stress-displacement curves along adhesive for BM 4600F adhesive

A comparison between the CZM and continuum method was performed. Figures 34 and 35 show a comparison of stress distribution within the adhesive at the damage initiation point and maximal force. The general behaviour and values are similar at the damage initiation point

with some peaks in the continuum model. At maximal force, an increased deviation between stress distributions for various models can be seen This deviation is lower prior to the damage initiation point since the material behaviour is linear.

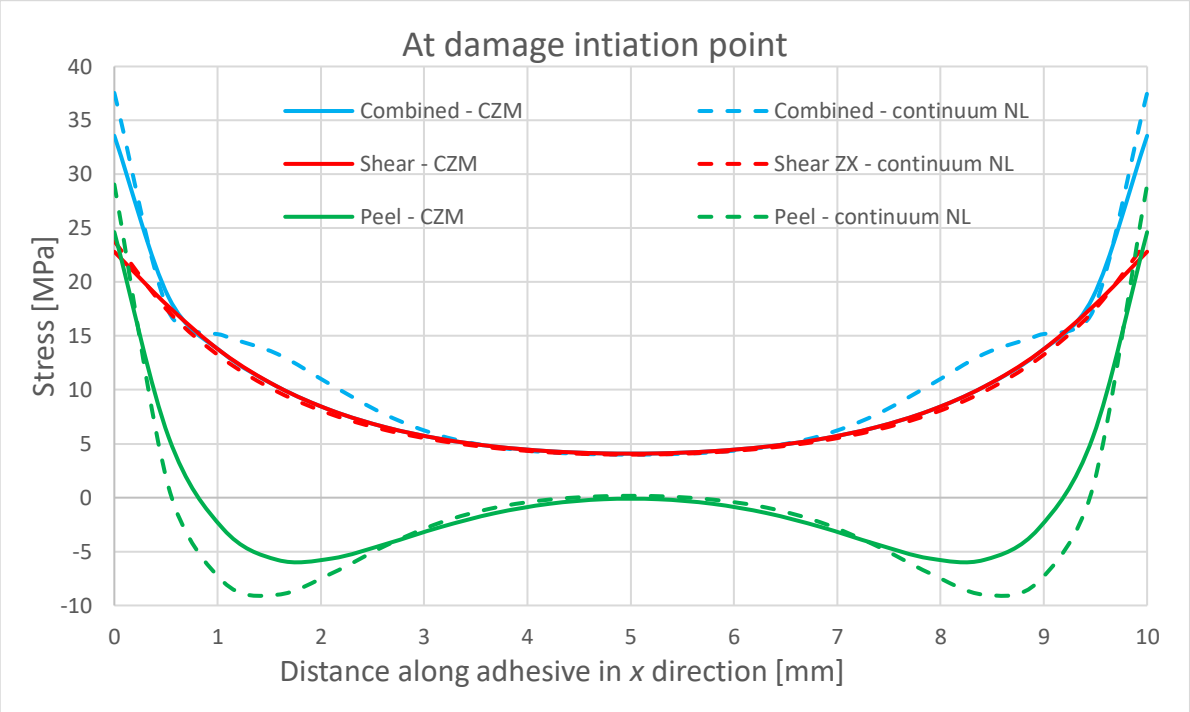

Figure 34. Comparison of stress distribution within adhesive at damage initiation point between CZM and continuum models

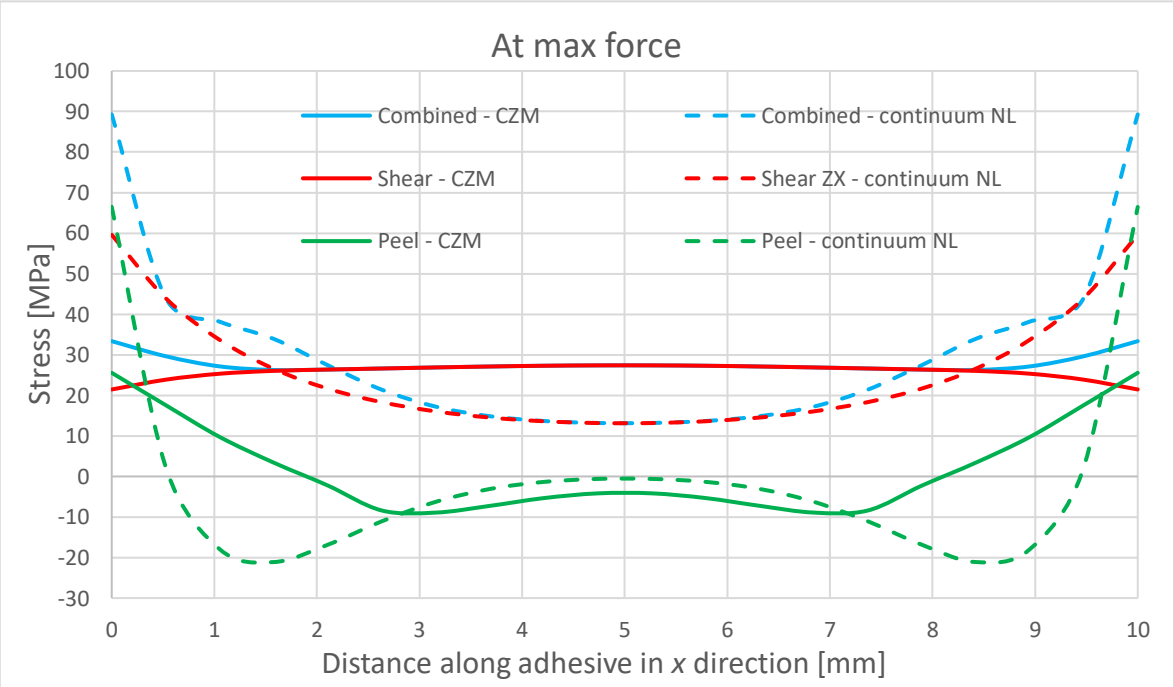

Figure 35. Comparison of stress distribution within adhesive at max force point between CZM and continuum models

Looking from the perspective of a full vehicle simulation, where a complex stress state occurs, it makes more sense, and it is also easier, to extract von Mises stress, σ_{vm}, and max shear stress, τ_{max}.

A comparison of combined, shear, peel and averaged stresses, for the CZM and continuum models was done, see Figures 36 – 38. The stress values are extracted at the damage initiation point. The point of interest lies in the adhesive behaviour prior to damage, making the state of damage initiation the maximum allowable load condition for the joint. Comparing the combined stress in continuum model, $\sigma_{C,C}$, with von Mises stress, σ_{vm}, combined stress shows lower deviation from the combined stress in CZM, $\sigma_{C,CZM}$, see Figure 36. This is due to the difference in expression used. Similarly, max shear stress τ_{max} deviates more than shear stress component τ_{zx}, when comparing to shear stress σ_{II} in CZM. Again, the reason is the different expression. Lastly, peel stress exhibit highest mismatch, see Figure 38, particularly on the adhesive edge and in compression (negative value of the peel stress). This is the main reason for the mismatch of combined stress shown in Figure 36.

Figure 39 shows deviation of the continuum model compared to the CZM. Von Mises stress deviates more compared to combined stress, but it exhibits a constant deviation except on the adhesive edges where the stress singularity is present. Additionally, shear stress τ_{zx} also exhibits a constant deviation. The deviation is calculated as:

$$deviation = \frac{\sigma_{CZM} - \sigma_{continuum}}{\sigma_{CZM}} \cdot 100. \quad \textbf{(19)}$$

In further text, a comparison is made between the combined stress, as well as the shear τ_{zx} stress, for the CZM and continuum model.

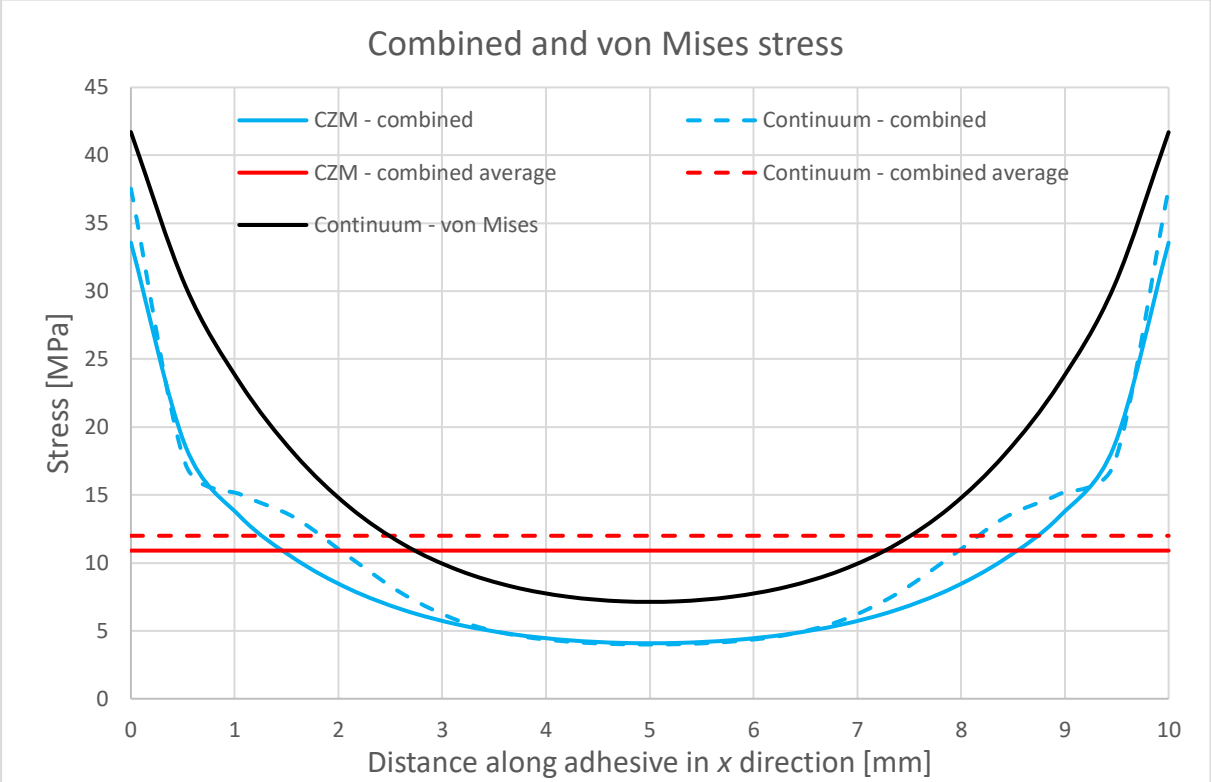

Figure 36. Distribution of combined and von Mises within adhesive at damage initiation point for CZM and continuum model

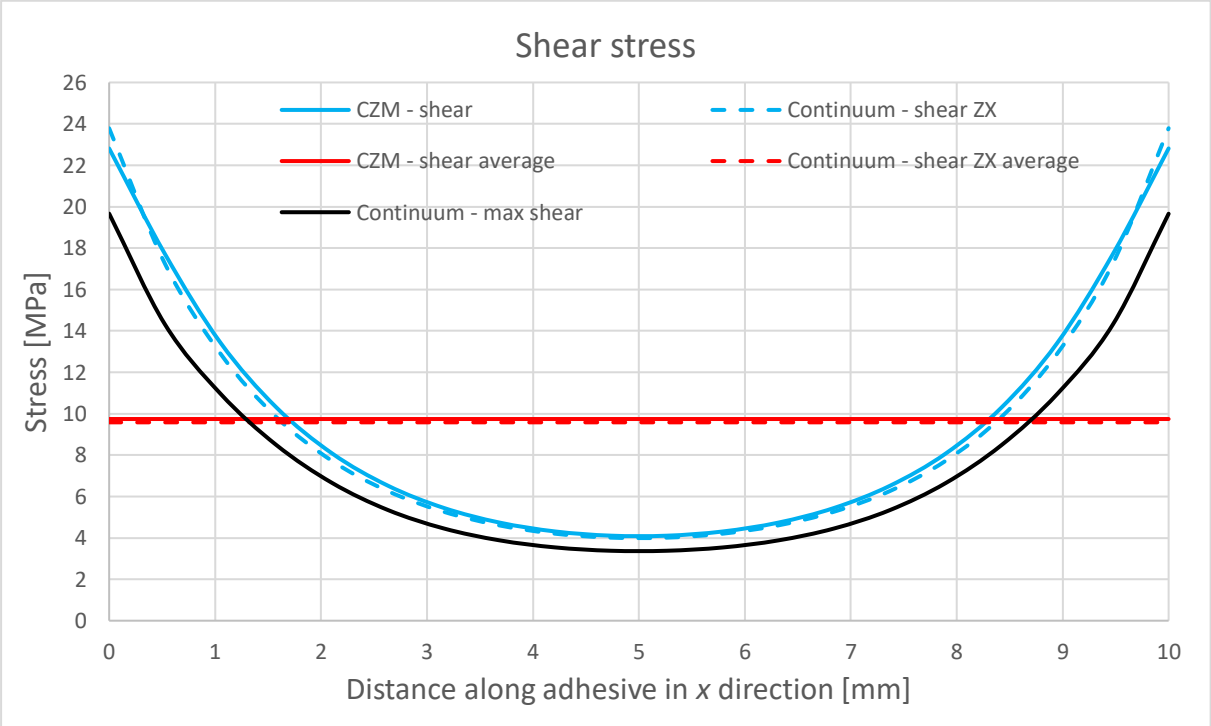

Figure 37. Distribution of shear stress within adhesive at damage initiation point for CZM and continuum model

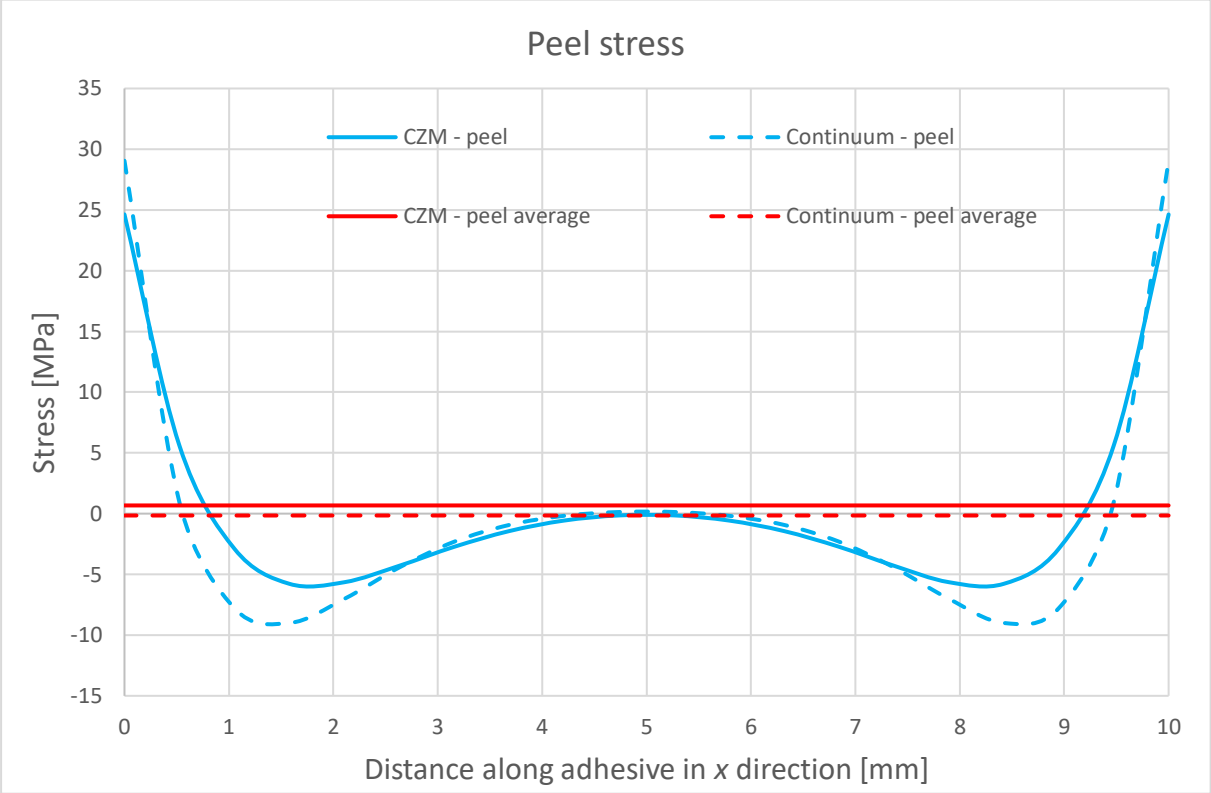

Figure 38. Distribution of peel stress within adhesive at damage initiation point for CZM and continuum model

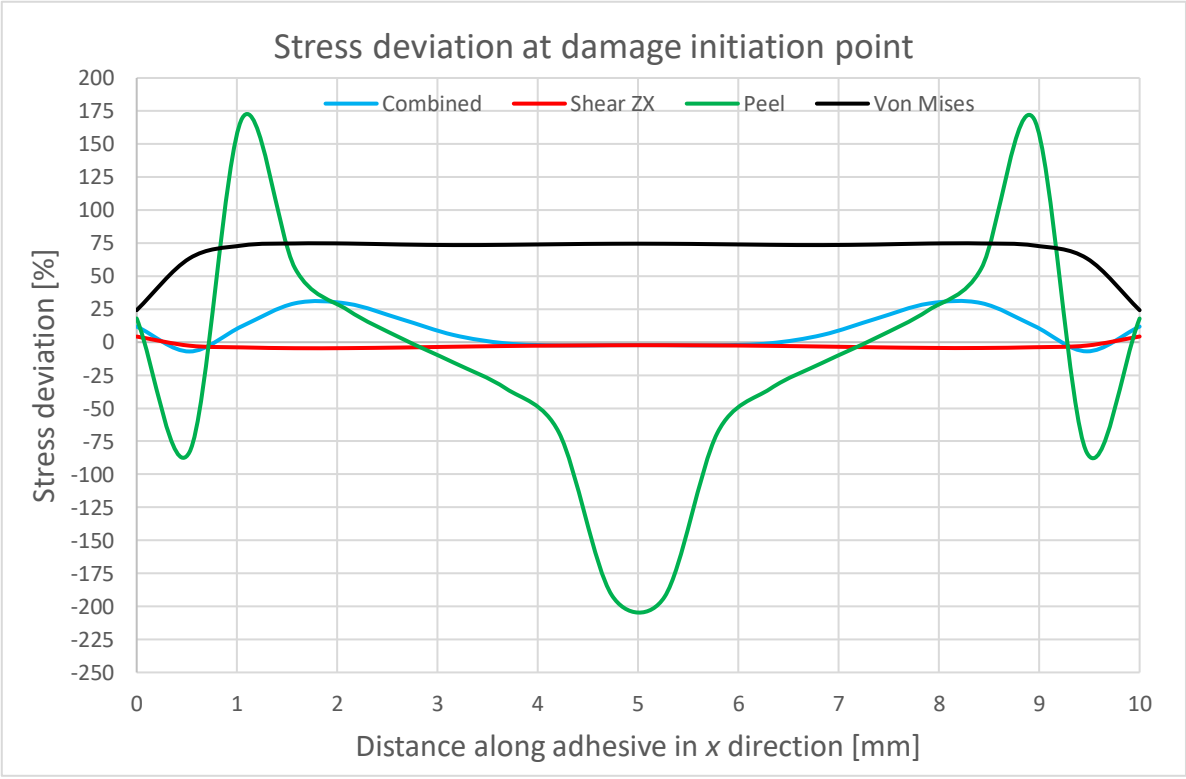

Figure 39. Stress deviation within adhesive at damage initiation point between CZM and continuum models

4.1.3. Connection type

Results presented in Figure 40 show no non-acceptable difference in stiffness regardless of connection type used. The continuum non-linear shell model with tie connection exhibits a lower stiffness compared to the rest of the continuum models. This is due to the gap between the substrates and adhesive since the adhesives were modelled with shell elements. When using tie connection with gap, error in results can occur [17]. Since in this case the substrate thickness is relatively small – 1,2 mm, the error is not significant but with increasing substrate thickness, as well as the gap, the error increases.

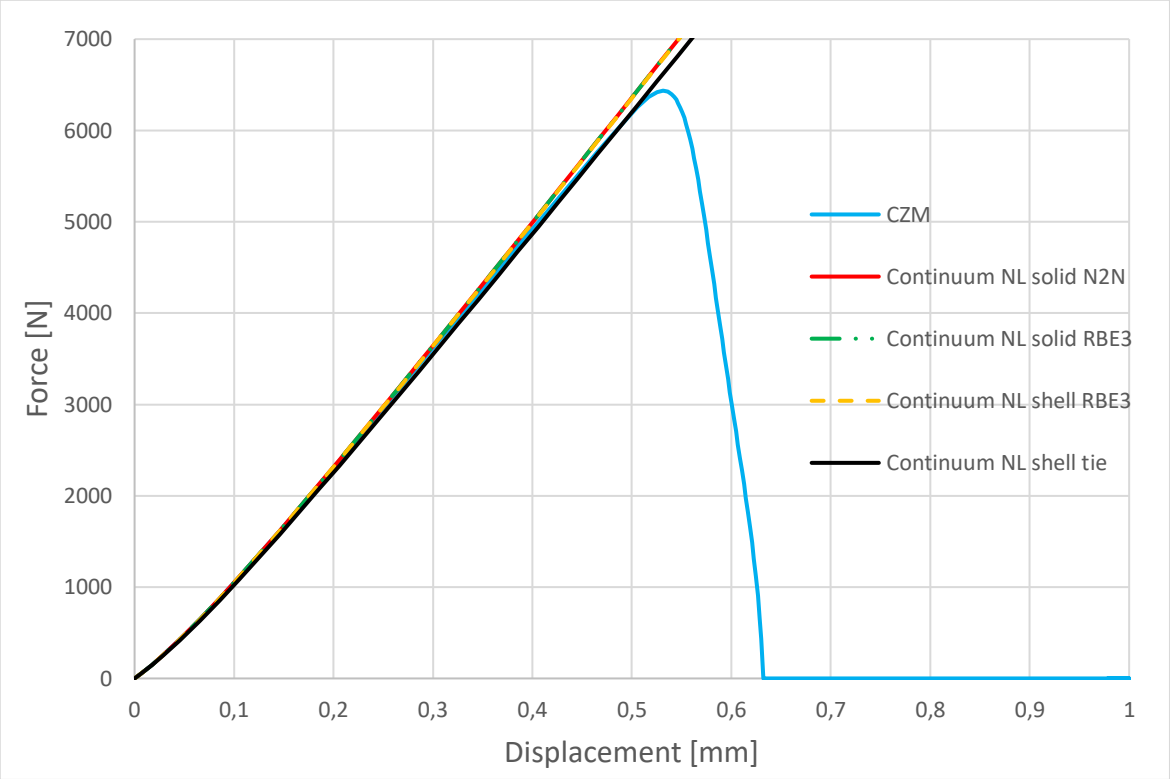

Figure 40. Different connection types for BM 4600F adhesive

4.2. Sensitivity study

4.2.1. Element size sensitivity

4.2.1.1. Stiffness analysis

A force – displacement curve comparison between CZM and continuum models for different element size was done, see Figure 41. The results show no significant change in the joint stiffness regardless of the element size.

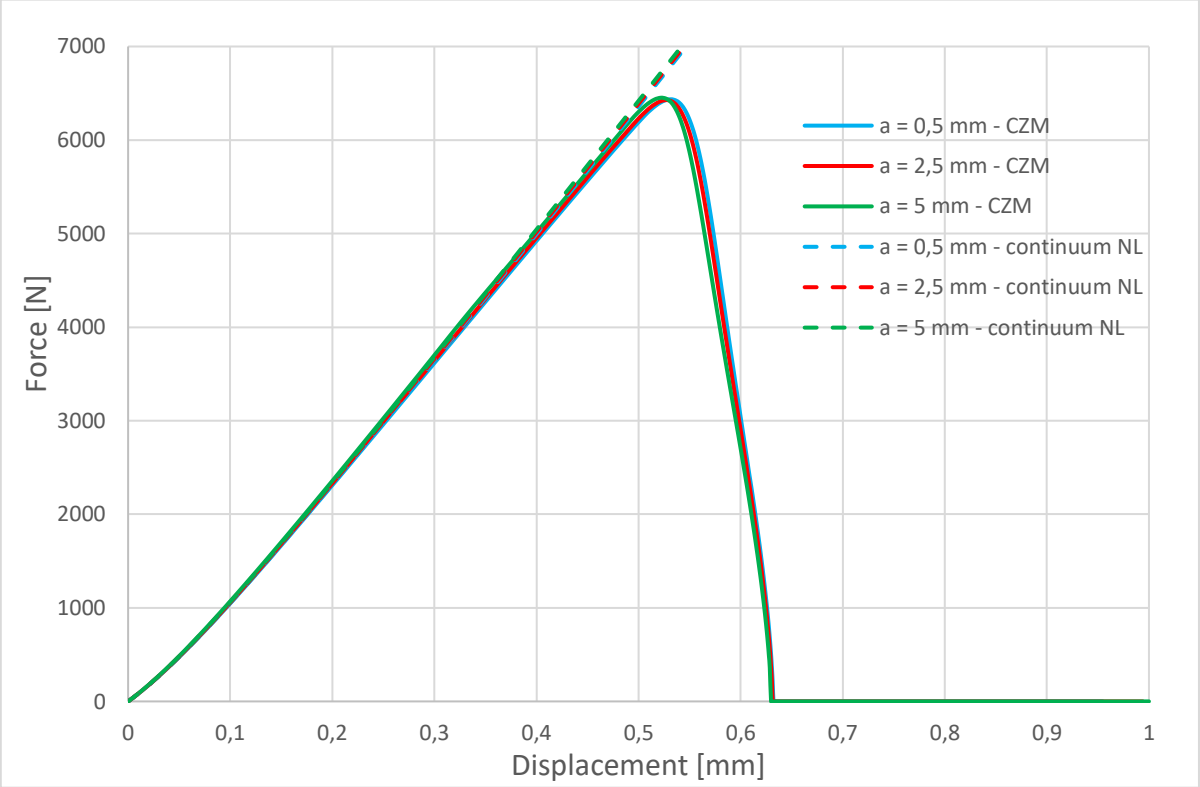

Figure 41. Force-displacement curve comparison between CZM and continuum models for different element sizes

4.2.1.2. Strength analysis

Figure 42 displays the maximum force of the joint, achieved with the CZM model, with respect to the element size used to discretize the adhesive. Maximum force is essentially constant regardless of the element size which indicates mesh independence of the CZM model as mentioned in chapter 2.6.2.

Figures 43 – 46 show discretization of the joint for different element sizes with a stress distribution of combined stress in CZM. As element size increases there is less elements across the adhesive resulting in a more uniform stress distribution. The deviation between the methods was increased with an increased element size, see Figure 46.

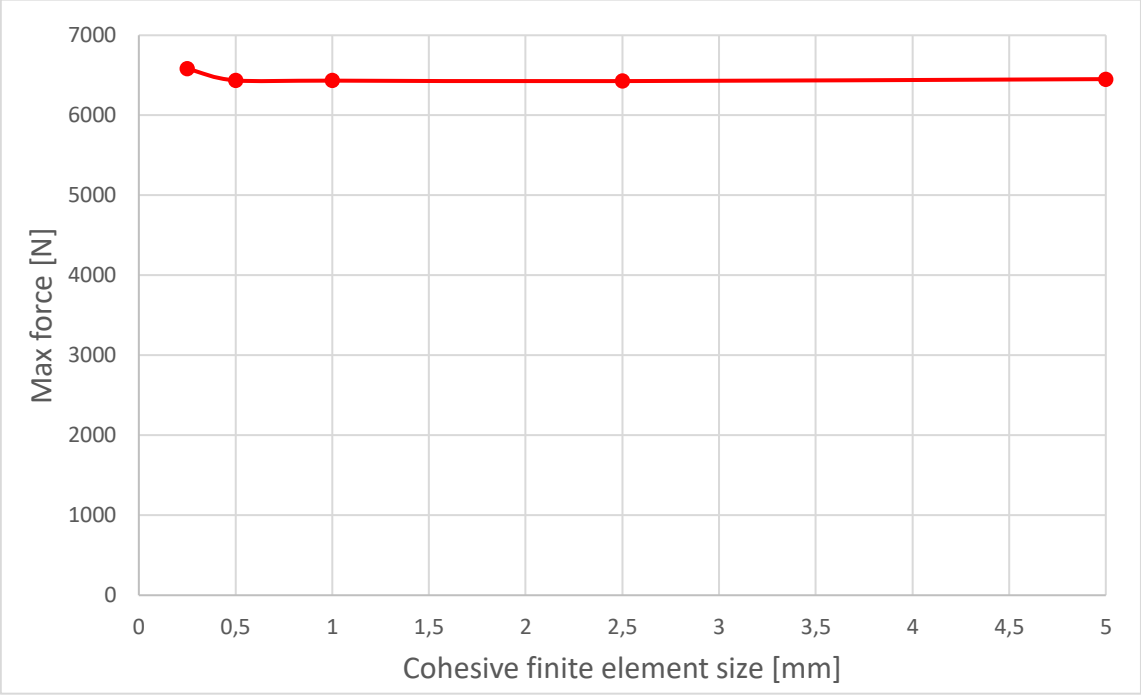

Figure 42. Maximal force of the joint with respect to cohesive element size for CZM model

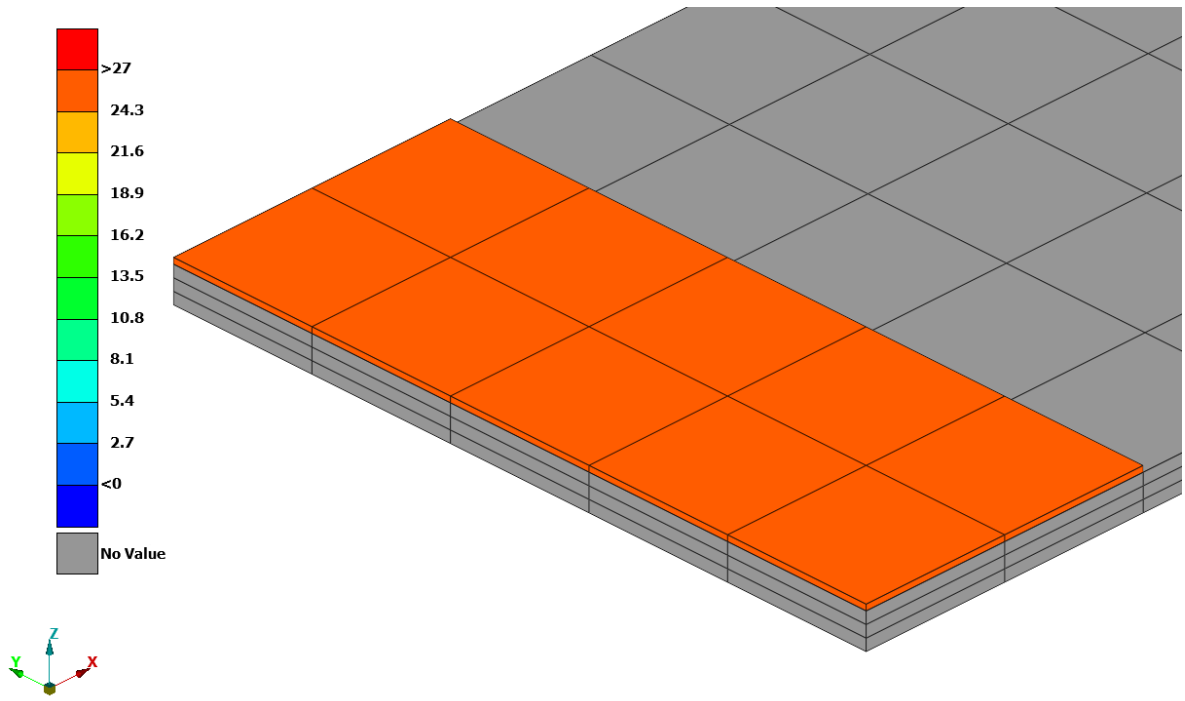

Figure 43. Distribution of combined stress at damage initiation point with element size of 5 mm

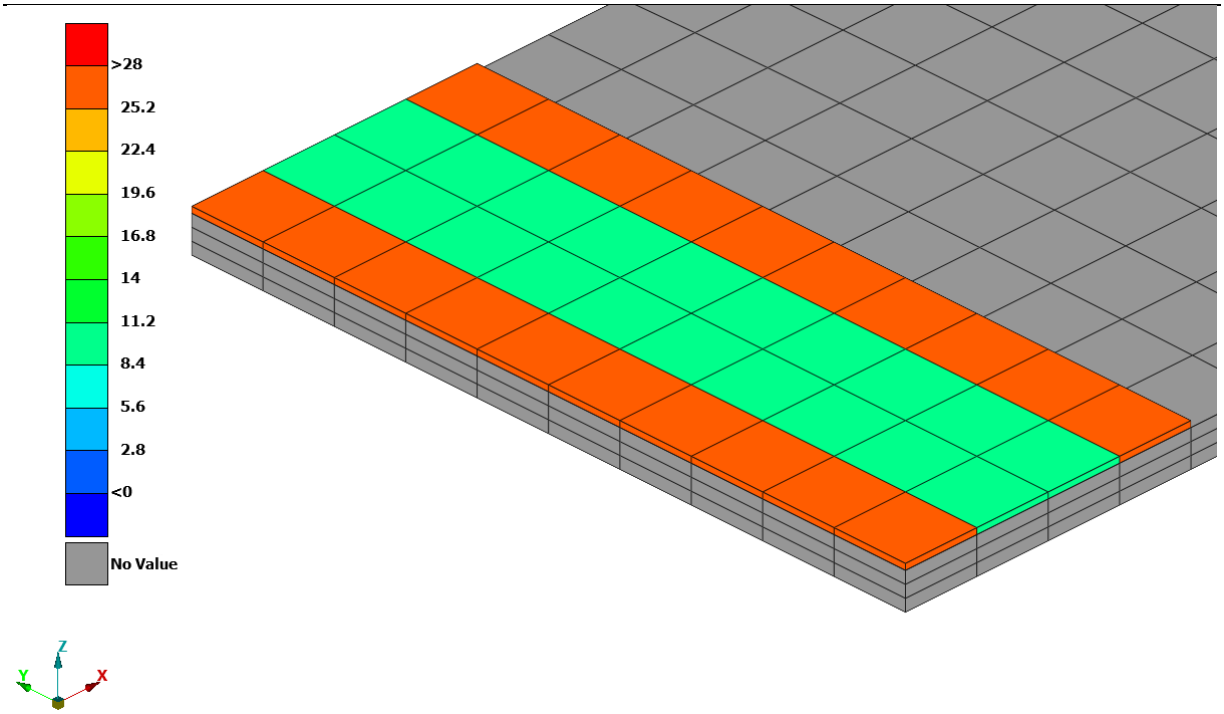

Figure 44. Distribution of combined stress at damage initiation point with element size of 2,5 m

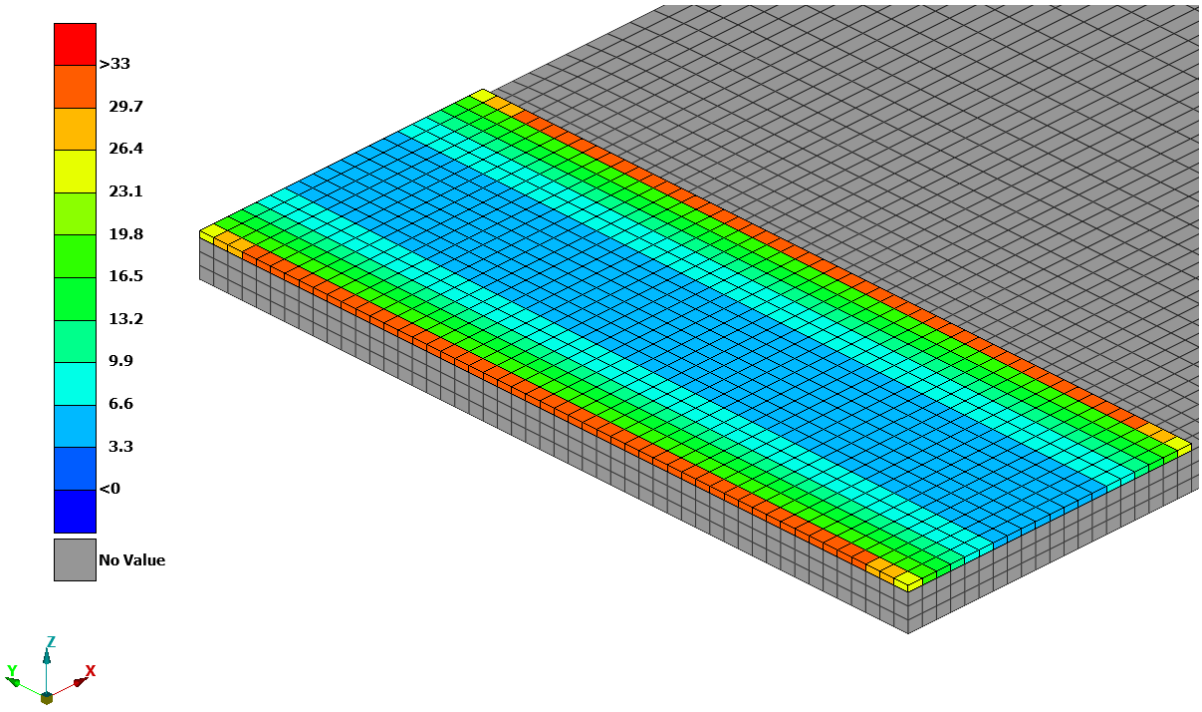

Figure 45. Distribution of combined stress at damage initiation point with element size of 0,5 mm

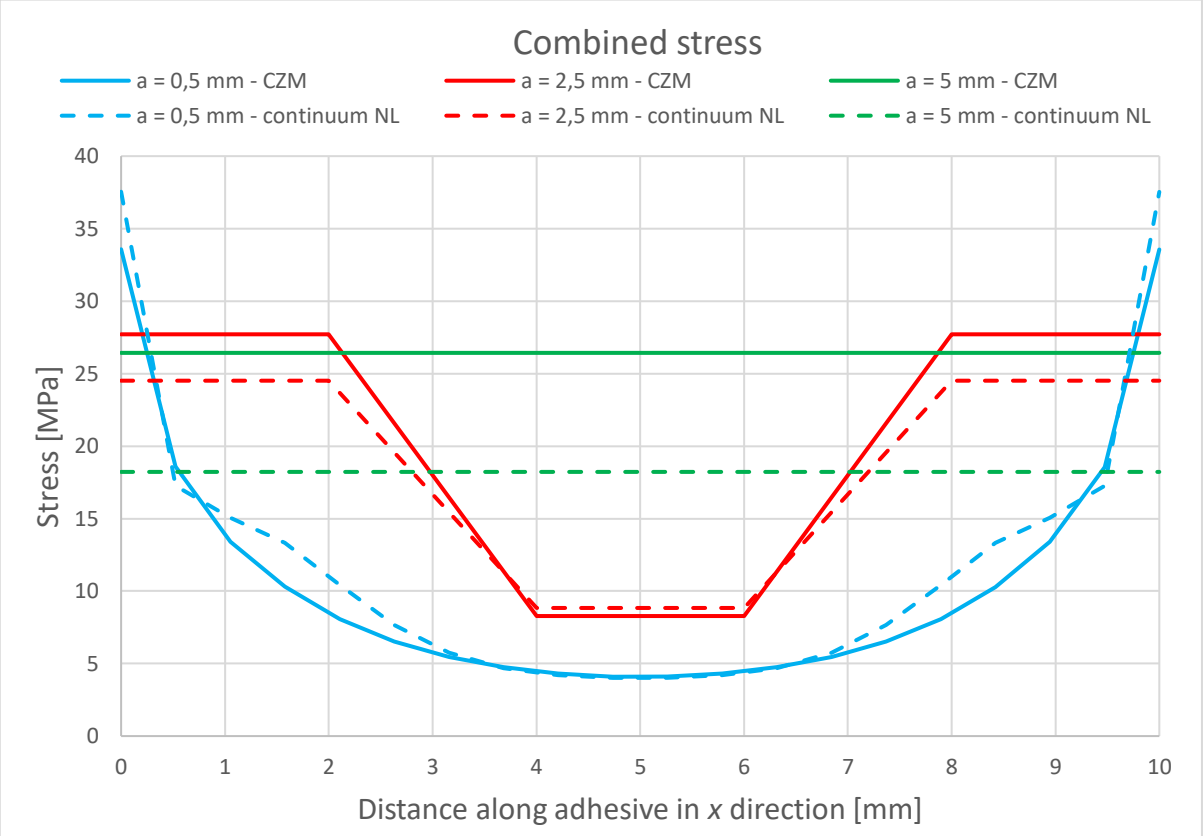

Figure 46. Comparison of combined stress distribution between CZM and continuum models for different element sizes

4.2.2. Adherend thickness

4.2.2.1. Stiffness analysis

A force – displacement curve comparison between CZM and continuum models for different adherend thicknesses was done, see Figure 47. Increased adherend thickness resulted in an increased joint stiffness. Both methods exhibit similar behaviour in terms of joint stiffness.

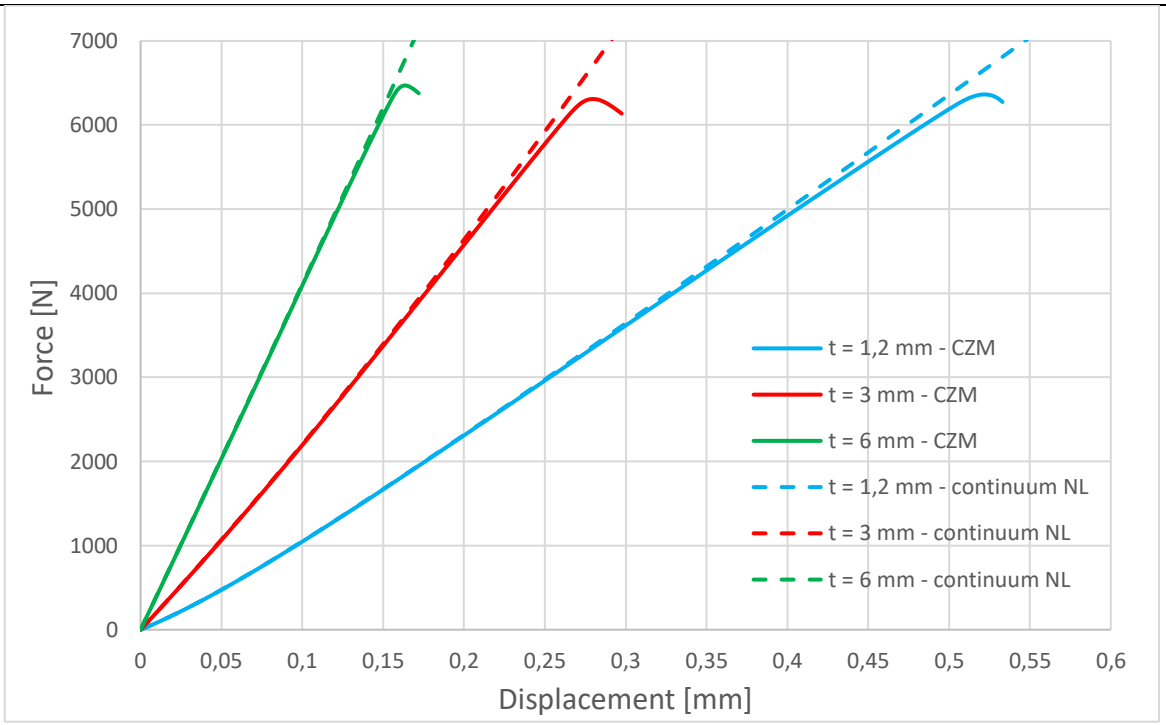

Figure 47. Force-displacement curve comparison between CZM and continuum models for different adherend thicknesses

4.2.2.2. Strength analysis

For the CZM model, maximum force and the force magnitude at the damage initiation point was extracted for different adherent thicknesses, see Figure 48. Max force is relatively constant which can be explained with the adhesive being the first component to fail meaning that the maximum strength of the joint is defined by the adhesive. Regardless of the change in substrate thickness, the adhesive is unchanged and therefore maximal force of the joint remains nearly constant.

The force at the damage initiation curve displays another phenomenon. With increased substrate thickness the force at which damage initiation occurs is increased. This suggests that the stress state is changed towards a more uniform stress distribution. With increased substrate thickness, the distance between forces acting on the joint is increased resulting in increased secondary bending. Moreover, bending moment is increased linearly while the substrate`s bending stiffness is increased to the power of three resulting in higher shear stress and a more uniform stress distribution.

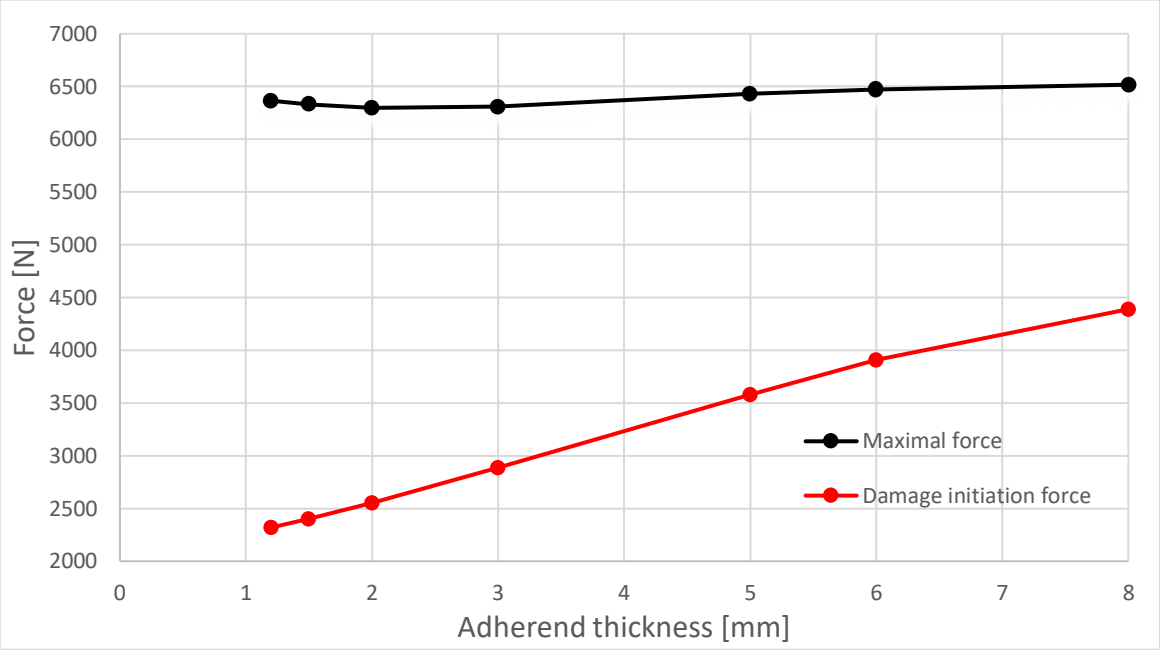

Figure 48. Max force and force at damage initiation point for different adherend thicknesses for CZM model

Stress distribution comparison between the CZM and continuum model for different substrate thicknesses was done, see Figures 49 - 52. Combined (Figure 49) and shear stresses (Figure 50) exhibit flattening of the stress distribution curve with increased substrate thickness. The combined and shear stress in the adhesive middle are increased. On the adhesive edge, both combined and peel stress exhibit an upward trend up to a substrate thickness of 3 mm, beyond which they begin to decline. The shear stress shows opposite behaviour. The probable cause of this is the difference in the bending stiffness of substrates as mentioned before. Since the substrates` bending stiffness is increased faster than the bending moment, the peel stress decreases at the break-even point. The continuum model shows constant deviation at the adhesive edge while at the adhesive middle the deviation is changed with increased adherend thickness. Shear stress shows lower deviation compared to combined and peel stress.

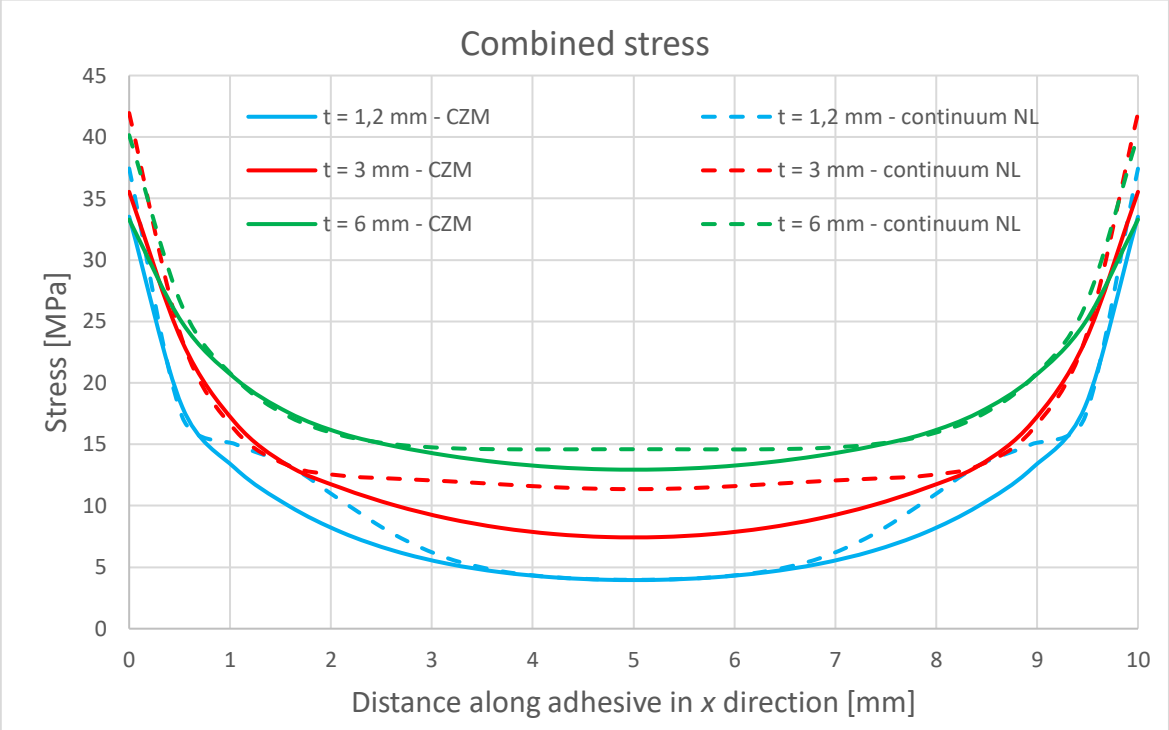

Figure 49. Combined stress comparison between CZM and continuum models for different adherend thicknesses

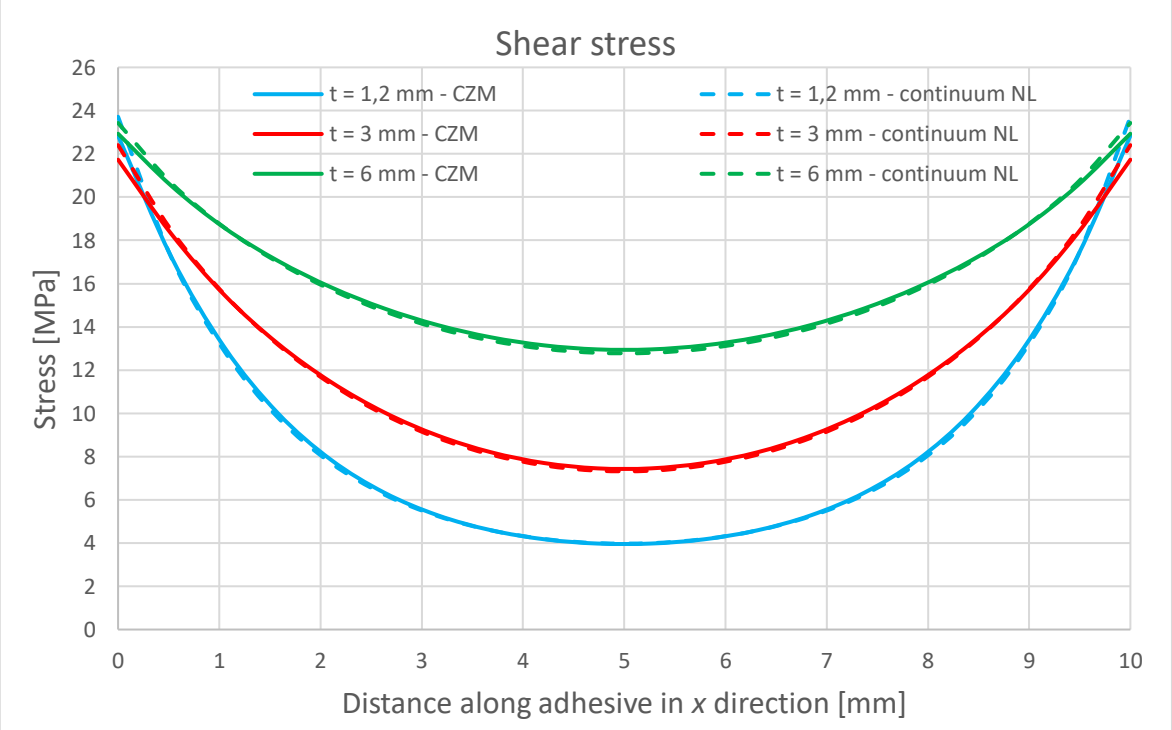

Figure 50. Shear stress comparison between CZM and continuum models for different adherend thicknesses

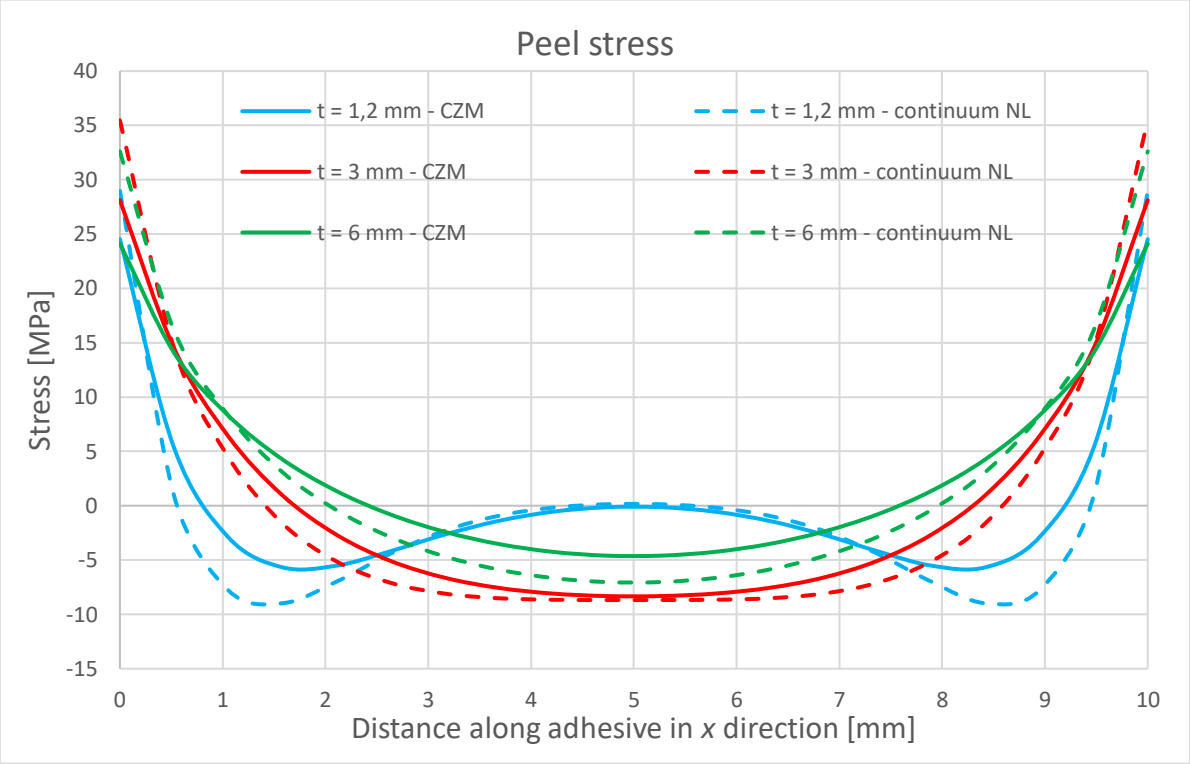

Figure 51. Peel stress comparison between CZM and continuum models for different adherend thicknesses

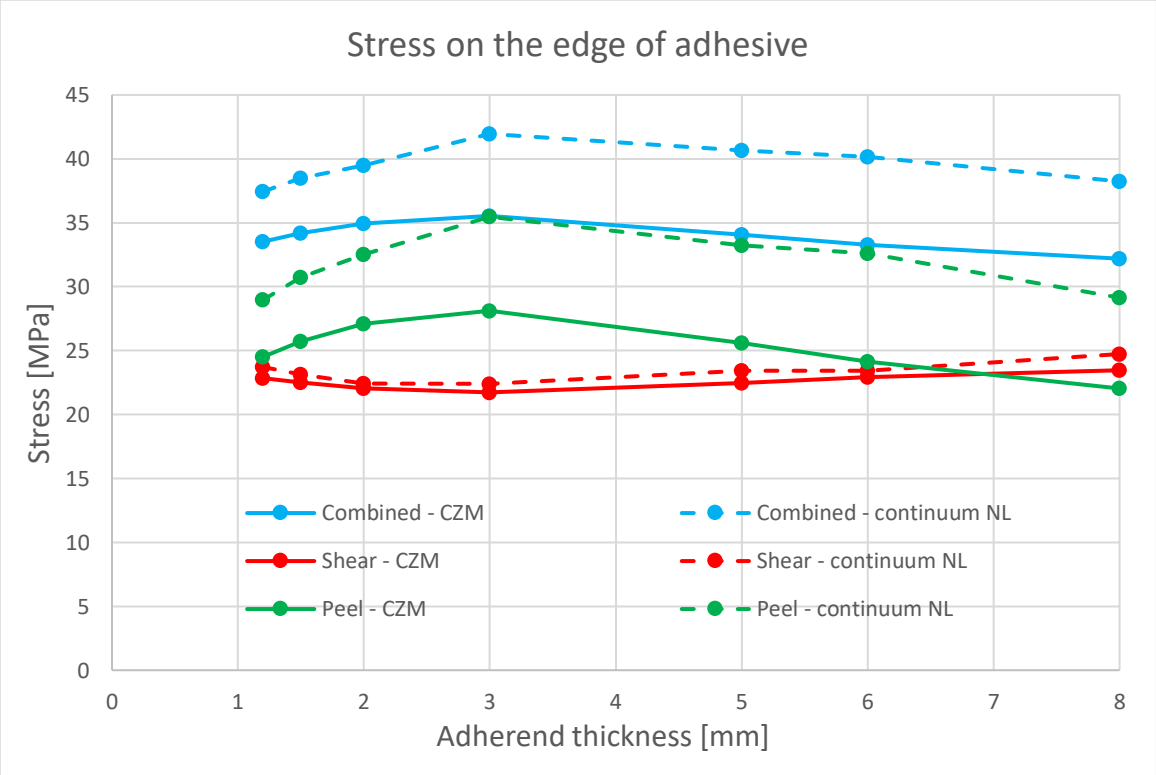

Figure 52. Comparison of the change in stress on the edge of adhesive between CZM and continuum models with the change of adherend thickness

4.2.3. Bondline thickness

4.2.3.1. Stiffness analysis

A comparison of a force – displacement curves between CZM and continuum model for different bondline thicknesses was made, see Figure 53. Models showed sufficient match in terms of joint stiffness. With increased bondline thickness, the joint stiffness is decreased. The 1,5 mm bondline thickness shows a more non-linear behaviour below 0,3 mm of displacement compared to thinner bondlines. As bondline thickness is increased, tensile forces acting on the joint are further separated resulting in an increased bending moment. Since the adhesive is less stiff compared to the aluminium substrates, it underwent greater deformation. Consequently, increased proportion of the adhesive in the joint resulted in decreased joint stiffness.

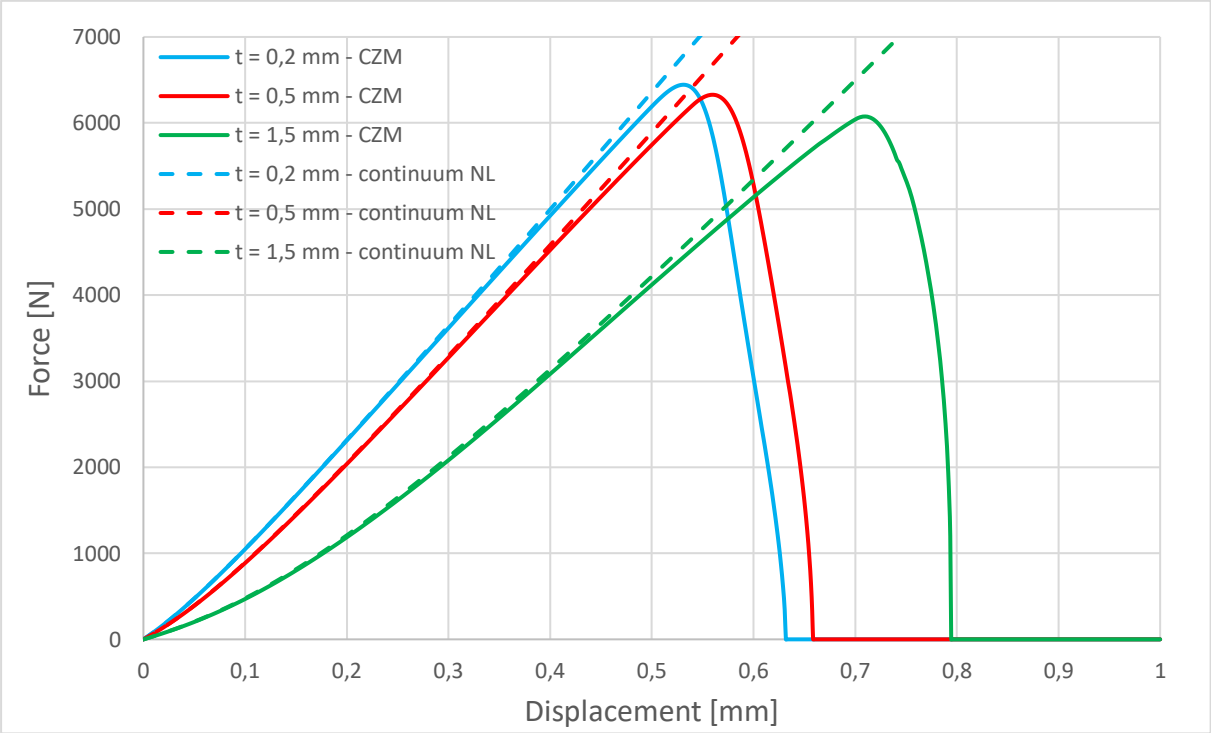

Figure 53. Force-displacement curve comparison between CZM and continuum models for different bondline thicknesses

4.2.3.2. Strength analysis

For the CZM model, maximum force and the force magnitude at the damage initiation point was extracted for different bondline thicknesses, see Figure 54. With increased bondline thickness, the max force of the joint is decreased. Contrary, the force at the damage initiation point is increased up to the thickness of 1 mm after which it remained nearly constant. With increased bondline thickness, shear stress became more uniform as seen in Figure 56. Shear

stress in the adhesive middle was increased up to certain value which corresponds to bondline thickness of 1 mm. This increased shear stress allowed the adhesive to withstand a higher load. However, further increase of bondline thickness past 1 mm did not result in increased shear stress in the adhesive middle, therefore the adhesive was not able to carry additional load. Consequently, the force at the damage initiation curve ceased to increase.

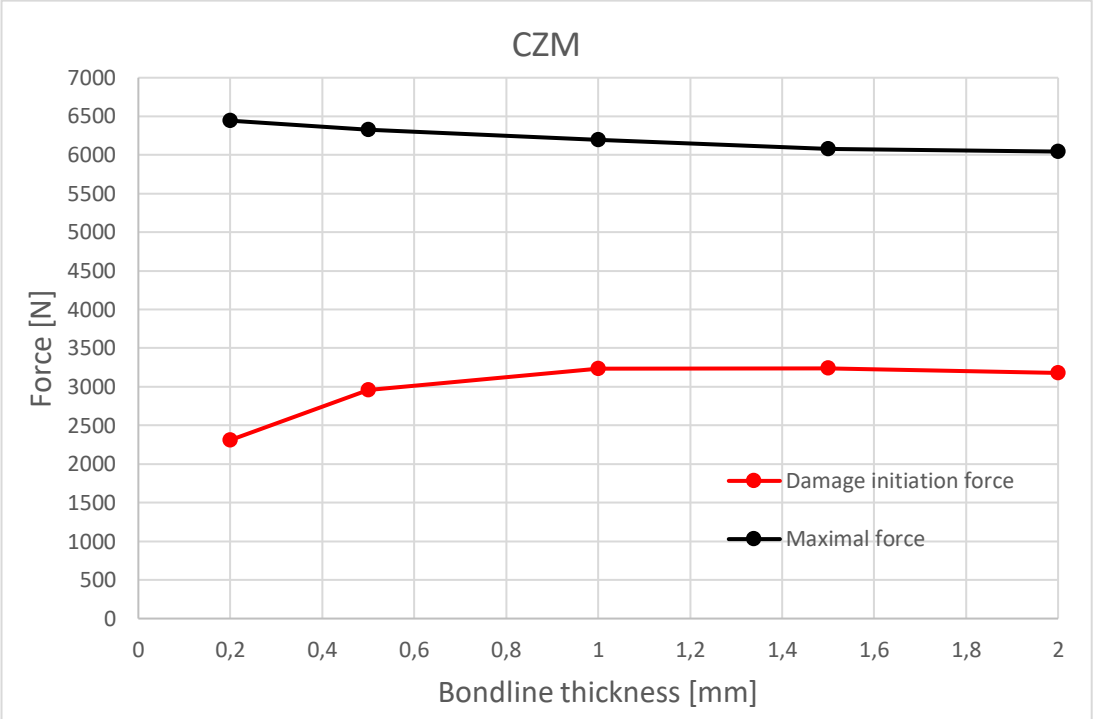

Figure 54. Max force and force at damage initiation point for different bondline thicknesses for CZM model

A comparison of stress distribution within the adhesive between the CZM and continuum models for different bondline thicknesses was performed, see Figures 55 - 58. Combined and shear stresses were increased in the adhesive middle with increased bondline thickness. Furthermore, shear stress exhibited a more uniform stress distribution but less pronounced compared to the adherend thickness sensitivity study. Combined stress appears to deviate more with increased bondline thickness.

Figure 58 displays the change of stress on the adhesive edge for the CZM and continuum model. Peel stress increased with increased bondline thickness due to increased bending moment. Furthermore, shear stress was decreased but at slower rate than the increase of peel stress resulting in overall increased combined stress.

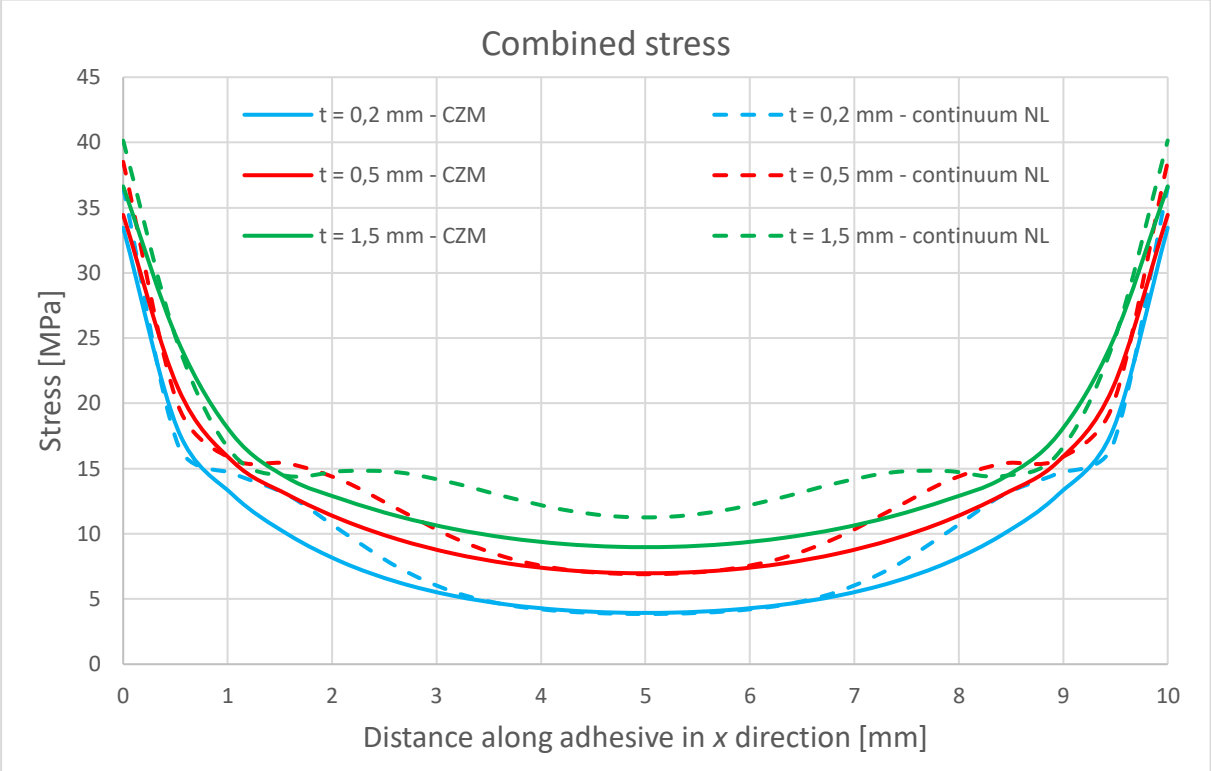

Figure 55. Combined stress comparison between CZM and continuum models for different bondline thicknesses

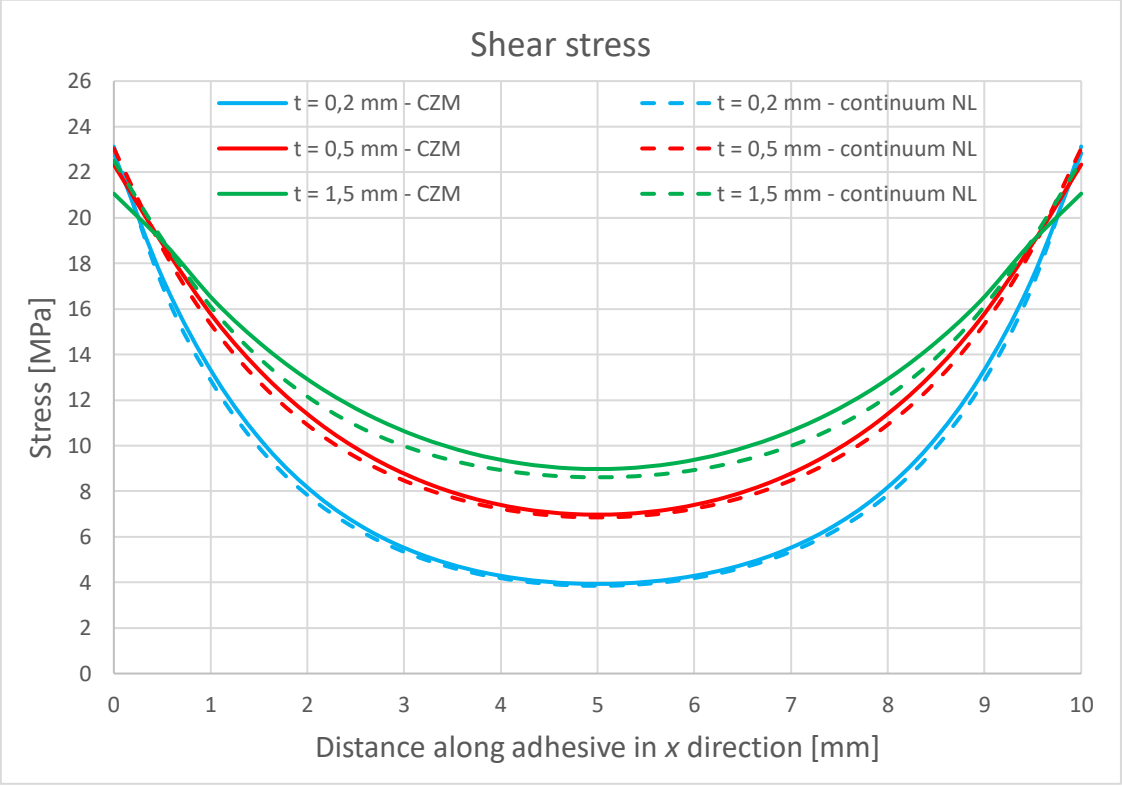

Figure 56. Shear stress comparison between CZM and continuum models for different bondline thicknesses

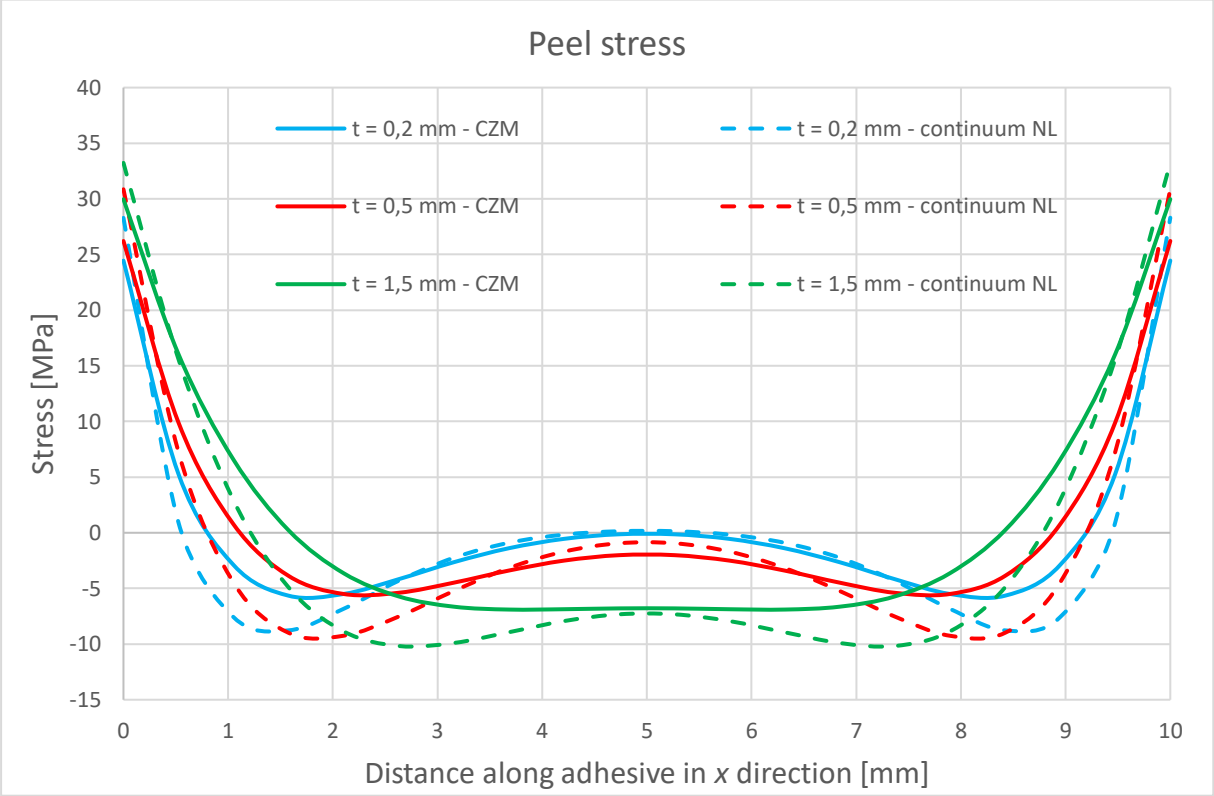

Figure 57. Peel stress comparison between CZM and continuum models for different bondline thicknesses

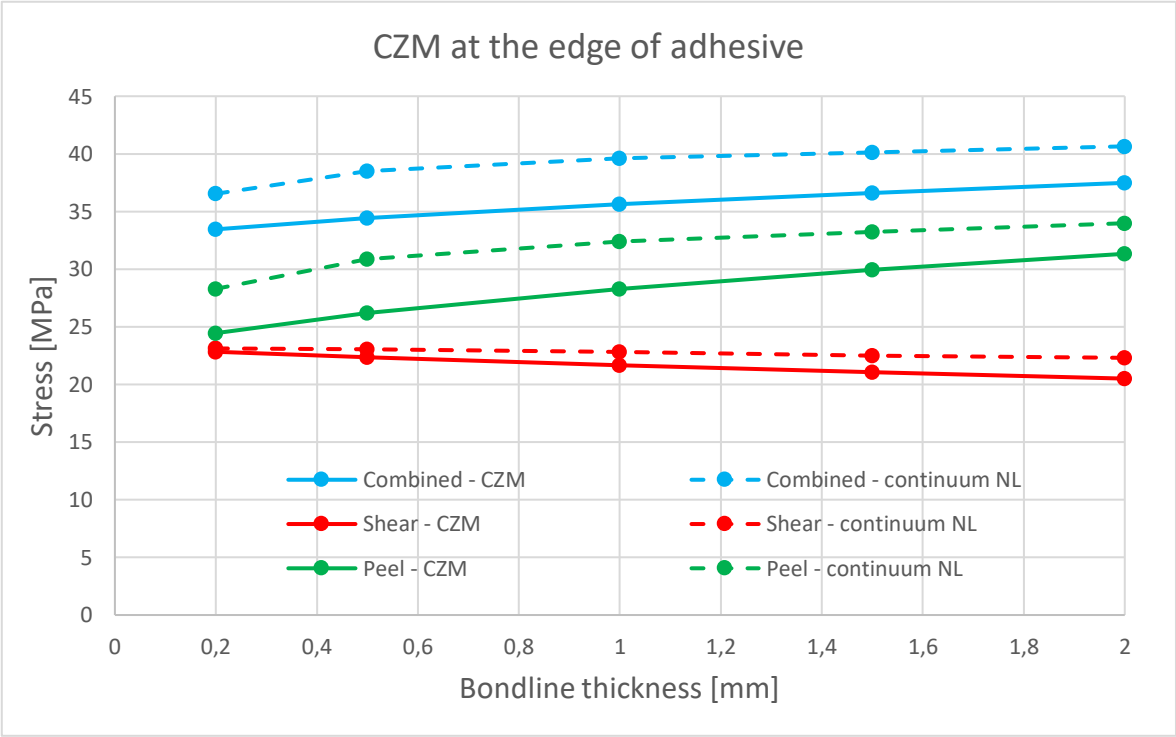

Figure 58. Comparison of the change in stress on the edge of adhesive between CZM and continuum models with the change of bondline thickness

4.2.4. Bondline length

4.2.4.1. Stiffness analysis

A comparison of force – displacement curves between CZM and continuum model for different bondline lengths was done, see Figure 59. Increased joint stiffness with the increased bondline length is exhibited. This is due to increased overlap, hence inertia of the joint is increased. Additionally, increased max strength of the joint is achieved for the CZM model. Since the adhesive area was increased, increased maximum force of the joint was expected. As the bondline length is increased, deviation of the continuum model from the CZM model occurred sooner. This is due to damage and bondline length. Damage initiation occurred at the adhesive edge, and due to the longer bondline length, the initiation of damage travelled a greater distance. Consequently, a larger portion of the joint experienced a reduction in stiffness, leading to earlier degradation of the joint stiffness.

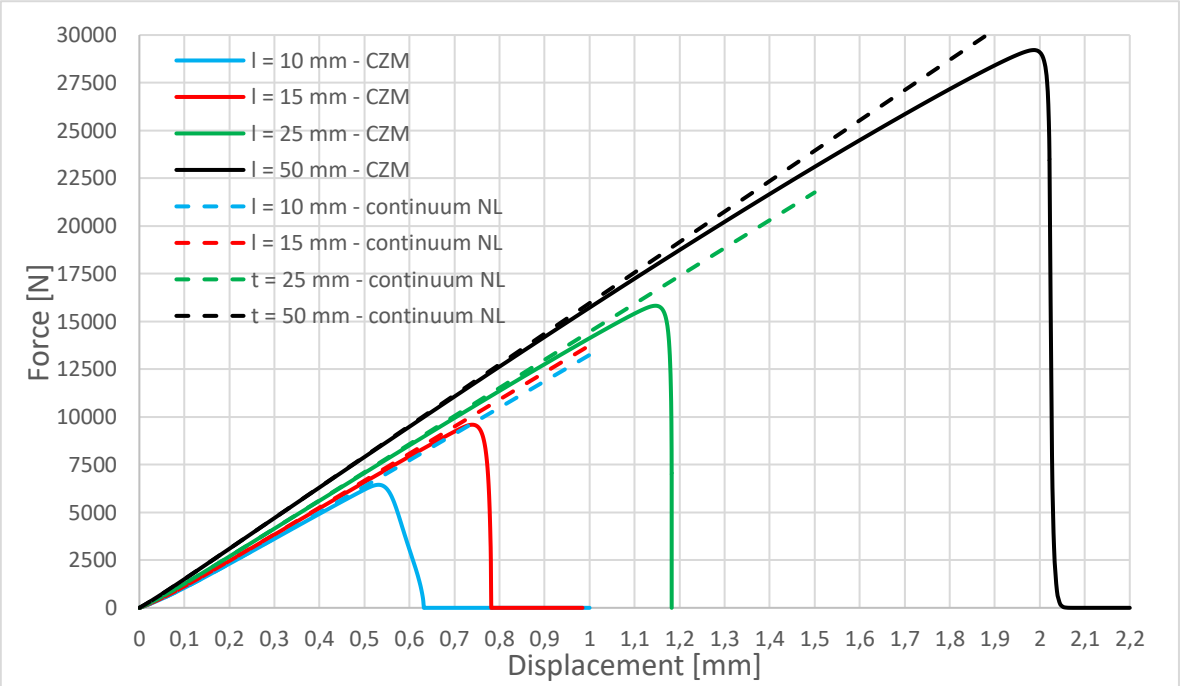

Figure 59. Force-displacement curve comparison between CZM and continuum models for different bondline lengths

4.2.4.2. Strength analysis

One of the biggest benefits of using adhesives is displayed in Figure 60 where the change of max force and force at the damage initiation point with varying bondline length is plotted. With increased bondline length, max force of the joint is increased linearly while the force at the damage initiation point increased slightly. This means that during exploitation if

adhesive enters plasticization, the failure will not occur right away if bondline is long enough. Most loaded part of the adhesive, usually edge, undergoes plastic deformation causing the load redistribution. Consequently, inner part of adhesive starts contributing more to the joint strength, i.e., the inner part of adhesive is being utilized better as stated in [15]. However, this represents a problem in a numerical analysis, especially in a full vehicle simulation. In a full vehicle simulation, usually only linear behaviour is simulated due to the run time. The problem is to determine failure criterion for adhesives. If the failure criterion is the plasticization of adhesive then a long bondline length, and therefore higher bondline strength, represents a safety factor. However, as seen in Figure 60, for bondline length of, for e.g., 50 mm, there is a big difference between the forces meaning that the failure criterion could be too conservative, thus resulting in overusing material.

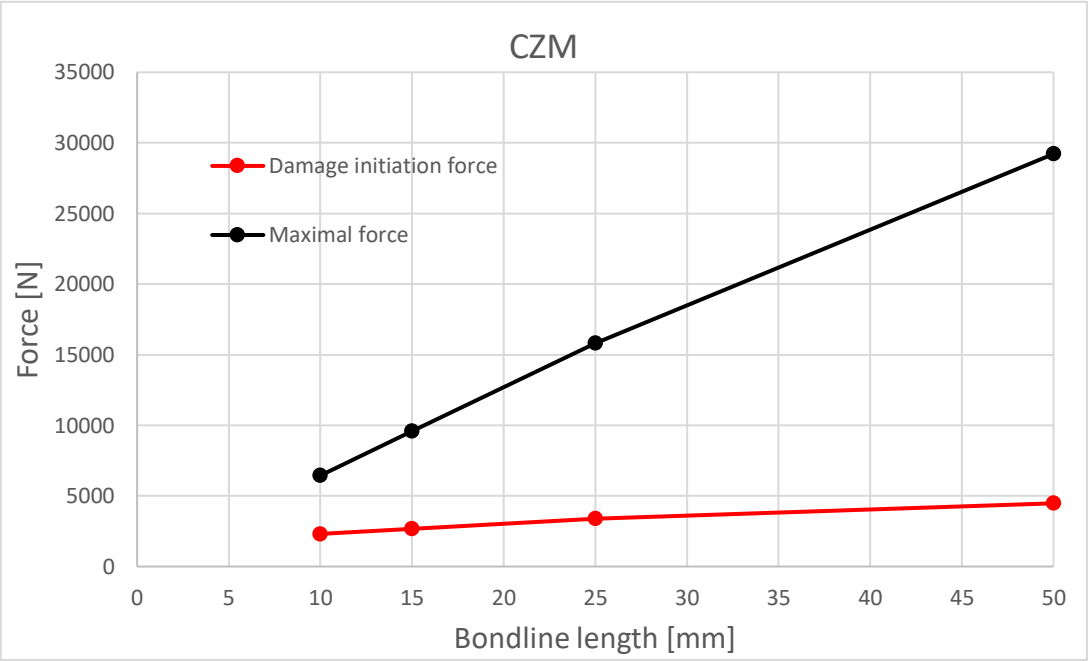

Figure 60. Max force and force at damage initiation point for different bondline lengths for CZM model

A comparison of stresses between the CZM and continuum models was done, see Figures 61 - 64. Shear stress showed acceptable matching, see Figure 62. Peel stress exhibits a deviation on the adhesive edge and in compression, but it appears that the difference is decreased with increased bondline length, see Figure 63. Consequently, deviation of combined stress decreased, see Figure 61.

Figure 64 displays the change of stress on the adhesive edge for the CZM and continuum models. With increased bondline length, peel stress was decreased while shear stress was

increased. The length between the grips was not changed while the bondline length was increased resulting in decreased secondary bending, i.e., decreased peel stress.

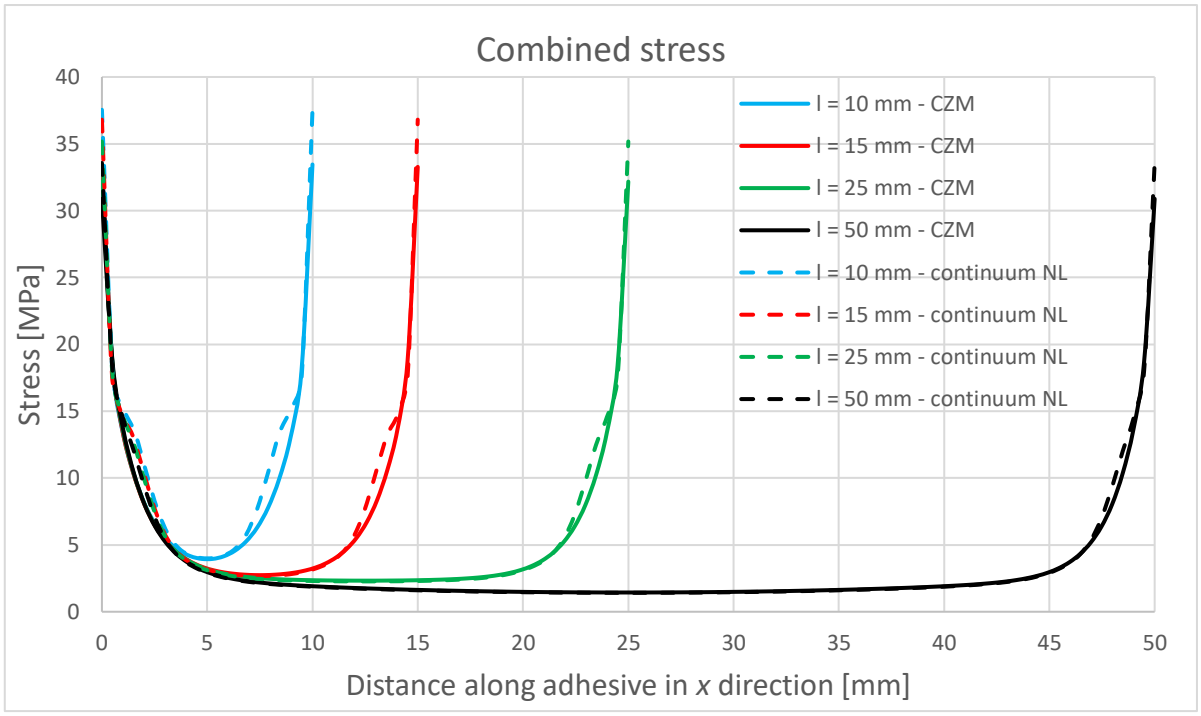

Figure 61. Combined stress comparison between CZM and continuum models for different bondline lengths

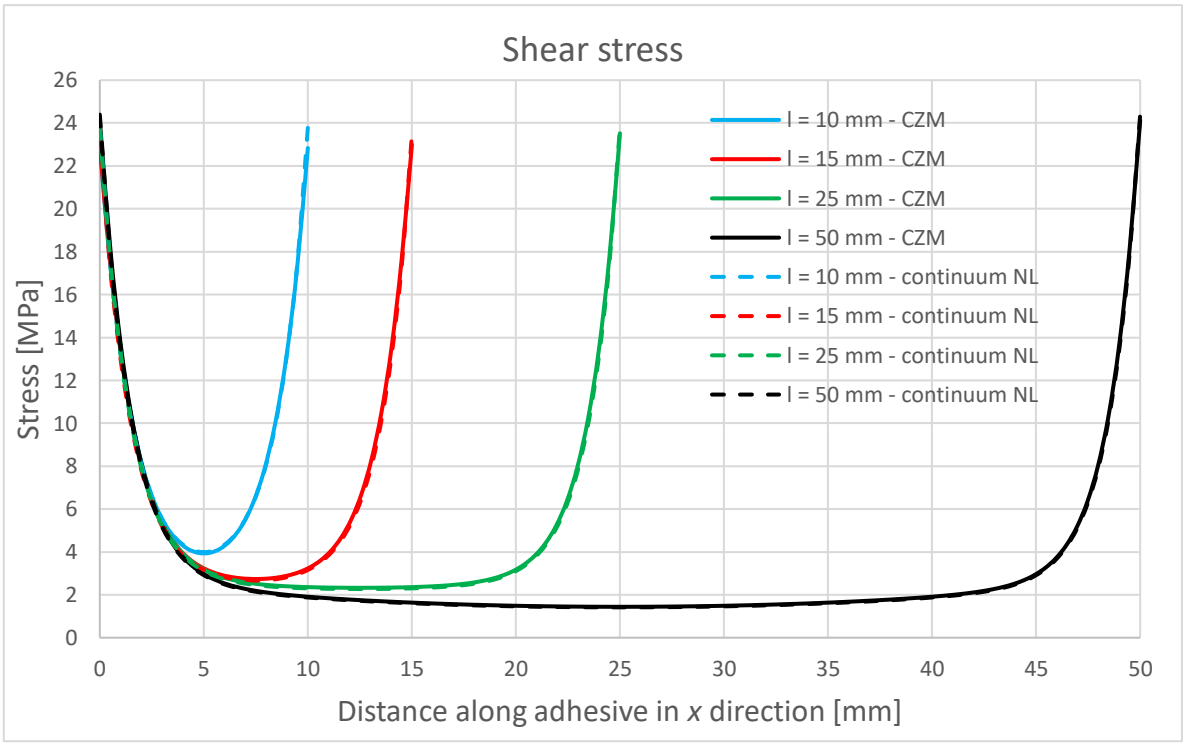

Figure 62. Shear stress comparison between CZM and continuum models for different bondline lengths

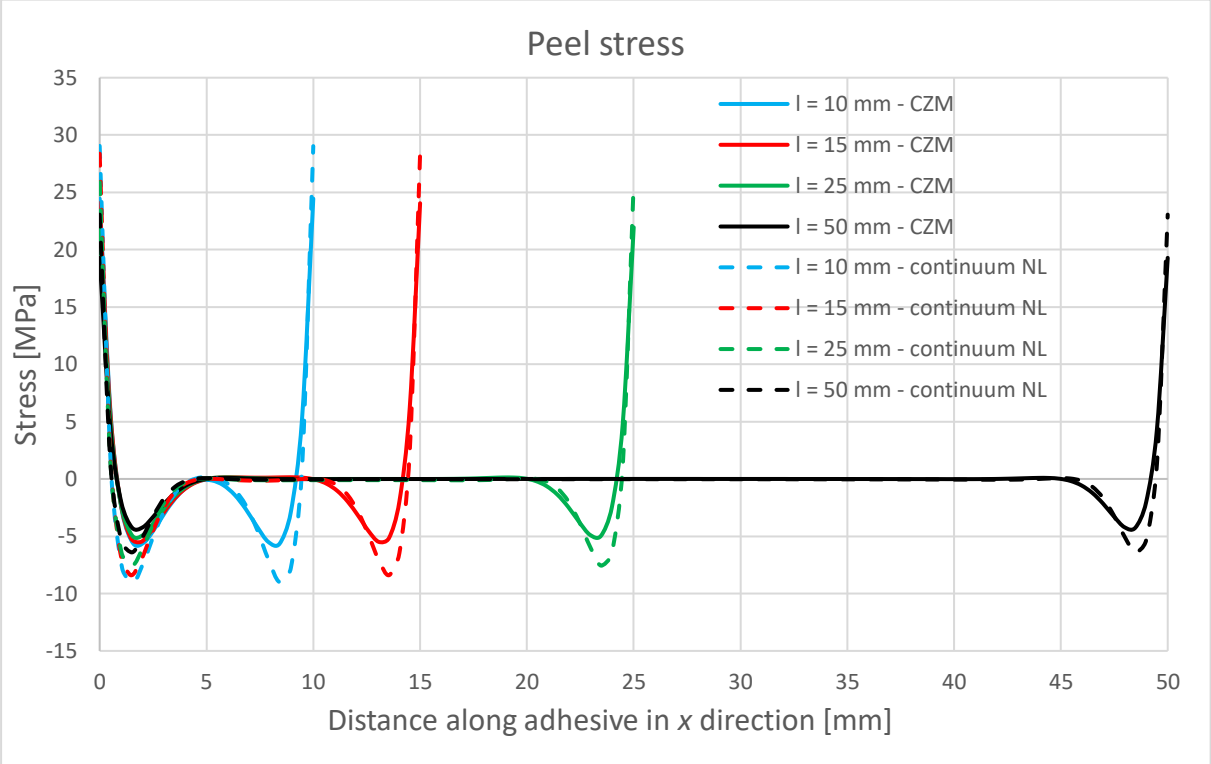

Figure 63. Peel stress comparison between CZM and continuum models for different bondline lengths

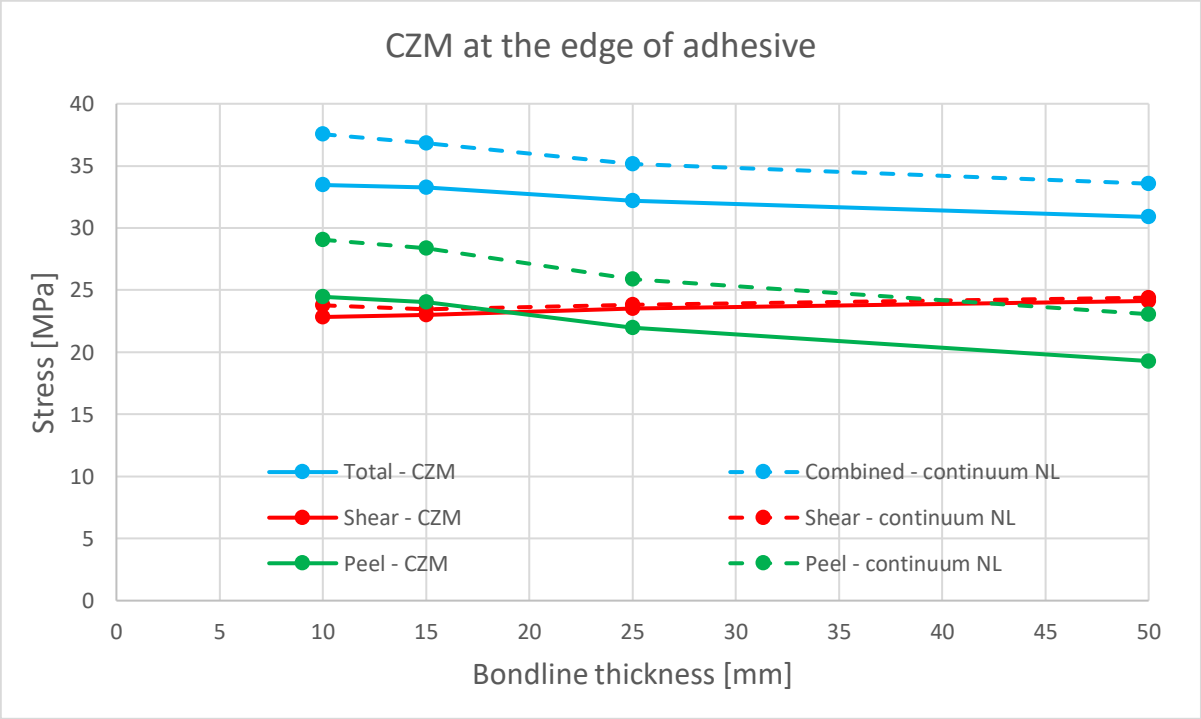

Figure 64. Comparison of the change in stress on the edge of adhesive between CZM and continuum models with the change of bondline length

5. CONCLUSION

The objective of this thesis was to make initial steps towards numerical modelling and analysis of structural adhesives. The intention was to come up with a solution for modelling adhesive in a full vehicle simulation. Since full vehicle simulations are computationally expensive due to the model size, it is desired that the solution for modelling adhesives can produce accurate results while considering only linear behaviour. Furthermore, the solution is supposed to predict stiffness and strength of an adhesively bonded joint with sufficient accuracy.

After detailed literature review, two modelling methods were chosen for detailed investigation and comparison – cohesive zone modelling and linear continuum method. Linear continuum method is computationally efficient and simple to implement, making it often used for initial evaluation. CZM is often used method for modelling adhesive behaviour since it combines the principles of continuum and fracture mechanics. Due to different formulation, CZM has an advantage of being mesh independent and the stress singularities being eliminated. However, with further investigation, it was found out that CZM cannot be used in linear analysis. Therefore, a comparison of CZM and continuum methods was conducted to determine difference in results.

No experimental data was available for adhesive of interest therefore test data from literature was used. First step was to compare the CZM and continuum models to the test data in terms of stiffness of a SLJ test. Adhesive data required for setting up the models was extracted from the literature. Results showed a mismatch with test data with both models exhibiting higher stiffness compared to test results. Furthermore, the CZM exhibited a slightly higher stiffness compared to the continuum model. Expecting similar behaviour, the same simulations were conducted for BM 4600F adhesive, which is the adhesive of interest. Results showed increased mismatch in stiffness with the CZM model being ≈50% stiffer than the continuum model. After rerunning the continuum model, but with including non-linear geometry, results showed improved matching of the CZM and continuum models. It was concluded that the continuum model needs to be run as a non-linear analysis, especially with thin adherends, to be able to capture bending and consequent stiffening effects. Since both models predicted stiffness with satisfactory accuracy further analyses were performed for the BM 4600F adhesive.

Next, a comparison of stress distribution was done at the point of damage initiation and at the point of max force. Results showed relatively similar behaviour for both models with

combined and peel stresses exhibiting larger deviation in certain areas compared to shear stress. Furthermore, comparison of von Mises to combined stress, and max shear to shear stress, resulted in significant difference in results. Subsequently, it was shown that comparing stresses calculated using the same formulation results in a better match. Additionally, difference in values of stress was increased as approaching to the max force of the joint. Deviation of the continuum model compared to the CZM was calculated at damage initiation point. Results showed a deviation of a few percent for shear stress while combined stress and peel stress deviated up to 30% and 200% respectively. It was concluded that only shear stress exhibits acceptable deviation. Due to high deviation of peel stress, combined stress exhibits relatively high deviation.

After initial analyses, next step was to perform sensitivity study on the following parameters: element size, adherend thickness, bondline thickness and bondline length. The aim was to study the effects of a particular parameter on stiffness and stress distribution of the joint, but also to verify the consistency of the previously acquired results for the CZM and continuum models. For the element size sensitivity study, to discretize the adhesive, five finite element sizes were used ranging from 0,2 to 5 mm. Results showed that both models were unaffected by element size in terms of the joint stiffness. Furthermore, the CZM exhibited constant value of maximal force of the joint regardless of element size confirming its mesh independency. As element size increased there was less elements in the adhesive which resulted in models´ inability to adequately capture stress field. Furthermore, stress deviation of the continuum model increased with increased element size.

For the adherend thickness sensitivity study, joints with seven adherend thicknesses ranging from 1,2 to 8 mm were simulated. Results showed increased joint stiffness with increased substrate thickness. Also, both models exhibited acceptable matching in terms of joint stiffness. A reduction in peel stress and a more uniform distribution of shear stress was exhibited. Combined and shear stresses exhibited an increase of the stress values in the adhesive middle. By analysing stress on the adhesive edge, it was showed that peel stress was increased up to the substrate thickness of 3 mm after which it decreased. Shear stress exhibited opposite behaviour. The probable cause of this is the difference in the bending stiffness of substrates. Since the substrates` bending stiffness is increased faster than the bending moment, the peel stress decreases at the break-even point. Furthermore, it was shown that only shear stress exhibited a sufficient match.

Bondline thickness sensitivity study showed the adhesive´s effect on the joint. Analysis was performed for bondline thicknesses ranging from 0,2 to 2 mm. Increased bondline thickness resulted in decreased joint stiffness. Furthermore, increased non-linear behaviour at the initial stages of the force – displacement curve was shown with increased bondline thickness. This behaviour was explained with increased bending moment, and increased adhesive´s ratio in the joint which has lower stiffness compared to the substrates, making the joint less stiff and consequently deforming more. Additionally, a sufficient match between the models was achieved in terms of the joint stiffness. With increased bondline thickness, shear stress decreased but became more uniform while peel stress increased.

In bondline length sensitivity study four different bondline lengths were used ranging from 10 to 50 mm. Increased bondline length resulted in increased joint stiffness and increased max force of the joint. This was expected since the area of the adhesive was increased. With increased bondline length, deviation of the continuum model from the CZM model occurred sooner due to larger portion of the joint experiencing a reduction in stiffness. With increased bondline length, max force of the joint is increased linearly while the force at the damage initiation point increased slightly. This meant that plastic deformation of the adhesive edge caused the load redistribution. Consequently, inner part of adhesive started contributing more to the joint strength. However, this represents a problem in a full vehicle simulation since usually only linear behaviour is simulated. Furthermore, it creates a problem in defining the failure criterion for adhesives. Also, an acceptable match of the models was exhibited in terms of shear stress distribution while combined and peel stresses exhibited higher deviation in certain areas. The difference between the models was decreased with increased bondline length. Furthermore, peel stress was decreased due to decreased secondary bending.

The CZM is not recommended to be used in a full vehicle simulation due to its inability to run linear analysis, unlike the continuum model. For the simulated models the joint stiffness deviation between the two methods was sufficiently low. Furthermore, the methods showed similar shear stress values. In general, the methods showed increased deviation of peel stress, and consequently combined stress, with continuum method exhibiting increased stress values. However, using the continuum method in a full vehicle simulation would mean using a more conservative approach resulting in higher safety factor compared to the CZM.

6. FUTURE WORK

First, it is recommended to perform physical tests and compare the test results to the numerical results presented in this thesis. It was possible only for the A2015 adhesive, extracted from the literature, to compare with test data.

Next, a study should be performed in which other types of adhesives would be analysed. The BM 4600F adhesive is a moderately ductile adhesive therefore an analysis of a ductile and brittle adhesive would be desirable. Due to variations in material behaviour, the sensitivity study may yield different results and conclusions. Also, CZM and continuum model might not be able to sufficiently predict the adhesive behaviour for complete range of varied parameters.

LITERATURE

[1] Steidler, S. M.: *Structural modelling of adhesive joints in automotive bodies*, 2000.

[2] Rodriguez, R. Q., de Paiva, W. P., Sollero, P., Rodrigues, M. R. B., Albuquerque, E. L.: *Failure criteria for adhesively bonded joints*, 2012.

[3] Fors, F.: *Analysis of metal to composite adhesive joints in space applications*, 2010.

[4] da Silva, L. F. M., Öchsner, A., Adams, R. D.: *Handbook of adhesion technology*, Second edition, 2018.

[5] Cabral, T. D.: *A first approach to structural health monitoring of adhesive bonded joints in pipelines using integrated fiber optic sensors*, 2016.

[6] 3M web page, https://www.3m.com/

[7] https://sites.google.com/site/juliamorrismengproject2009/background-information

[8] Banea, M. D., da Silva, L. F. M.: *Adhesively bonded joints in composite materials: An overview*, 2009.

[9] Mehrabadi, F. A.: *Experimental and numerical failure analysis of adhesive composite joints*, 2012.

[10] Quini, J. G., Marinucci, G.: *Polyurethane Structural Adhesives Applied in Automotive Composite Joints*, 2012.

[11] ASTM International web page, https://www.astm.org/

[12] ISO Standards web page, https://www.iso.org/standards.html

[13] Yang, C., Tomblin, J. S.: *Investigation of adhesive behaviour in aircraft applications*, report no. DOT/FAA/AR-01/57, 2001.

[14] Bajpai, A., Martin, R., Faria, H., Ibarboure, E., Carlotti, S.: *Epoxy based hybrid nanocomposites: Fracture mechanisms, tensile properties and electrical properties*, 2020.

[15] de Sousa, C. C. R. G., Campilho, R. D. S. G., Marques, E. A. S., Costa, M., da Silva, L. F. M.: *Overview of different strength prediction techniques for single-lap bonded joints*, 2016.

[16] Steidler, S. M.: *Structural modelling of adhesive joints in automotive bodies*, 2000.

[17] Altair, *OptiStruct*, version 2021.2 user guide, User Guide (altair.com)

[18] 3M: *Introduction to modelling structural adhesives*, 2020.

[19] Ramalho, L. D. C., Campilho, R. D. S. G., Belinha, J., da Silva, L. F. M.: *Static strength prediction of adhesive joints: a review*, 2019.

[20] Tonković, Z., Finite element analysis course literature, 2020.

[21] BETAMATE 4600F adhesive datasheet, BETAMATE™ 4600F (gluespec.com)

[22] Abaqus, version 6.6 user's manual, ABAQUS Analysis User's Manual (v6.6)

[23] META, version 23.0. user guide, BETA CAE Systems (beta-cae.com)

APPENDIX A

Analytical methods

In the Volkersen´s model the expression for shear stresses, τ, is [15]:

$$\tau = \frac{P}{BL_O}\frac{w}{2}\frac{\cosh(wX)}{\sinh(w/2)} + \left(\frac{t_{P1}-t_{P2}}{t_{P1}+t_{P2}}\right)\frac{w}{2}\frac{\cosh(wX)}{\sinh(w/2)}, \quad \textbf{(20)}$$

where P is the load, t_{P1} and t_{P2} are the upper and lower adherend thickness, $X = x/L_O$ (the origin of the longitudinal co-ordinate x is at the middle of the overlap), where $-0{,}5 \leq X \leq 0{,}5$, and

$$w = \sqrt{\frac{G_A L_O^2}{E_P t_{P1} t_A}\left(1+\frac{t_{P1}}{t_{P2}}\right)}, \quad \textbf{(21)}$$

where E_P is the adherend modulus and G_A is the adhesive shear modulus.

A bending moment factor (k) in the Gland and Reissner model is calculated as [15]:

$$k = \frac{\cosh(u_2 c)}{\cosh(u_2 c) + 2\sqrt{2}\sinh(u_2 c)}, \quad \textbf{(22)}$$

with c being $L_O/2$ (Figure 9.) and

$$u_2 = \sqrt{\frac{3(1-\nu^2)}{2}}\frac{1}{t_P}\sqrt{\frac{\bar{P}}{t_P E_P}}, \quad \textbf{(23)}$$

where ν is the adherends Poisson's ratio. The expression for the adhesive shear stress is

$$\tau = -\frac{1}{8}\frac{\bar{P}}{c}\left\{\frac{\beta_C}{t_P}(1+3k)\frac{\cosh\left(\frac{\beta_C}{t}\frac{x}{c}\right)}{\sinh\left(\frac{\beta_C}{t}\right)} + 3(1-k)\right\}, \quad \textbf{(24)}$$

and

$$\beta = 8\frac{G_A}{E_P}\frac{t_P}{t_A}. \quad \textbf{(25)}$$

The elastic model of Hart-Smith considered an alternative expression for the Goland and Reissner's bending moment factor [15]

$$k = \left(1+\frac{t_A}{t_P}\right)\frac{1}{1+\xi_C+\frac{\xi_C^2}{6}}, \quad \textbf{(26)}$$

where $\xi = \sqrt{\bar{P}/D}$ (D is the adherend bending stiffness).

In Hart-Smith plastic model, τ stresses in the elastic region are given by [15]:

$$\tau = A_2\, cosh(\,2\lambda' x) + \tau_P(1-K), \quad \textbf{(27)}$$

and the shear strains in the plastic region by

$$\gamma = \gamma_C\{1 + 2K[(\lambda' x')^2 + \lambda' x' tanh(\lambda' d)]\}, \quad \textbf{(28)}$$

where τ_P is the plastic adhesive shear stress, K is the adhesive shear stiffness and

$$A_2 = K\tau_P/(cosh(\lambda' d)). \quad \textbf{(29)}$$

The values of K and d are iteratively solved by using the equations

$$\frac{\bar{P}}{L_O \tau_P}(\lambda' L_O) = 2\lambda'\left(\frac{L_O - d}{2}\right) + (1-K)(\lambda' d) + K\tanh(\lambda' d), \quad \textbf{(30)}$$

$$\left[1+3k(1-v^2)\left(1+\frac{t_A}{t_P}\right)\right]\frac{\bar{P}}{\tau_P}\lambda^2\left(\frac{L_O - d}{2}\right) = 2\left(\frac{\gamma_P}{\gamma_C}\right) + K\left[2\lambda'\left(\frac{L_O - d}{2}\right)\right]^2, \quad \textbf{(31)}$$

$$2\left(\frac{\gamma_P}{\gamma_C}\right) = K\left\{\left[2\lambda'\left(\frac{L_O - d}{2}\right) + \tanh(\lambda' d)\right]^2 - \tanh^2(\lambda' d)\right\}, \quad \textbf{(32)}$$

where γ_e and γ_P are the elastic and plastic adhesive shear strains, respectively. The process consists of introducing an initial value for k and solving the system of equations for P, K and d until achieving convergence for k.

In the global yielding (GY) failure criterion, the entire adhesive layer is subjected to the shear failure strength of the adhesive (τ_f), i.e., [15]:

$$P_m = \tau_f B L_O, \quad \textbf{(33)}$$

where P_m is the maximum load, B is the bondline width and L_O is the bondline length.

APPENDIX B

Element size sensitivity study

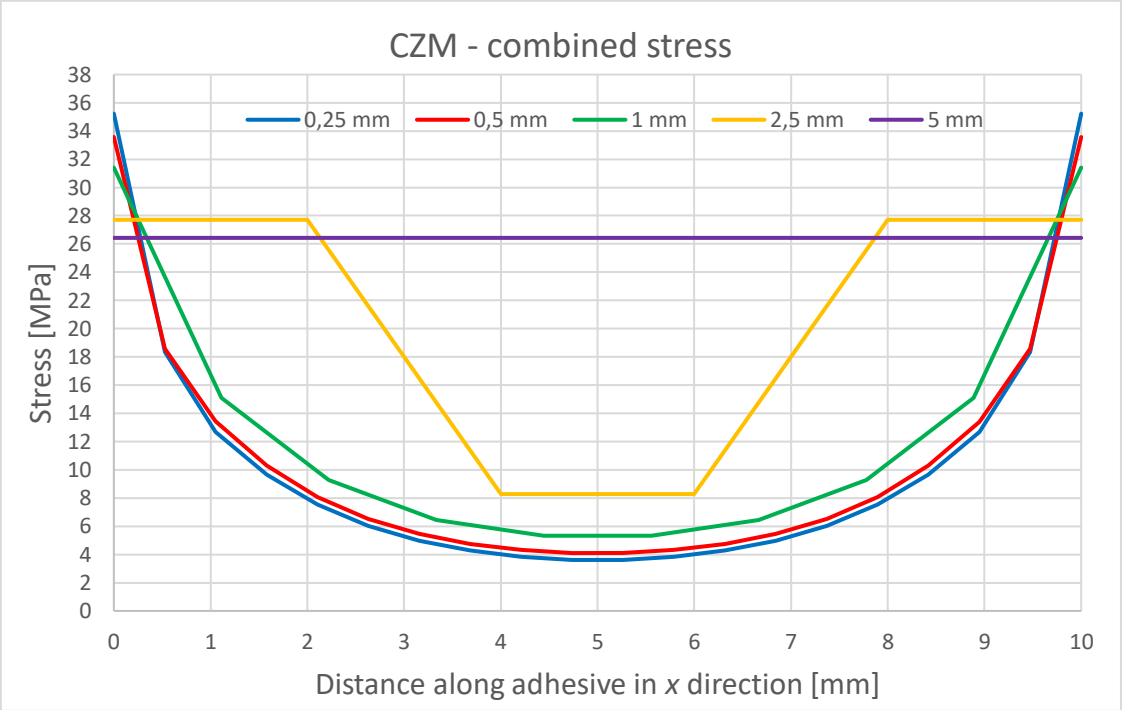

Figure 65. Distribution of combined stress through adhesive at damage initiation point for different cohesive element size for CZM model

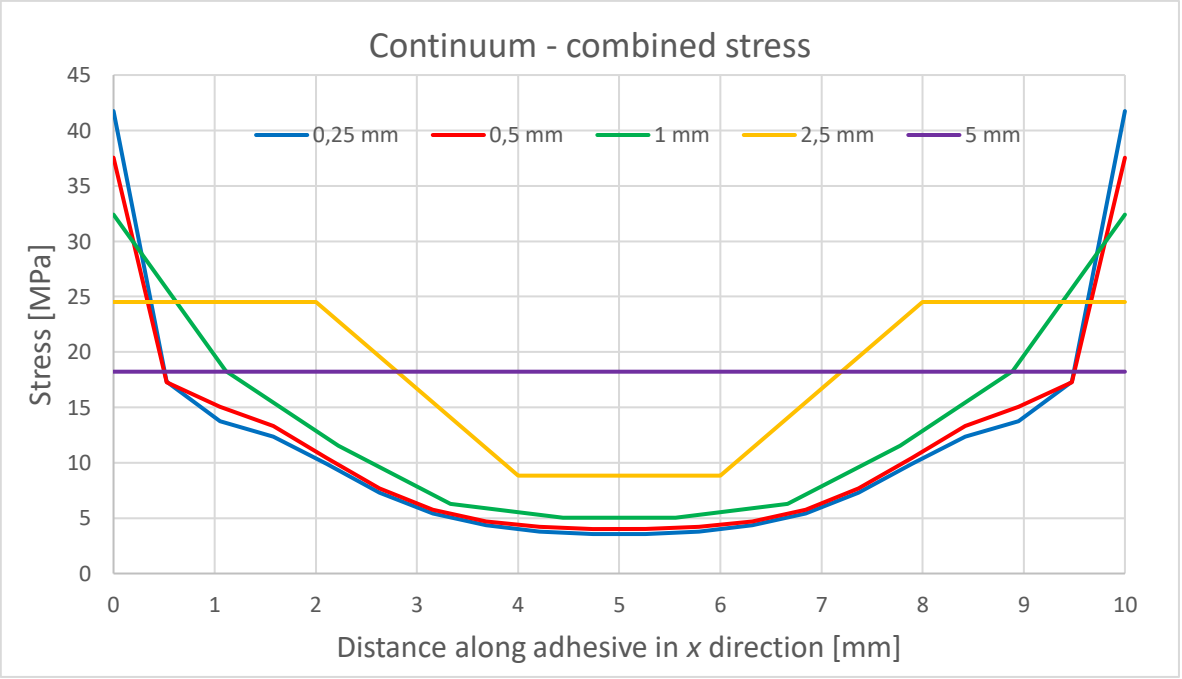

Figure 66. Distribution of von Mises stress through adhesive at damage initiation point for different finite element size for continuum model

APPENDIX C

Adherend thickness sensitivity study

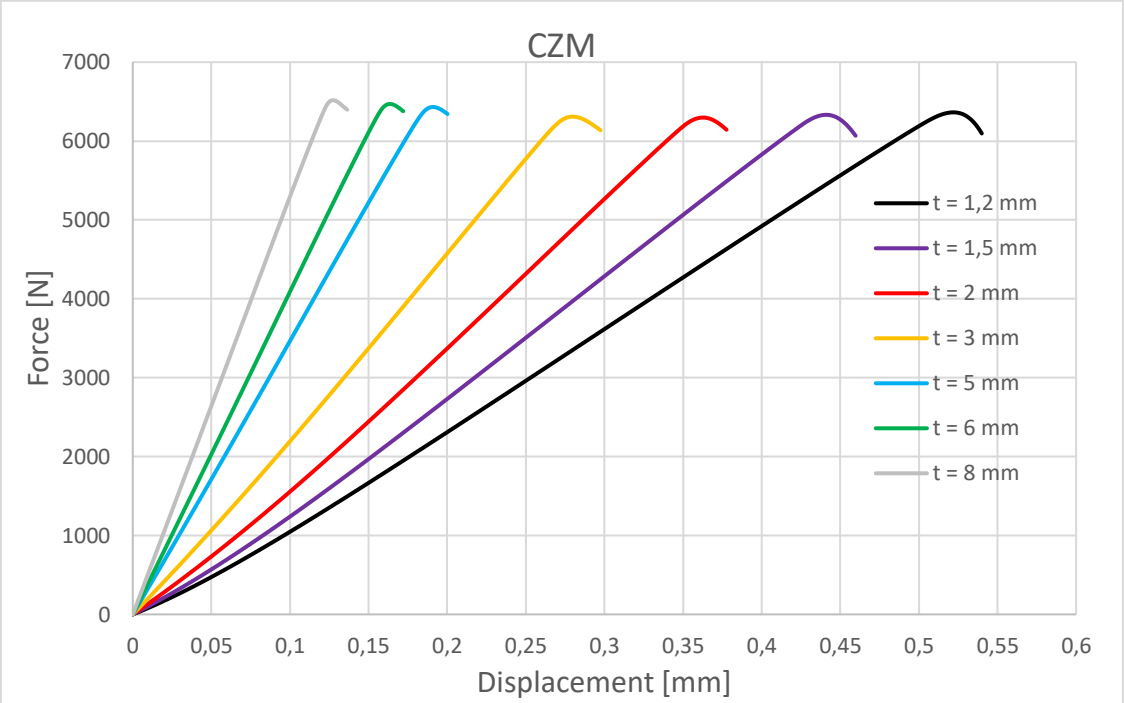

Figure 67. Force vs. displacement curves for different adherend thicknesses for CZM model

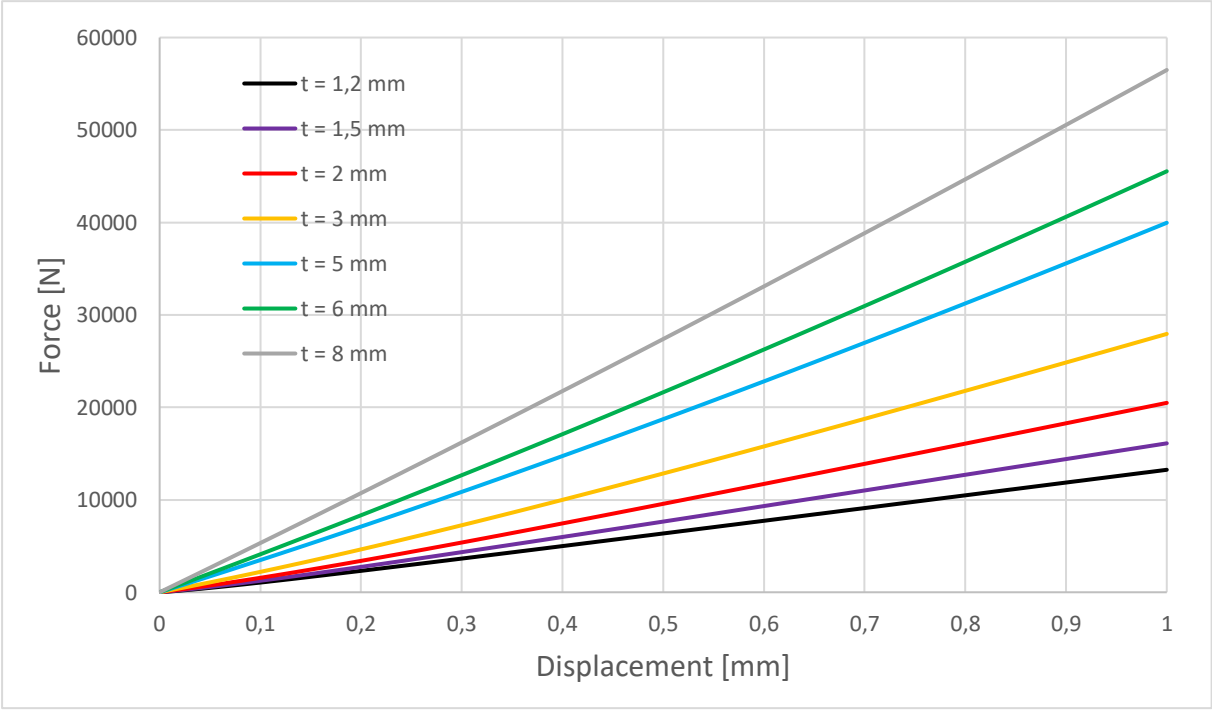

Figure 68. Force vs. Displacement curves for different adherend thicknesses for continuum model

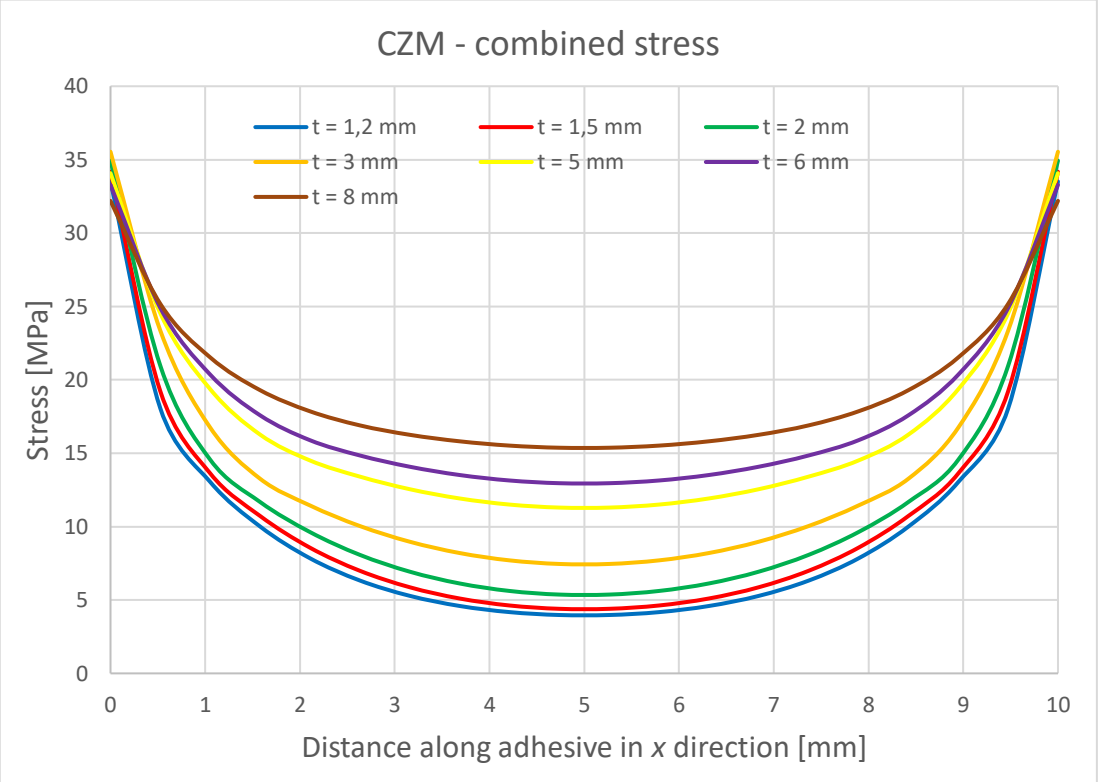

Figure 69. Distribution of combined stress within adhesive for different adherend thicknesses for CZM model

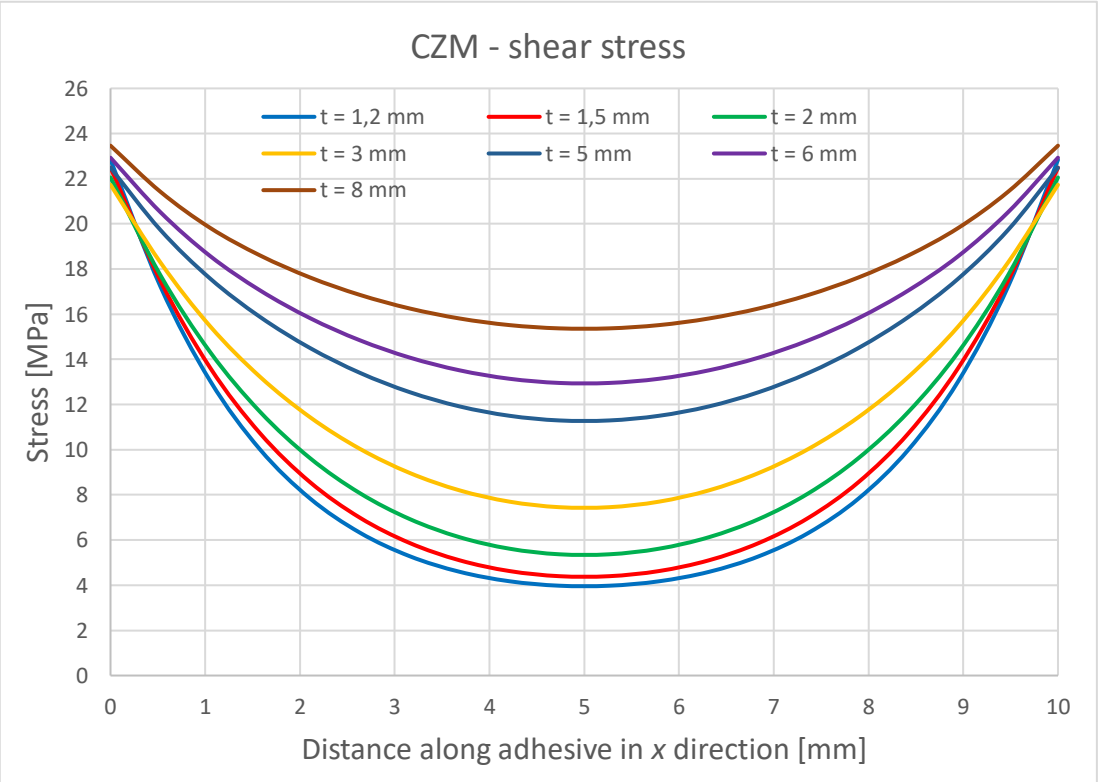

Figure 70. Distribution of shear stress within adhesive for different adherend thicknesses for CZM model

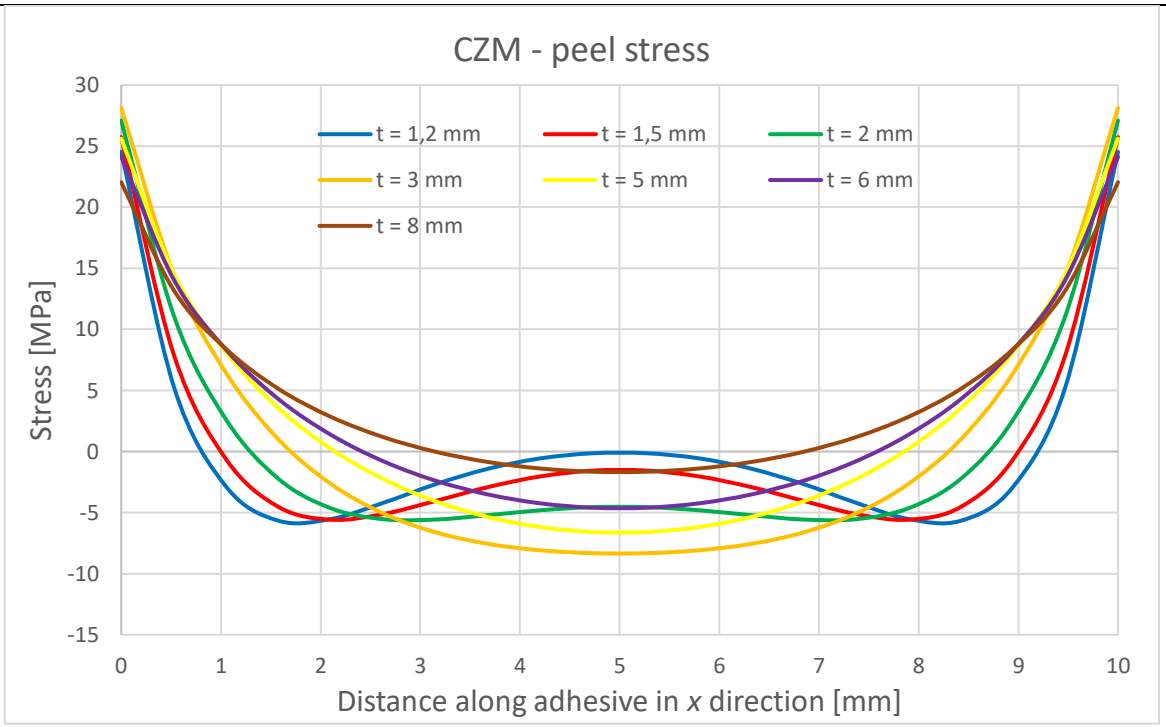

Figure 71. Distribution of peel stress within adhesive for different adherend thicknesses for CZM model

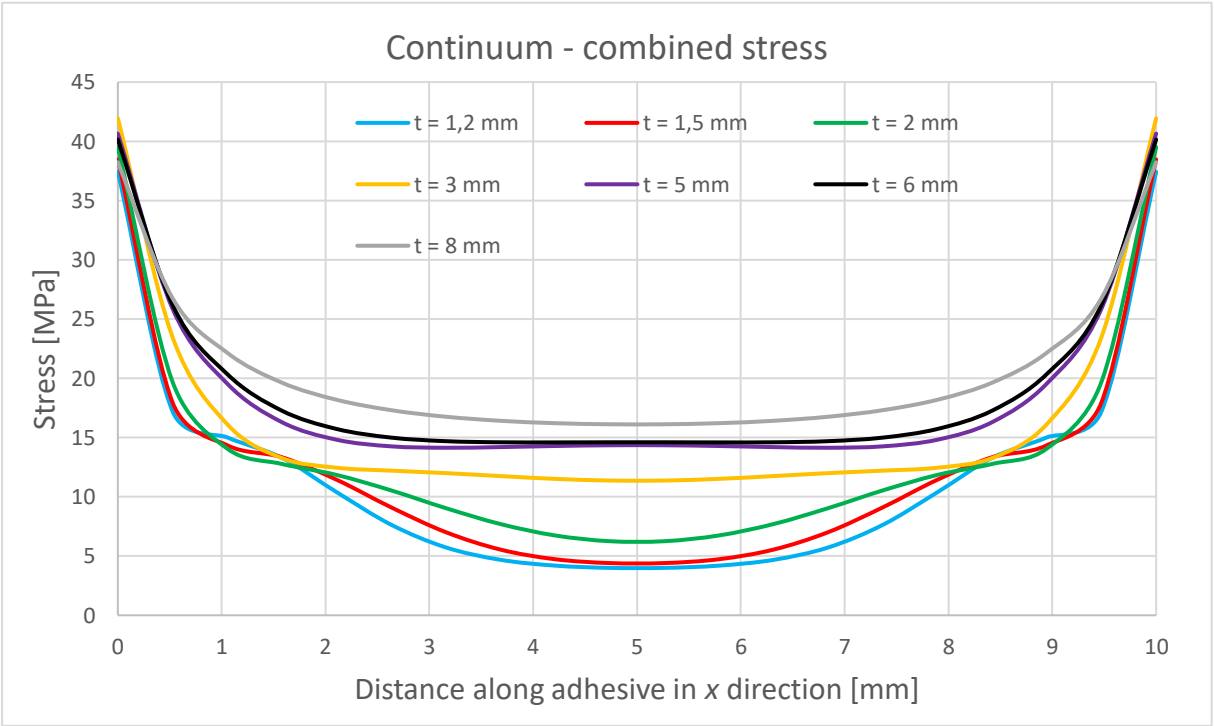

Figure 72. Distribution of combined stress within adhesive for different adherend thicknesses for continuum model

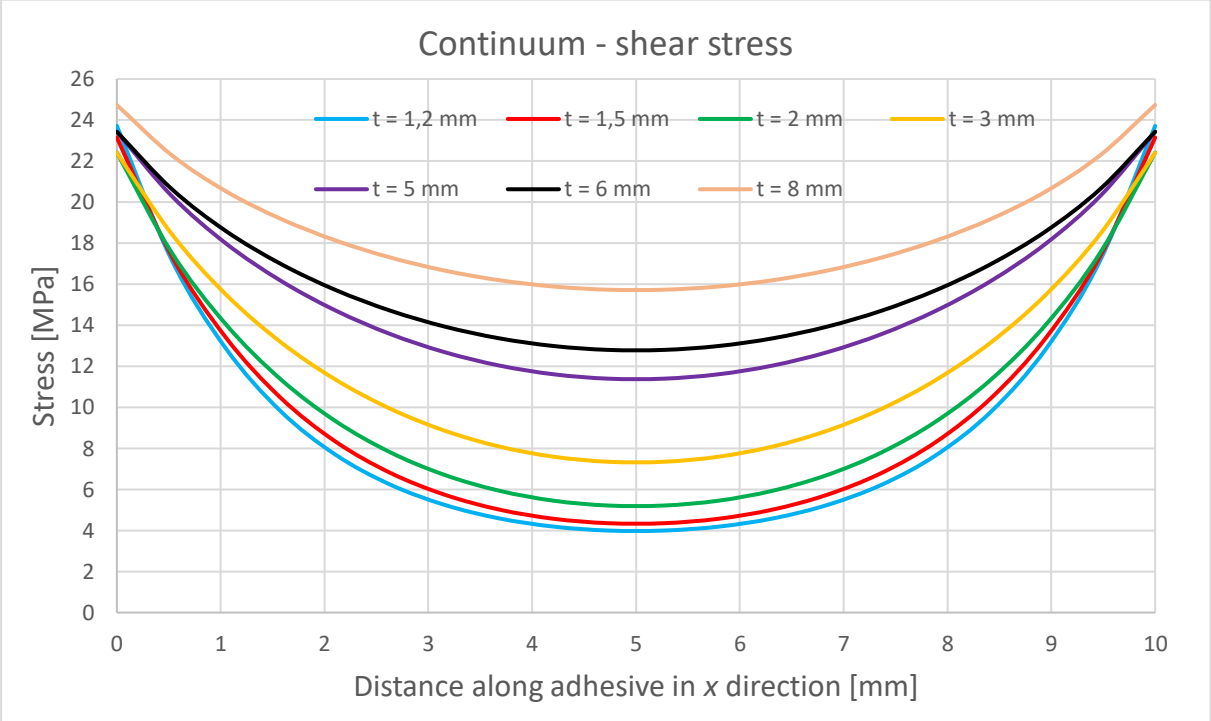

Figure 73. Distribution of shear stress within adhesive for different adherend thicknesses for continuum model

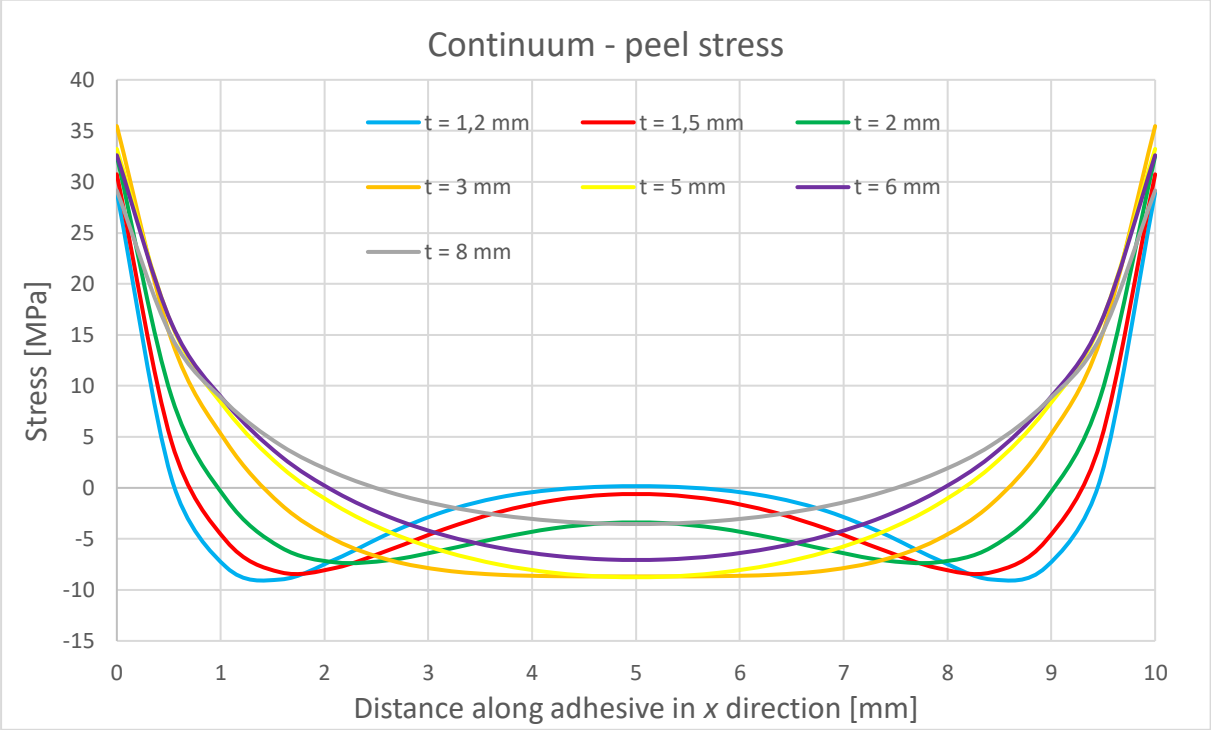

Figure 74. Distribution of peel stress within adhesive for different adherend thicknesses for continuum model

APPENDIX D

Bondline thickness sensitivity study

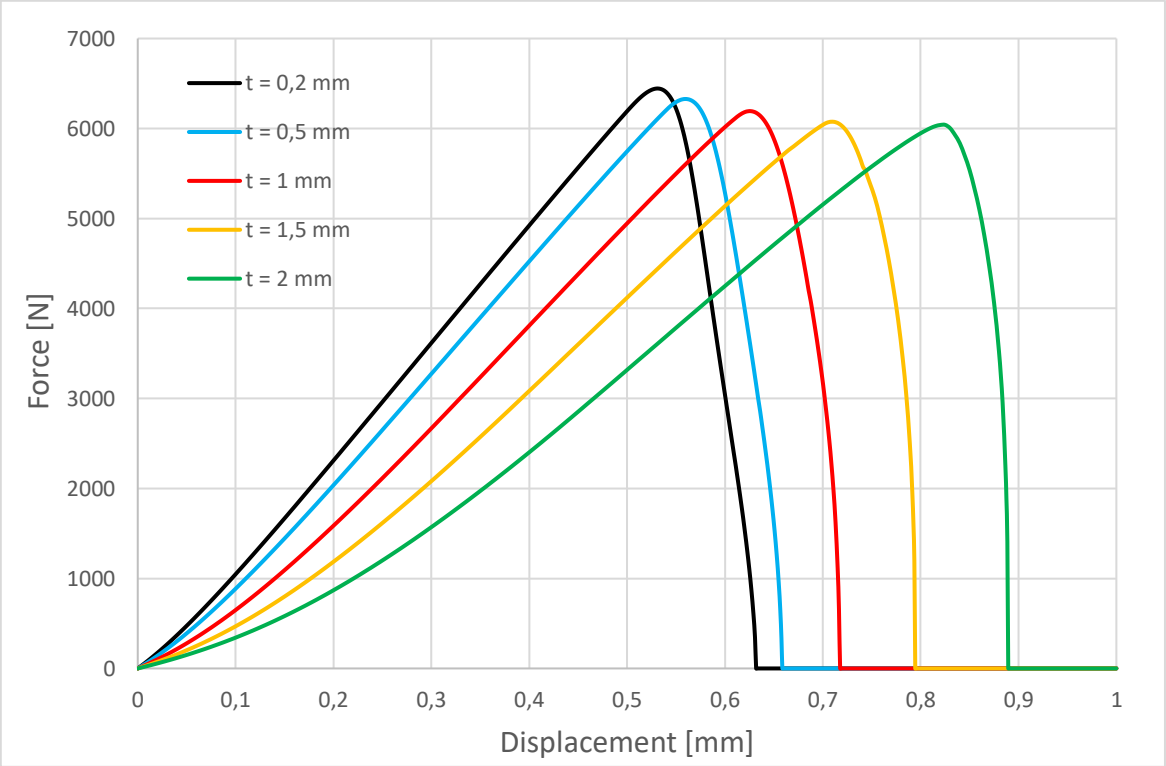

Figure 75. Force-displacement curves for different bondline thicknesses for CZM model

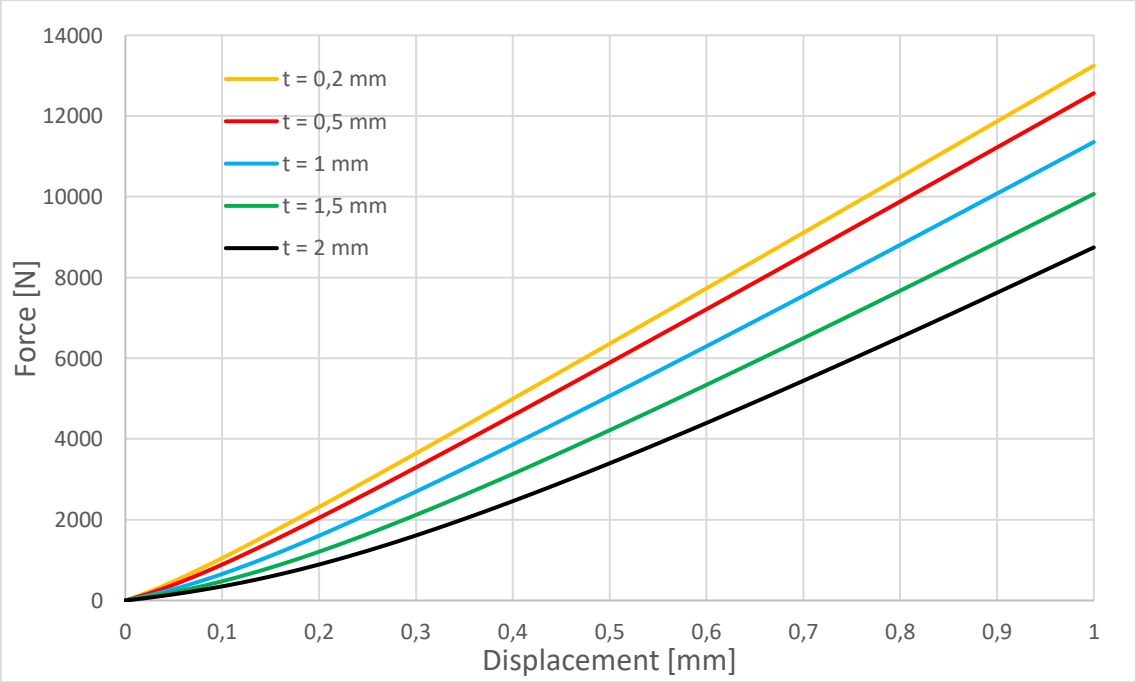

Figure 76. Force-displacement curves for different bondline thicknesses for continuum model

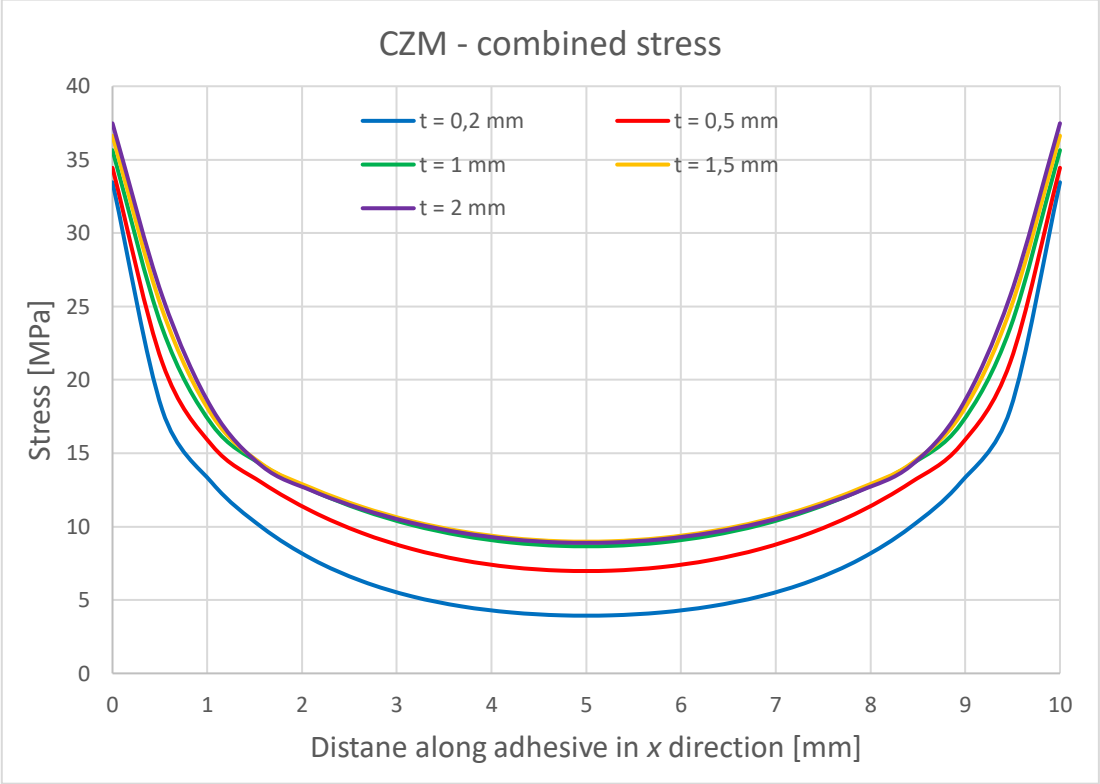

Figure 77. Distribution of combined stress within adhesive for different bondline thicknesses for CZM model

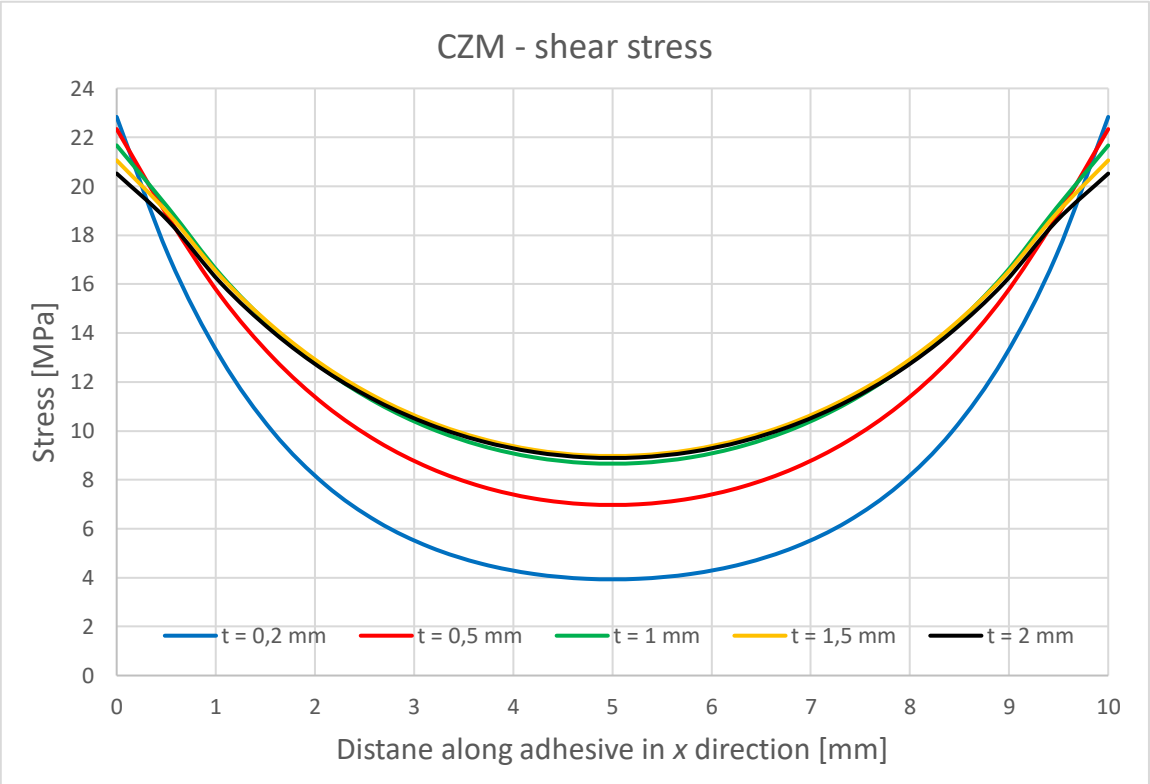

Figure 78. Distribution of shear stress within adhesive for different bondline thicknesses for CZM model

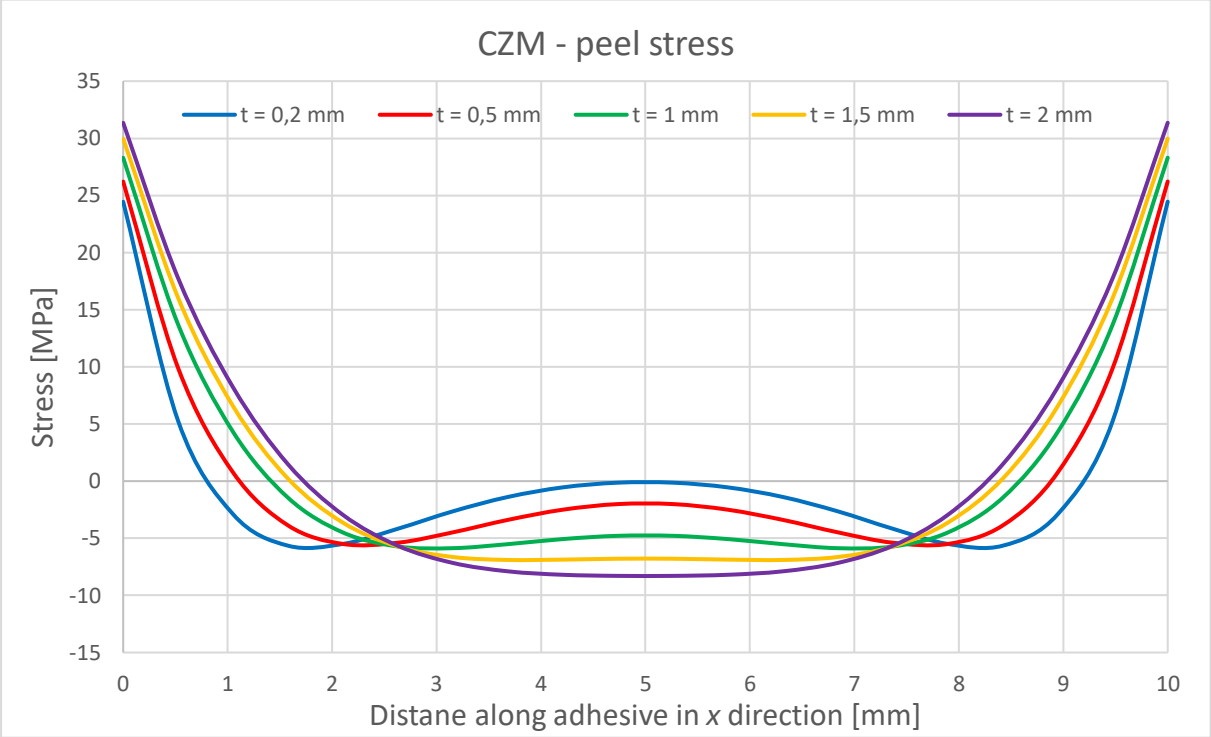

Figure 79. Distribution of peel stress within adhesive for different bondline thicknesses for CZM model

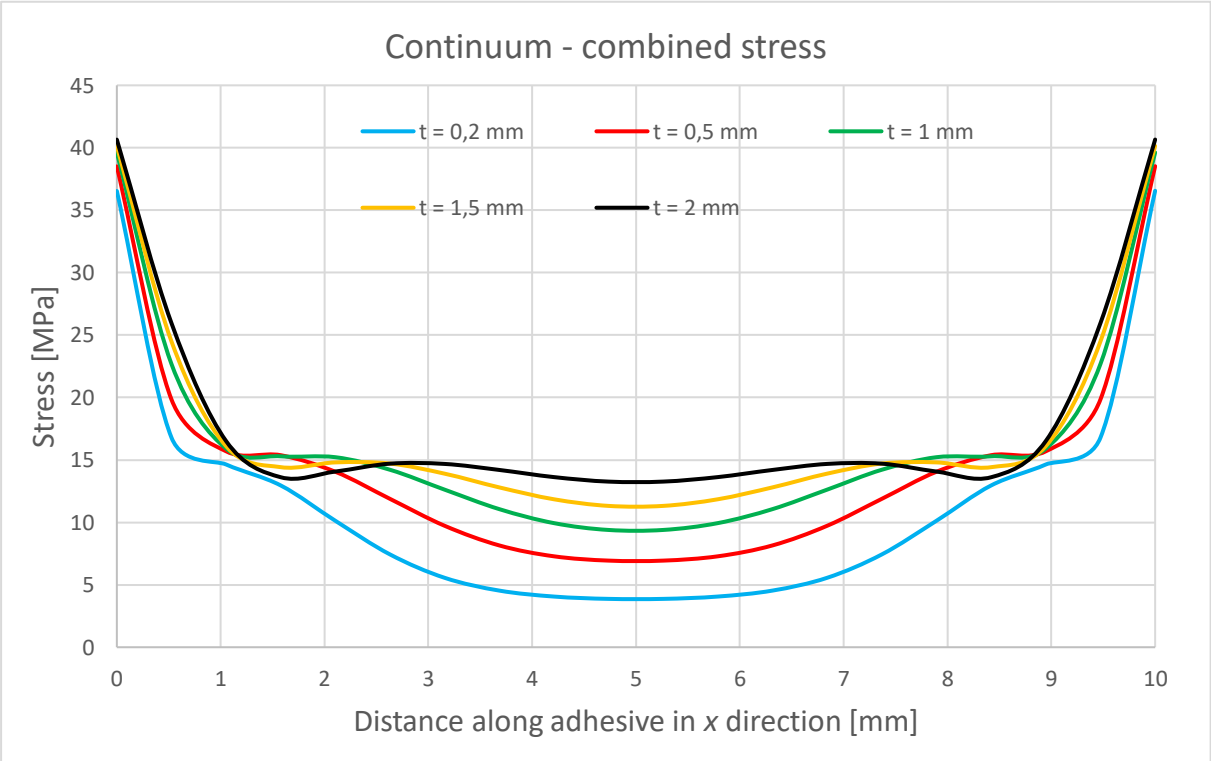

Figure 80. Distribution of combined stress within adhesive for different bondline thicknesses for continuum model

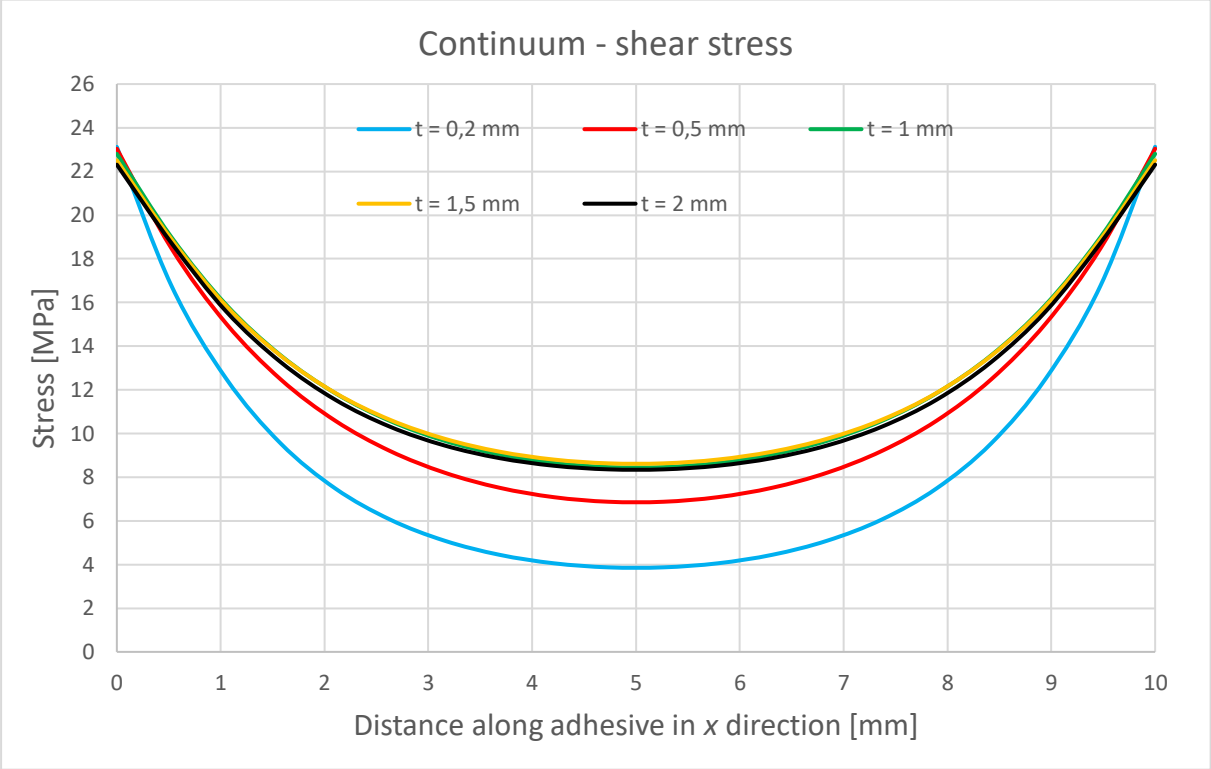

Figure 81. Distribution of shear stress within adhesive for different bondline thicknesses for continuum model

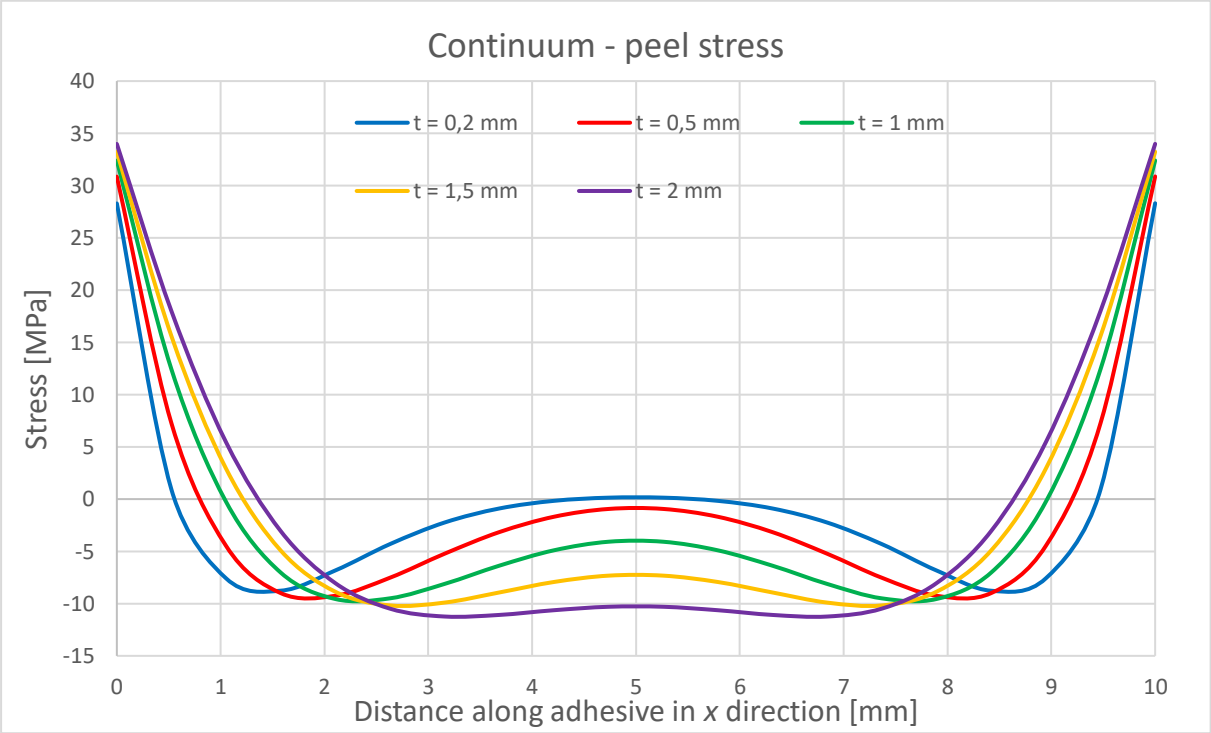

Figure 82. Distribution of peel stress within adhesive for different bondline thicknesses for continuum model